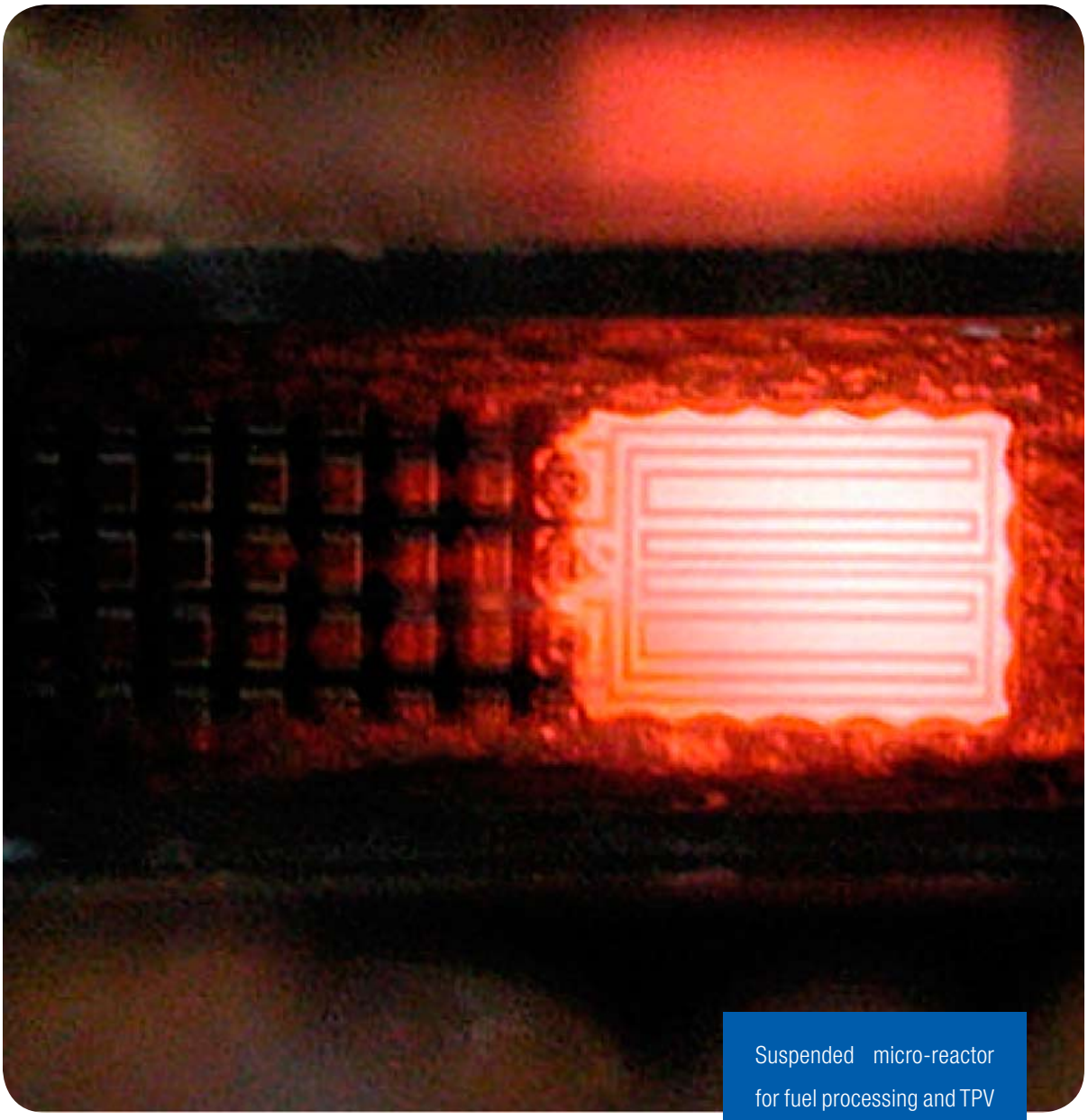

Suspended micro-reactor for fuel processing and TPV energy conversion. Photo by Ole Mattis Nielsen

MEMS

TABLE OF CONTENTS

Nanoscale Manipulation of Biological Entities Using Magnetic Particles and Fields

A. Balducci, D. Pregibon, H. Singh, L. Gonzalez, P. Matsudaira, T.A Hatton, P. Doyle
Sponsorship: NSF

An increasing number of "lab-on-a-chip" technologies and therapeutic treatments rely on the rapid isolation of clinically or scientifically relevant proteins, cells, and nucleic acids. Magnetic fields and forces provide a useful means of sorting and manipulating such biological entities. Researchers have successfully used magnetic particles, often decorated with target-specific antibodies, for applications in human leukocyte antigen (HLA) diagnostics, cell enrichment or depletion, protein isolation, biomechanics measurements, and the electrophoresis of nucleic acids. The goal of our research is to use uniform and non-uniform magnetic fields in MEMS devices to manipulate magnetic particles or bound entities for the purpose of developing tools that can more rapidly and efficiently sort DNA, blood cells, and cellular organelles.

We have previously demonstrated the electrophoresis of DNA in a microchannel using an array of self-assembled posts of magnetic particles [1]. We intend to investigate the effect of column spacing on separation efficiency and also the use of "blinking" magnetic fields (Figure 1) as a more rapid means to separate long-chain DNA, which tends to migrate very slowly in a static matrix. In addition, we have demonstrated, experimentally and through simulation, the ability to direct columns of magnetic beads laterally across a microfluidic channel, using patterned materials and a uniform magnetic field (Figure 2). This mechanism is the first step toward our development of a continuous, incubation-free cell-sorting device. Furthermore, we have utilized "saw-tooth" magnetic fields with aqueous ferrofluids to sort submicrometer (510 and 840nm) non-magnetic particles [2]. We believe this magnetophoresis will be useful in sorting subcellular, like-sized biological bodies, such as organelles and viruses.

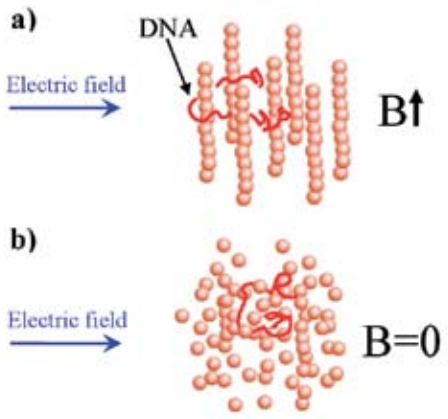

Figure 1: Conceptual electrophoresis of DNA using magnetic beads in a "blinking" magnetic field. (a) DNA caught on a post in a vertical field. (b) Release of DNA and destruction of posts when magnetic field is turned off.

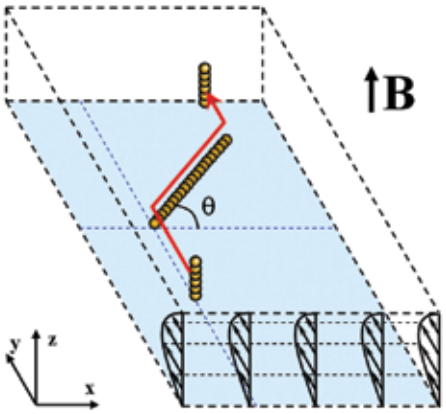

Figure 2: Schematic demonstrating the guidance of a magnetic bead column along a rail of similar beads patterned to the floor of a microfluidic channel.

REFERENCES:

[1] Doyle, P.S., J. Bibette, A. Bancaud, J.L. Viovy, "Self-Assembled Magnetic Matrices for DNA Separation Chips," *Science*, vol 295, pp. 2237, March 2002.

[2] Park, E.S., L.A. Gonzalez, K.A. Smith, T.A. Hatton, "Magnetophoretic Size-Based Trapping and Separation of Nonmagnetic, Submicrometer Particles in a Microsystem," submitted to *Analytical Chemistry*.

Suspended Microchannel Resonators for Biomolecular Detection

T.P. Burg, S.R. Manalis
Sponsorship: NIH, AFOSR

We have demonstrated a new approach for detecting biomolecular mass in the aqueous environment. Known as the suspended microchannel resonator (SMR), target molecules flow through a suspended microchannel and are captured by receptor molecules attached to the interior channel walls [1]. As with other resonant mass sensors, the SMR detects the amount of captured target molecules via the change in resonance frequency of the channel during the adsorption (Figures 1,2). However, what separates the SMR from the myriad of existing resonant mass sensors is that the receptors, targets, and their aqueous environment are confined inside the resonator, while the resonator itself can oscillate at high Q in an external vacuum environment, thus, yielding extraordinarily high mass resolution.

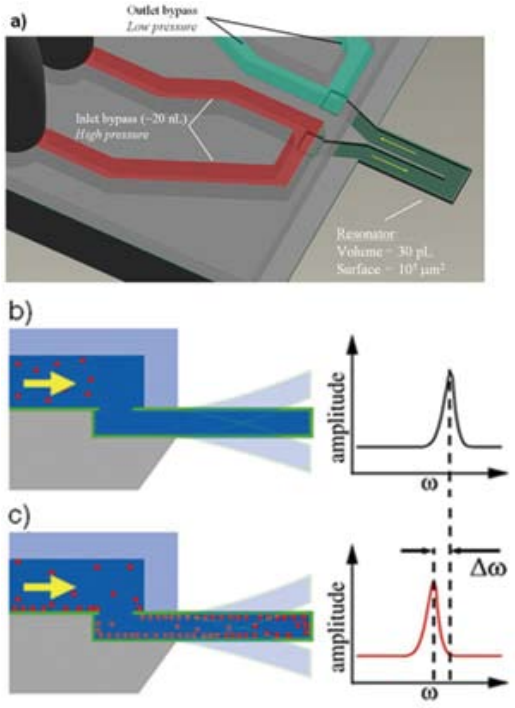

Figure 1: a) Suspended microchannel resonator (SMR); b) Cross-section of vibrating SMR; c) Targets bind to immobilized receptors (not shown), and the high surface concentration lowers the resonant frequency. Since biomolecules are more dense than solution (~1.4 g/cm^3), the resonant frequency is reduce by $\Delta\omega$.

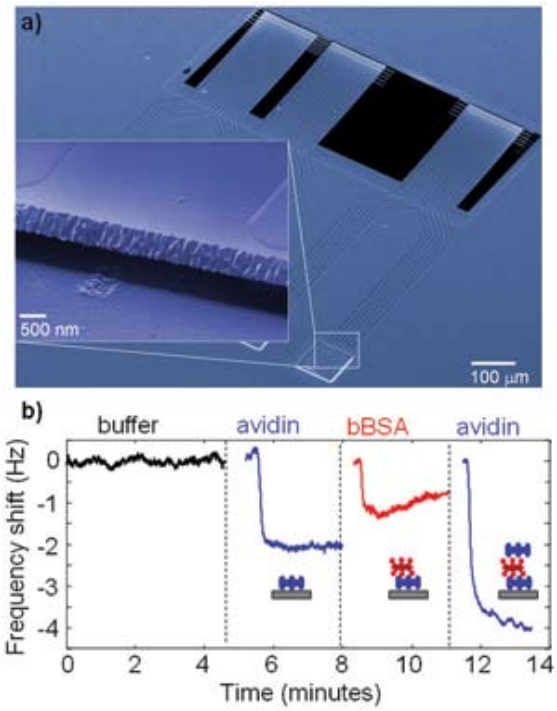

Figure 2: a) Electron micrograph of three suspended microchannel resonators; b) Relative frequency shift for a 40 kHz resonant microchannel after injection of the following solutions: buffer (black), avidin (blue), bBSA (red), and avidin (blue). The adsorption of the biomolecules to the interior channel walls increases the overall mass and lowers the resonant frequency.

REFERENCES:

[1] Burg, T., S.R. Manalis, "Suspended Microchannel Resonators for Biomolecular Detection," *Appl. Phys. Lett.* 83: 2698-2701 (2003).

A Combined Microfluidic/Dielectrophoretic Microorganism Concentrator

N. Gadish, J. Voldman
Sponsorship: Charles Stark Draper Laboratory, Siebel Scholarship

This project focuses on the development of a microorganism concentrator for pathogen detection applications. A common problem in microfluidic systems is the mismatch between the volume of a sample and the volume that a device, such as a detector, can process in a reasonable amount of time. Concentrators can, therefore, be used in pathogen detection and other microfluidics applications to reduce sample sizes to the micro-scale without losing particles of interest.

The concentrator, illustrated in Figure 1, is an active filter that uses dielectrophoresis to concentrate bacterial spores in low-conductivity solution. Dielectrophoresis uses spatially nonuniform, alternating electric fields to move particles by polarizing them and then acting on the induced dipole [1]. This concentrator uses positive dielectrophoresis, pulling particles toward electric field maxima. In operation, we set up the electric fields by lining the bottom of the channel with interdigitated electrodes. We combine a passive mixer [2] with these electrodes to enable trapping at high flowrates: the mixer circulates the liquid, bringing particles to the bottom of the channel where they are trapped by the electrodes. When enough particles have been collected, they are all released at once in a small volume, thereby producing a concentrated sample. Figure 2 shows a plot of output concentration over time as a sample of beads is released. The plot was produced by sampling discrete droplets at the output of the device and measuring their bead concentration using a spectrophotometer. This result shows a concentration enhancement of 25x between the input (C_0) and output (Drop #5) concentrations.

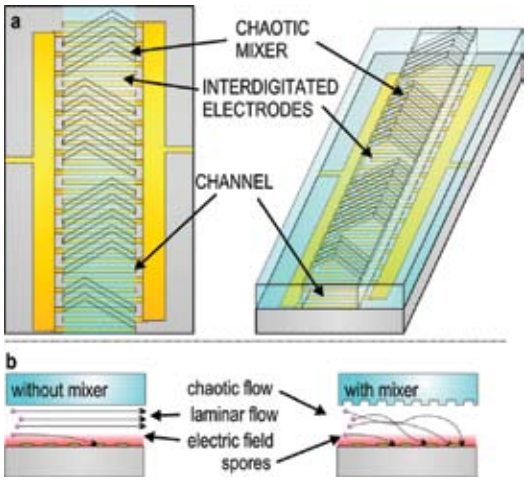

Figure 1: Illustration of the proposed concentrator. Interdigitated electrodes (a) on the bottom of the channel trap particles, and a passive mixer (b) circulates the liquid to enable trapping at high flowrates.

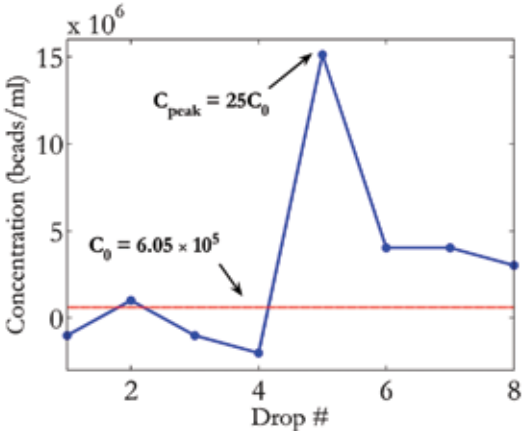

Figure 2: Experimental data of sample concentration. The blue curve shows the output concentration as it varies over time, measured in discrete drops. The peak concentration (C_{peak}) is 25 times the input concentration (C_0, indicated by the red line).

REFERENCES:

[1] Pohl, H.A, Dielectrophoresis, Cambridge University Press, Cambridge, UK, 1978.
[2] Stroock, A.D., *et al.*, "A Chaotic Mixer for Microchannels," *Science* 295, 647-651, 2002.

Single Molecule Analysis of DNA in Electric Fields

G. Randall, P. Doyle
Sponsorship: NSF

Recent advances in gene therapy and crime investigation have spurred a demand for rapid "gene mapping" of large (kbp-Mbp) DNA molecules. Because current electrophoresis technologies are inadequate for large DNA, several promising MEMS designs for DNA mapping have been recently proposed that require either: 1) a DNA molecule negotiating an obstacle course in a microchannel or 2) stretching a DNA coil for linear analysis. The goal of our research is to experimentally probe the fundamental physics that underlie these DNA mapping designs. In general, the governing physics is complex due to the confinement of the microchannel, the coiled-nature of long DNA molecules, and the induced electric field gradients from obstacles and changes in channel dimensions.

With single molecule microscopy, we have demonstrated many of the governing physical mechanisms at play in these gene mapping microfluidic devices [1-3]. For example, we have shown the experimental scaling for the diffusion coefficient of DNA in a confined channel (Figure 1a) and the probability distribution for the "collision time" of a DNA molecule unhooking from a small obstacle (Figure 1c). In addition, we have thoroughly investigated DNA stretching in electric field gradients created by a contraction and an obstacle (Figure 2). Just as a flow gradient stretches a polymer, an electric field gradient can stretch a charged polymer like DNA. Because electric field gradients have no local rotational components, a charged polymer will experience *purely extensional* deformation. These findings will aid the design of DNA separation devices that contain many obstacles and contractions, and they also offer an attractive way to completely stretch DNA for linear analysis.

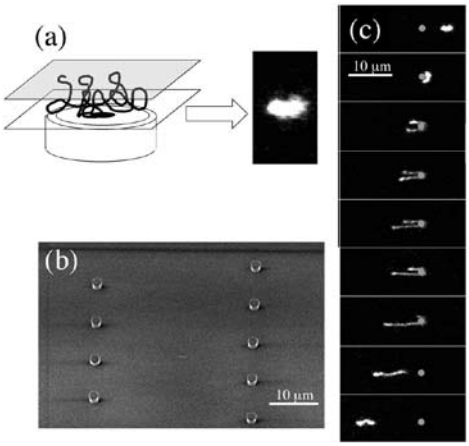

Figure 1: (a) Cartoon of a long DNA molecule in a thin slit over a microscope objective and a sample experimental image. (b) SEM image of a disperse array of small PDMS (polydimethylsiloxane) obstacles (R_{obs}=0.8 μm, height=2 μm). (c) A hooking collision of λ−DNA with one of the small obstacles (0.17 s intervals, DNA moving right to left).

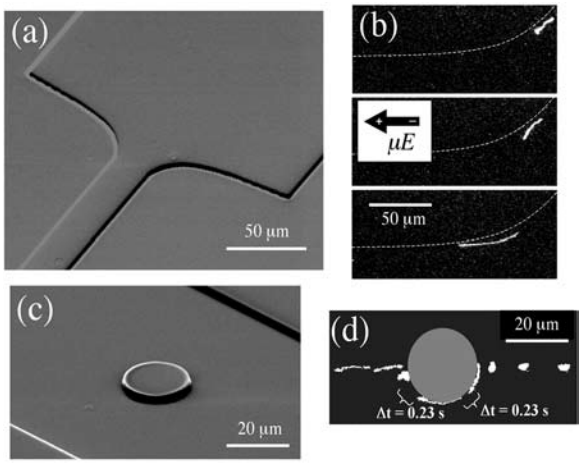

Figure 2: (a) SEM image of a hyperbolic PDMS contraction (height=2 μm). (b) A 2λ−DNA stretching near full extension in a hyperbolic contraction (DNA moving right to left). (c) SEM image of a large PDMS obstacle (R_{obs}=10 μm, height=2 μm). (d) A center-line collision of DNA with the large obstacle (0.33 s intervals unless noted, DNA moving right to left).

REFERENCES:

[1] Randall, G.C., P. S. Doyle, "Electrophoretic Collision of a DNA Molecule with an Insulating Post," *Phys. Rev. Lett.*, vol. 93, pp. 058102, July 2004.

[2] Chen, Y.-L., M.D. Graham, J. J. dePablo, G. C. Randall, M. Gupta, P. S. Doyle, "Conformation and Dynamics of Single DNA in Parallel-Plate Slit Microchannels," *Phys. Rev. E*, vol. 70, pp. 060901, December 2004.

[3] Randall, G.C., P.S. Doyle, "DNA Deformation in Electric Fields: DNA Driven Past a Cylindrical Obstruction," *Macromolecules*, vol. 38, pp. 2410-2418, February 2005.

Microfabricated Mechanical Biosensor with Inherently Differential Readout

C.A. Savran, T.P. Burg, J. Fritz, S.R. Manalis
Sponsorship: AFOSR, NSF

Intermolecular forces that result from adsorption of biomolecules can bend a micromachined cantilever and enable the detection of nucleic acids and proteins without any prior labeling of target molecules. Often, the cantilever deflection is detected using the optical lever method, i.e., by focusing a laser beam at the tip of the cantilever and measuring the changes in position of the reflected beam. Researchers have also shown that, by using the optical lever method to separately measure the bending of two identical cantilevers, the reliability of the signal resulting from the molecular binding reaction is improved by monitoring the relative or differential bending. [1]

We developed an interferometric sensor that inherently measures the differential bending between two adjacent cantilevers, thereby eliminating the need for two separate optical setups and alignment steps. The two cantilevers constitute a sensor-reference pair, whereby only the sensing surface is functionalized with receptors that are specific to the ligand to be detected (Figure 1). The two cantilevers have closely matched responses to background disturbances. Hence, disturbance-induced nonspecific deflections are suppressed upstream, i.e., before the optical signal is measured. We have previously shown that in air, the resolution of the interferometric cantilever-based sensor at high frequencies (40-1000 Hz) is limited by its sub-angstrom thermomechanical noise (~0.2 $Å_{RMS}$). However, at lower frequencies, the sensor exhibits a flicker or 1/f-type behavior, which yields noise levels that are much higher (~10 $Å_{RMS}$) than the thermomechanical noise. For biological applications of cantilever-based sensors, it is the low-frequency behavior in liquid that governs the detection limit. We have measured the low-frequency behavior of the sensor in liquid and demonstrated that it can be improved by differential detection (Figure 2) [2].

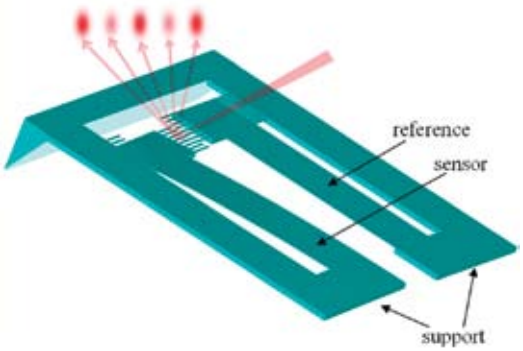

Figure 1: Schematic of the sensor. The pair of flexible sensor/reference cantilevers is supported by L-shaped thick structures that connect them to the die. The die is placed in a fluidic chamber. The differential bending is measured directly using the interference between two sets of interdigitated fingers.

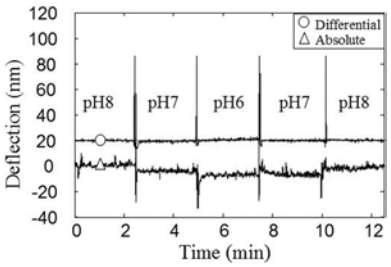

Figure 2: Absolute and differential cantilever bending due to pH changes in aqueous environment. Spikes represent injections. Absolute response (triangle) of a single cantilever to pH changes is significantly reduced by the differential detection (circle). Differential response was intentionally plotted with a DC offset for clarity.

REFERENCES:

[1] Savran, C., T. Burg, J. Fritz, S.R. Manalis, "A Mechanical Biosensor with Inherently Differential Readout," *Appl. Phys. Lett. 83*: 1659-1661 (2003).

[2] Fritz, J., M.K. Baller, H.P. Lang, H. Rothuizen, P. Vettiger, E. Meyer, H.J. Guntherodt, C. Gerber, J.K. Gimzewski, "Translating Biomolecular Recognition into Nanomechanics," *Science,* 288, 5464 (2000).

Micromechanical Detection of Proteins Using Aptamer-Based Receptor Molecules

C.A. Savran. S.M. Knudson, A.D. Ellington, S.R. Manalis
Sponsorship: AFOSR, NSF

Numerous studies have been conducted on using antibodies as receptors for detecting proteins. Although antibodies can be used to detect proteins with high sensitivity and specificity, they are generally produced *in vivo*, which introduces difficulties in engineering their properties. In contrast, aptamers (nucleic-acid binding species) can be selected *in vitro* and have been produced against a wide range of targets, from small molecules, to proteins, to whole cells. Aptamers are DNA or RNA molecules, which can form tertiary structures that recognize and bind to their respective targets.

We have investigated the capability of an aptamer-protein binding event to generate changes in surface stress that bend a flexible micromachined cantilever (Figure 1) [1]. We used a receptor-ligand system that was previously investigated and characterized in solution. The ligand, i.e. the target molecule, was Thermus aquaticus (Taq) DNA polymerase, an enzyme that is frequently used in polymerase chain reaction (PCR). The recognition element (receptor) of the sensor was an anti-Taq aptamer modified with a thiol group at one end to enable covalent linking onto a gold surface. The sensor cantilever was functionalized with aptamer molecules, and the reference cantilever was functionalized with oligonucleotides of nonspecific sequence. The differential bending between the two cantilevers was determined directly by using interferometry. We characterized the system in terms of its response to variation in ligand concentration, as well as, its ability to recognize a particular ligand in a complex mixture and to discriminate against nonspecific binding (Figure 2). Our results indicate that aptamers can be used with cantilever-based sensors for sensitive, specific, and repeatable protein detection.

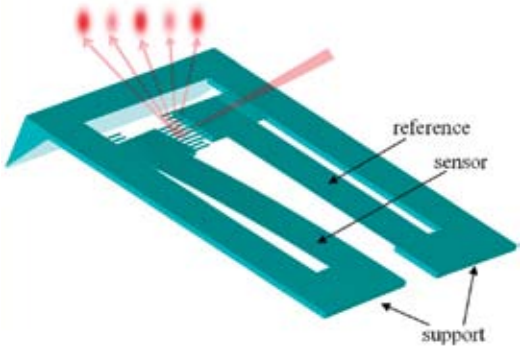

Figure 1: Schematic of the sensor. The pair of flexible sensor/reference cantilevers is supported by L-shaped thick structures that connect them to the die. The die is placed in a fluidic chamber. The differential bending is measured directly using the interference between two sets of interdigitated fingers.

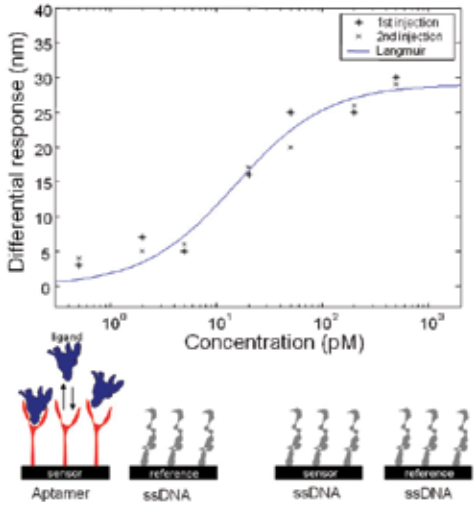

Figure 2: Variation of micromechanical sensor response with Taq DNA polymerase concentration. The experiment was performed twice for each concentration. A Langmuir-isotherm fit to the data revealed a Kd of 15pM.

REFERENCES:

[1] Savran, C., S. Knudson, A.D. Ellington, S.R. Manalis, "Micromechanical Detection of Proteins Using Aptamer-Based Receptor Molecules," *Analytical Chemistry,* 76: 3194-3198 (2004).

Plasmon Microscopy on Gold and Gold/Oxide Surfaces

L. Chao, M. Steinback, A.P. Gast
Sponsorship: MIT ChemE

Surface plasmon resonance has primarily been used as a technique for measuring the thicknesses of very thin organic and polymer films on metallic surfaces with low lateral resolution. Its ability to sense unlabeled molecules and its speed of measurement are advantageous when observing real-time adsorption, desorption, or reactions, of biological molecules.

In this study, we will use the surface plasmon technique to create an imaging microscope to study planar lipid bilayers. We develop imaging optics that collect the plasmon reflectivity in a CCD (charged-coupled device) camera to provide real images of the optical thickness of absorbates as shown in Figure 1. To improve the lateral resolution, we will utilize protein barriers to restrict the motion of the lipids and to uniformly divide the observational field. We print these with a PDMS (polydimethylsiloxane) stamp made from photoresist masters created in the MTL Technology Research Laboratory. To provide a surface commensurate with other experimentation on the lipids, we coat the metallic interface with a 10 nm layer of silicon dioxide, which has a minimal effect on sensitivity. The metallic surface and the silicon dioxide coating are evaporated in the MTL Exploratory Materials Laboratory. In Figure 2, we show a static corral pattern with 50x50 μm^2 areas of 40% 1,2-dioleoyl-sn-glyceri-3-phosphocholine (DOPC)/30% egg-sphingomyelin/30% cholesterol surrounded by 10 micrometer wide BSA (Bovine Serum Albumin) protein spacers. The width is foreshortened by the experimental setup.

After improving the lateral resolution, this technique will be able to image the domain dynamics caused by enzyme reactions in a high throughput way.

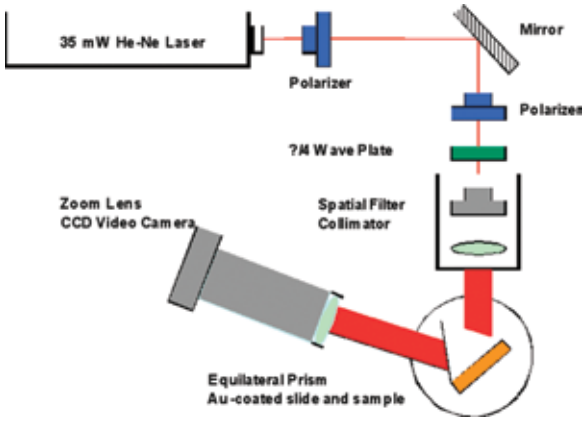

Figure 1: Optical layout of the surface plasmon microscope.

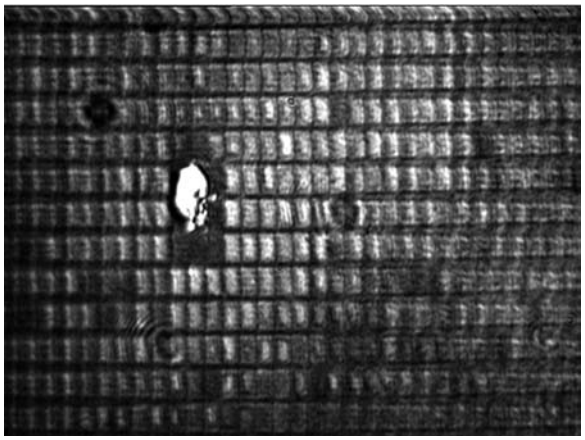

Figure 2: BSA corrals containing lipid layer. Size is 50x50 μm^2 with 10 µm separations.

Use of Stamped Protein Corrals in High Throughput Studies of Lipid Membrane Model Systems

L. Chao, M. Steinback, A.P. Gast
Sponsorship: MIT ChemE

Supported lipid bilayers are useful *in vitro* mimics for natural biological membranes, and various biotechnological applications are facilitated by their planar geometry. In this study, variable compositions or conditions will be created on supported planar lipid bilayers in order to study the coupled effects of enzyme, membrane, and solution composition on the sphingomyelinase enzymatic reaction. We combine gradients produced by microfluidic flows with membranes confined to surface patterned corrals in order to achieve a high throughput experimental system in which the preparation and measurement times can be greatly reduced. We employ poly(dimethylsiloxane) (PDMS) stamps, which are made from photoresist masters created in the MTL Technology Research Laboratory, to print proteins [1] onto glass surfaces to create barriers capable of restricting the motion of lipids to specific regions of the surface called corrals, as shown in Figure 1. The various membrane conditions in the corrals can be created by incorporating the patterned surface within a microfluidic device. The laminar flow in the micofluidic channel causes fluid elements to follow streamlines, mixing across the streamlines only by diffusion. To create varying lipid bilayer compositions, vesicles are deposited from solution and irreversibly stick to form a continuous bilayer within each corral. As a consequence, a particular vesicle composition in the microfluidic channel is captured by the surface and is restricted in each corral, as shown in Figure 2. Likewise, we can create gradients in the bulk solutions (e.g. enzyme concentration or buffer conditions) by varying the composition in neighboring laminar streams. The desired corralled lipid composition gradient or desired solution condition gradient upon corralled lipid can be adjusted by flow parameters and scale of corral size.

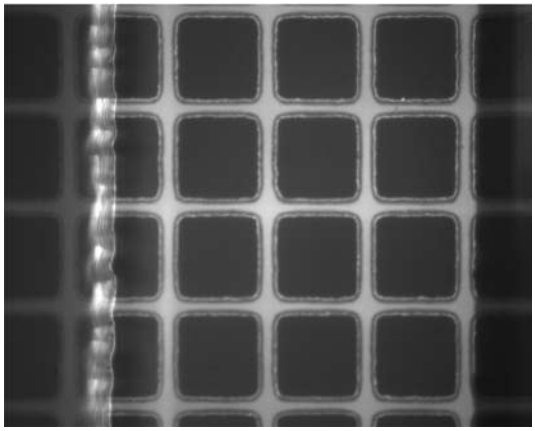

Figure 1: A Texas-Red labeled Bovine Serum Albumin (TR-BSA) corral printed on a glass coverslip in a 200μm wide microchannel. The size of each corral is 50μm x 50μm.

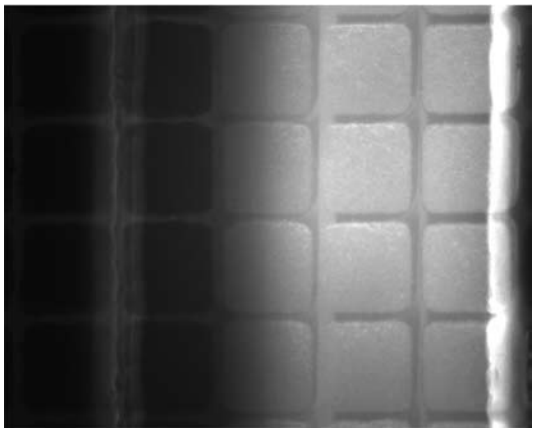

Figure 2: A preliminary lipid bilayer composition gradient formed in a 200μm wide and 50 μm high channel. Neighboring streams of vesicles are flowed over the glass coverslip patterned with BSA. The vesicles deposit a supported lipid bilayer, and the excess is washed away with the buffer. The corrals capture the composition gradient after the flow is stopped.

REFERENCES:

[1] Kung, L.A., L.Kam, J.S. Hovis, S.G. Boxer, "Patterning Hybrid Surfaces of Proteins and Supported Lipid Bilayers," *Langmuir*, vol. 16, p. 6776, 2000.

Use of Microfluidic Device to Study Protein-Polymer Interactions

P.A. Achurra[§], C.R. Robertson[§], A.P. Gast*
Sponsorship: E&J Gallo Winery

In recent years, the importance of polymer architecture on their physical properties has been recognized. We are studying the effect of a polymer's macromolecular architecture on its ability to interact with other molecules, in particular with proteins.

In order to study a variety of protein-polymer interactions we developed a microfluidic platform. We monitor polymer-protein interactions by means of fluorescence resonance energy transfer (FRET), where the polymer molecules are unlabeled and two populations of protein molecules are fluorescently labeled with a FRET donor and an acceptor pair. Because a FRET signal is highly distance-dependent, without interaction we observe little FRET, and upon complexation, we observe a strong FRET signal (Figure 1).

We are interested in the effects of polymer branching on protein aggregation and have chosen a model system of different generations of Poly(amidoamine) PAMAM dendrimers and fluorescently labeled Streptavidin. We can manipulate the overall charge of PAMAM dendrimers either by selecting dendrimers generation (G0, G2, G4, etc) or by adjusting the solution pH.

We create a microfluidic device from polydimethylsiloxane (PDMS). The laminar flow in these channels allows us to directly compare polymer or control solutions interacting with the protein solution by interdiffusion. Our initial results show qualitative differences between Streptavidin/PAMAM (G2) and Streptavidin/PAMAM (G4) interactions (Figure 2). As molecules move along the channel, they start interacting. We observe both a shift in peak position, as well as, changes in intensity profiles as the molecules move away from the junction point. The peak position shift indicates that, indeed, both polymers interact with Streptavidin and that changes in intensity profiles are not solely caused by diffusion. Differences between the intensity profiles of Streptavidin/PAMAM G2 and Streptavidin/PAMAM G4 show that indeed both polymers interact differently with Streptavidin molecules; we are currently analyzing these FRET profiles to provide a quantitative measure of protein-polymer interaction.

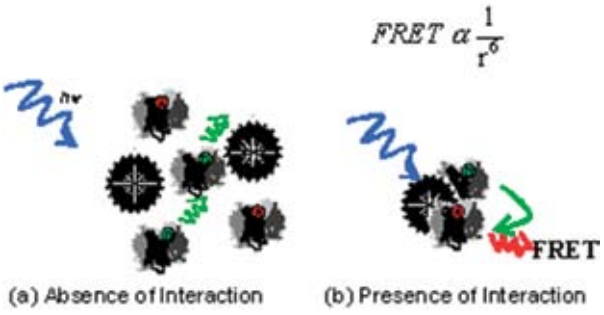

Figure 1: Schematic of FRET experiment. In the absence of interaction, there is little or no FRET signal observed; in the presence of interaction significant energy transfer occurs between donor and acceptor molecules, and FRET is observed D: FRET donor, A: FRET acceptor.

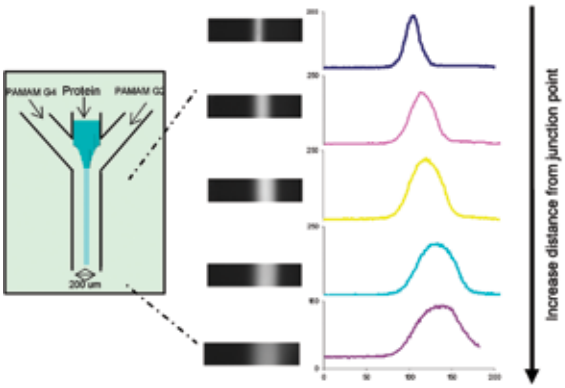

Figure 2: A microfluidic device for studying protein/polymer interactions. On the left is a diagram of the device; in the center are FRET images at different distances from the junction; on the right are intensity profiles from FRET images.

§ Department of Chemical Engineering, Stanford University.
* Department of Chemical Engineering, Massachusetts Institute of Technology.

Super-Hydrophobic Surfaces for Hemocompatibility

A.J. Schrauth, N. Saka, N.P. Suh
Sponsorship: Korean Institute of Machinery and Materials

It is well known that in fluid systems, as geometric scale decreases, the effect of surface forces increases relative to body forces. This property has been exploited to modify the wetting behavior of fluids on a surface by structuring the surface. By reducing feature size, surfaces have been developed that have a contact angle with water that approaches 180° when the flat-surface contact angle of the material is closer to 100° [1]. Our project focuses on making these so-called super-hydrophobic surfaces practical to manufacture. We have manufactured surfaces with water contact angles above 160° by casting poly-dimethylsiloxane (PDMS), a material with a flat-surface water contact angle of approximately 100°. Our methods are limited by the size of a low temperature oven, not by wafer size. Thus, we can scale production size up beyond the limits of typical microfabrication techniques.

Additionally, we are interested in the application of super-hydrophobic surfaces in bio-medical systems to improve hemocompatability. A material is hemocompatable if it does not react unfavorably in the presence of blood. Hemocompatible surfaces are crucial to the performance of many biomedical devices. One of the requirements for such surfaces is the ability to resist the coagulation of proteins from blood. The increase in contact angle for super-hydrophobic surfaces is driven by a reduction in the interaction between the fluid and the surface. We are investigating the hypothesis that reducing the fluid-surface interaction between blood and a surface by microstructuring will decrease protein deposition on the surface.

REFERENCES:

[1] Krupenkin *et al.*, "From Rolling Ball to Complete Wetting: The Dynamic Tuning of Liquids on Nanostructured Surfaces," *Langmuir*, 20, pp.3824-3827, 2004.

Electrical Properties of the Tectorial Membrane Measured with a Microfabricated Planar Patch Clamp

R. Ghaffari, D.M. Freeman
Sponsorship: NIH

The tectorial membrane (TM) is a mechanical structure in the cochlea that plays a critical role in hearing. Although its composition suggests that it contains an abundance of charged molecules–charges that may contribute to its mechanical properties–measuring the concentration of this fixed charge has been difficult. Since the TM lacks an insulating cell membrane, traditional micropipette techniques have not yielded stable measurements of the electrical potential of the TM.

We have developed a microfabricated chamber that overcomes this problem by placing the TM as an electrochemical barrier separating two fluid baths. The chamber consists of a small aperture into a microfluidic channel (Figure 1), similar to previous planar patch clamp designs [1]. The aperture diameter was chosen to be small enough to be covered by the TM, while large enough to contribute little electrical resistance. The microfluidic channel allows perfusion of the fluid below the TM, so the ionic composition of fluids in both baths can be rapidly changed. Varying the ionic concentration of the baths changes the electrical potential between baths in a manner that depends on the fixed charge of the TM. The microfabricated chamber has enabled the first stable, repeatable measurements of this electrical potential (Figure 2). The results suggest that the TM contains sufficient charge to completely account for its mechanical rigidity.

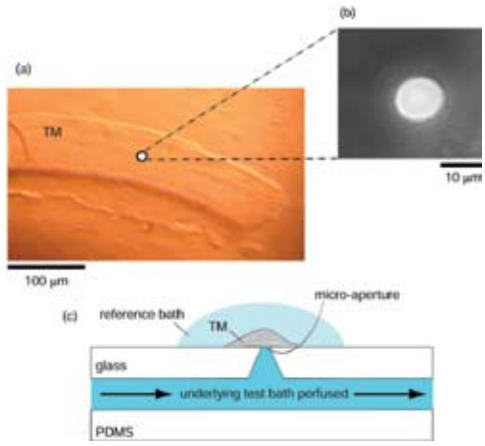

Figure 1: Microfabricated planar patch clamp setup. (a) Top view of a section of TM placed on the planar patch clamp containing a micro-aperture, drawn as a white circle for visibility. (b) Closer view of the micro-aperture with the TM removed. (c) The test bath in the underlying fluidics channel was perfused with solutions of different ionic strength during voltage recordings.

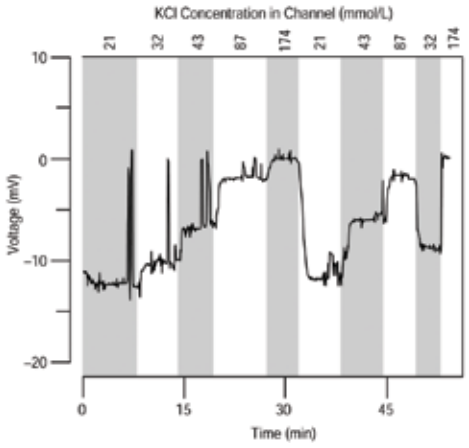

Figure 2: Voltage measurements with varying test solutions. Voltages were found to be stable and repeatable over several minutes up to hours during perfusion and TM voltage recordings. The shaded regions indicate times with different perfusates. The large transient voltage spikes result from intentionally shorting the two baths to check for drift in the measurement system.

REFERENCES:

[1] Sigworth, F.J., K.G. Klemic, "Patch Clamp On A Chip," *Biophys J*, vol. 82, 2002, pp. 2831-2832.

Microfabricated Shearing Probes for Measuring Material Properties of the Tectorial Membrane at Audio Frequencies

J.W. Gu, A.J. Aranyosi, W. Hemmert, D.M. Freeman
Sponsorship: NIH

The tectorial membrane (TM) is ideally located to exert shearing forces on sensory hair cells in the cochlea in response to sound. Consequently, measuring the shear impedance of the TM is important for understanding the mechanical basis of hearing. However, few direct measurements of TM shear impedance exist, because the small size of the TM and the need to measure its properties at audio frequencies render traditional impedance measurement methods infeasible. We have overcome these limitations by designing and microfabricating shearing probes that are comparable in size to the TM and that can exert forces at audio frequencies.

The probes consist of systems of cantilevers designed to apply forces in two dimensions (Figure 1). Forces applied to the base of the probe are coupled through the cantilevers to a shearing plate, which is brought into contact with the TM. By measuring the relative deflection of the base and plate and knowing the probe stiffness, we can determine the shear impedance of the TM. A variety of probes with different stiffnesses and geometries allow measurement of impedance over many orders of magnitude. Figure 2 shows a probe whose shearing plate is in contact with the TM. To determine TM impedance at audio frequencies, we have coupled these probes to a computer microvision system that allows measurements of nanometer-scale motions at high frequencies [1]. The probes were calibrated, and could exert forces with amplitudes in the range 3-300 nN at frequencies from 10-9000 Hz, a large fraction of the hearing range. Measurements of TM shear impedance, using these microfabricated probes, have helped to characterize this enigmatic component of the cochlea.

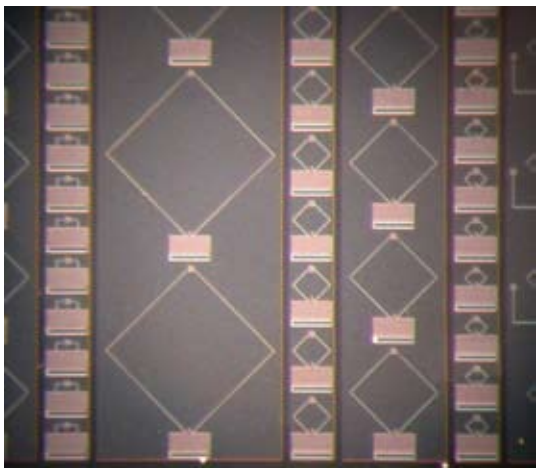

Figure 1: Microfabricated shearing probes on a silicon chip. Each probe consists of a base, a pair of cantilevered arms, and a small shearing plate. The probe stiffness depends on its size.

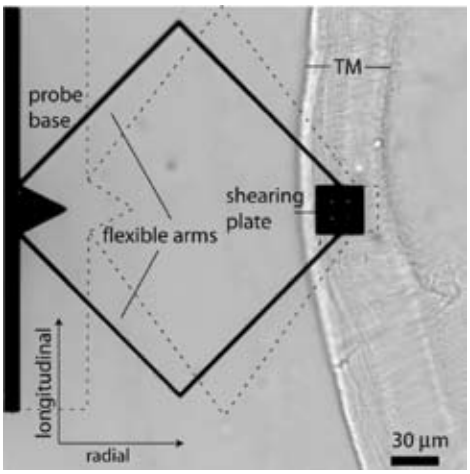

Figure 2: Stop-action video image of microfabricated probe on TM specimen. Displacements of the base cause relative motion of the base and plate (dotted line); this relative motion varies with TM impedance. Probe motions are greatly exaggerated for clarity.

REFERENCES:

[1] Davis, C.Q., D.M Freeman, "Using A Light Microscope To Measure Motions With Nanometer Accuracy," *Opt Eng,* vol. 37, pp. 1290-1298, 1998.

Implantable MEMS for Drug Delivery

H.L. Ho Duc, R.S. Langer, M.J. Cima
Sponsorship: NIH, NCI

We have developed an implantable silicon microelectromechanical system (MEMS) device for biomedical applications [1]. This device contains an array of wells that hermetically store its contents. Activation of the device electrochemically dissolves gold membranes covering the wells, by application of an anodic voltage through a wire-bonded connector (Figure 1). The well contents are then exposed to the surrounding environment. This system allows temporal control of several activations and the ability to store a variety of contents separately. Targeted application for this device is local drug delivery.

We have focused our drug delivery efforts on carmustine (BCNU), a potent brain cancer drug. Local delivery of BCNU from an implanted device results in efficacious concentrations at the tumor site, coupled with reduced systemic toxicity, which is a major drawback of the systemic delivery of BCNU [2]. We have achieved successful *in vitro* and *in vivo* release of BCNU, and have shown it to significantly impede tumor growth in rats as a result of co-formulation with polyethylene glycol (PEG) to improve release kinetics, and of the development of a new, Pyrex-based package that increases the capacity of the device [3]. Combination therapy of BCNU with Interleukin-2 (IL-2), however, has been shown to be more effective than either alone against tumors [4]. We, therefore, plan to use our device to achieve combination releases, to fully utilize the advantages of our MEMS, i.e., temporal control and multi-drug releases.

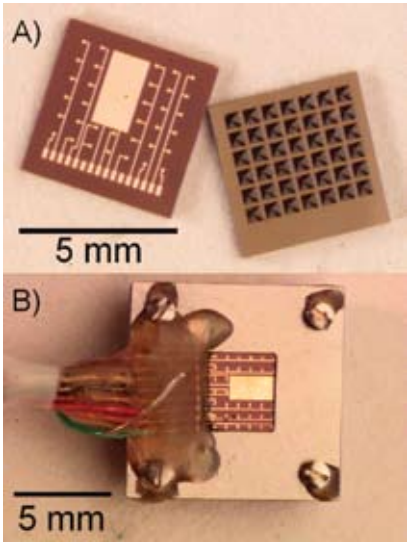

Figure 1: Photographs showing (A) top and bottom of the silicon microchip, and (B) a packaged device with wire-bonded connector

REFERENCES:

[1] Santini, J.T., M.J. Cima, R.S. Langer, "A Controlled-Release Microchip," *Nature*, vol. 397, pp. 335-338, January 1999.

[2] Brem, H., R.S. Langer, "Polymer-Based Drug Delivery to the Brain," *Sci Am Sci Med*, vol. 75, pp. 922-929, 1996.

[3] Li, Y.W., H.L. Ho Duc, B. Tyler *et al.*, "*In vivo* Delivery of BCNU from a MEMS Device to a Tumor Model," *Journal of Controlled Release*, accepted for publication.

[4] Sampath, P., J. Hanes, F. DiMeco *et al.*, "Paracrine Immunotherapy with Interleukin-2 and Local Chemotherapy is Synergistic in the Treatment of Experimental Brain Tumors," *Cancer Research*, vol. 59, pp. 2107-2114, May 1999.

A Peristaltic Oxygenating Mixer for Miniature Integrated Bioreactors

H.L.T. Lee, R.J. Ram
Sponsorship: Dupont-MIT Alliance

We have developed a mixer and corresponding fabrication process to address problems involved in the development of a miniaturized parallel integrated bioreactor array system, whose functional objectives include: (1) the ability to support cell growth of aerobic micro-organisms without oxygen limitation, (2) scalability to a large number of reactors, (3) online sensing of culture parameters, and (4) individual control over pH. In order to achieve these design objectives, we have developed a flat form factor, all PDMS (silicone elastomer), peristaltic oxygenating mixer (Figure 1), using a fabrication process that allows integrating multiple scale (100μm-1cm) and multiple depth (100μm-2mm) structures in a simple molding process. The flat form factor ensures a high surface area to volume ratio for high oxygen transfer rates, and the peristaltic action achieves in-plane homogeneous mixing within 5-20 seconds, depending on the depth of the well and actuation parameters, which is three orders of magnitude faster than lateral mixing from diffusion alone. The peristaltic action also contributes to mixing in the vertical direction, which further improves the oxygen transfer rate. The volumetric oxygen transfer coefficient (k_La) was measured by a gassing-in method [1], using an integrated platinum-octaethylporphyrine based dissolved oxygen sensor [2]. Calibrated measurements of the oxygen transfer coefficient (Figure 2) in devices of various well depths agree with theoretically expected oxygen transfer coefficients for unmixed devices. For devices mixed with various actuation frequencies, the measured oxygen transfer coefficient falls short of the theoretical values due to non-instantaneous vertical mixing. Even with non-optimized devices, preliminary results from eight simultaneous bacteria growth experiments, using four different medium compositions with online measured optical density and dissolved oxygen concentration, indicate that the oxygen transport is sufficient to maintain a greater than 55% dissolved oxygen concentration for the duration of the bioreaction.

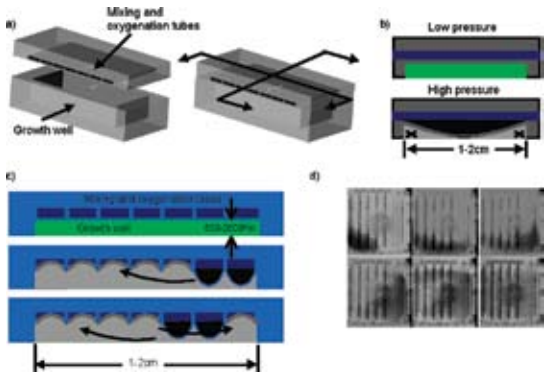

Figure 1. a) Exploded view of peristaltic oxygenating mixer. b) Low and high pressure cross sections along a mixing tube. X's indicate the return path for fluid flow. c) Cross -section across mixing tubes showing the actuation pattern, which approximates peristalsis. Arrows indicate direction of fluid flow. d) Photographs of a 750µm deep 15mm x 15mm device for 0, 1, 2, 4, 6, and 10 seconds after mixing at 25Hz and 4psi was initiated.

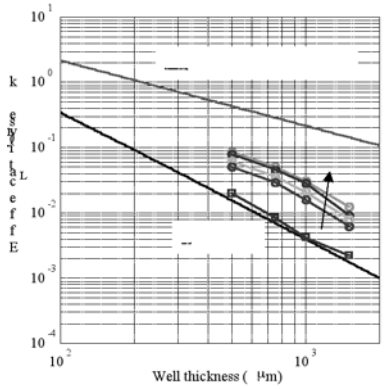

Figure 2: Calibrated oxygen transfer coefficient measurements for 500µm, 750µm, 1000µm and 1500µm deep wells and a 50µm thick peristalsis membrane. Actuation pressure was 4psi, and the arrow indicates increasing actuation frequency from 6, 12, 25, and 40Hz.

REFERENCES:

[1] Linek, V., P. Benes, V. Vacek, "Measurement of Aeration Capacity of Fermenters," *Chemical Engineering and Technology*, vol. 12, 1989, pp 213-217.

[2] Papkovsky, D.B., J. Olah, I.V. Troyanovsky, N. A. Sadovsky, V.D. Rumyantseva, A.F. Mironov, A.I. Yaropolov, and A.P. Savitsky, "Phosphorescent Polymer Films for Optical Oxygen Sensors," *Biosensors and Bioelectronics*, vol. 7, 1991, pp. 199-206.

Microfluidic Platform for High-Density Multiplexed Biological Assays

J. A. Benn, J. Hu, T. Thorsen
Sponsorship: Deshpande Center for Technological Innovation

We have developed a microfluidics-based technology that will support the ongoing need to reduce the cost and increase the capabilities of genetic testing in areas such as: population studies for the identification of inherited disease genes, more effective evaluation of drug candidates, and rapid determination of gene expression in tissues for disease management. This technology will also reduce the cost of the clinical testing of novel genetic targets related to disease risk and drug response.

Specific improvements promised by this technology are the following:

- Provides a flexible microfluidic enabling platform for genomic, proteomic and cellular array-based assays;
- Can be used with current diagnostic protocols and instrumentation;
- Tests many samples in parallel on the same microarray;
- Reduces the time it takes to perform genetic tests on microarrays from hours to minutes.

The elastomeric microfluidic device can print high-density DNA microarrays with dimensions as small as 10 µm. The device (Figure 1), which hermetically seals to a glass slide, patterns hundreds of DNA targets in parallel as lines on the glass surface. DNA samples are introduced into the sample entry ports and drawn along the channels, where they are exposed to and bind to the slide. After patterning, subsequent probe-target hybridization is simply achieved by running fluorescently labeled samples orthogonally over the target DNA-patterned glass slide, using a second microfluidic chip. Hybridization is achieved in less than 5 minutes; orders of magnitude faster than conventional DNA microarrays that require 16 hours for the same process. Using 10 µm wide microchannels, the hybridization spot density can be increased to over 400,000 assays per cm^2.

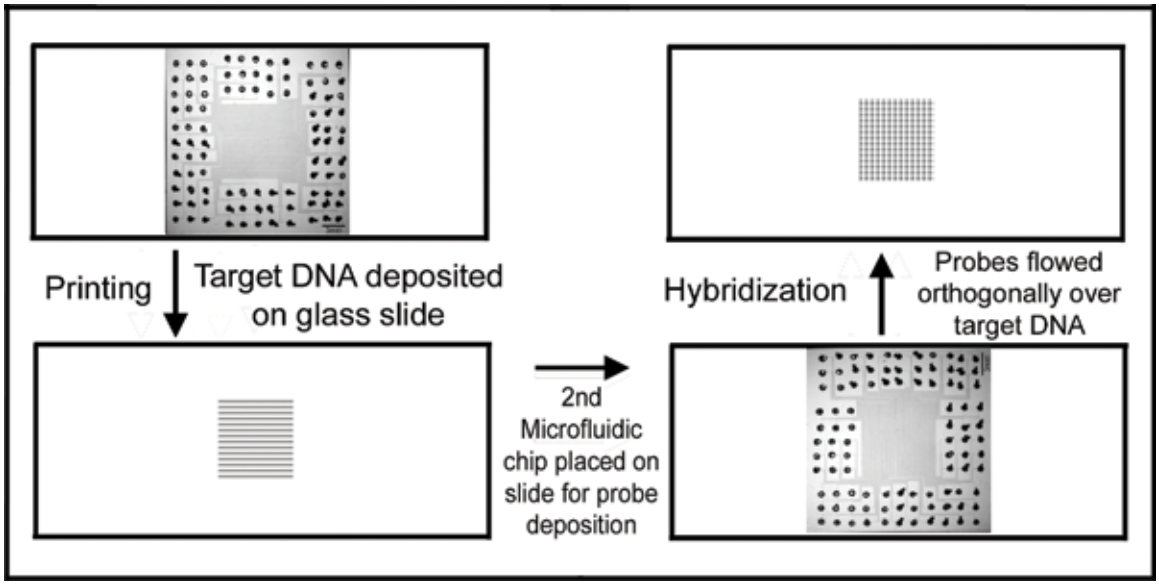

Figure 1: Illustration of DNA target printing and subsequent probe hybridization using a microfluidic array device.

Polymer-Based Microbioreactors for High Throughput Bioprocessing

Z. Zhang, G. Perozziello, N. Szita, A. Zanzotto, P. Boccazzi, A.J. Sinskey, K.F. Jensen
Sponsorship: Dupont-MIT Alliance

This project aims to develop high-throughput platforms for bioprocess discovery and developments, specifically automated microbioreactors; each with integrated bioanalytical devices, and operating in parallel. By microfabrication and precision machining of polymer material such as poly(dimethylsiloxane) (PDMS) [1] and poly(methylmethacrylate) (PMMA) [2, 3], we realize microliter (5~150 µl) microbioreactors (Figure 1) with integrated active magnetic mixing and dissolved oxygen, optical density, and pH optical measurements (Figure. 2) for monitoring nutrients and products. Reproducible batch and fed-batch [2] fermentation of *Escherichia coli* and *Saccharomyces cerevisiae* have been demonstrated in the microbioreactor. With the integration of local temperature control, cell-resistance surface modification, and pressure-driven flow at ~µL/min rates, the microbioreactor was also proven to be capable for chemostat continuous cell culture [3], which is a unique and powerful tool for biological and physiological research. As examples of bioanalysis, HPLC [1] and gene expression analysis [4] using microbioreactors have demonstrated potential applications in bioprocess developments.

Parallel microbial fermentations were undertaken in a multiplexed system demonstrating the utility of microbioreactors in high-throughput experimentation [5]. A key issue for high-throughput bioprocessing is to have inexpansive and disposable microbioreactors to save operation time and labor. Current works include the integration of plug-n-pump microfluidic connections [6] in the microbioreactor system, as well as, incorporation of fabricated polymer micro-optical lenses and connectors for biological measurements to produce "cassettes" of microbioreactors.

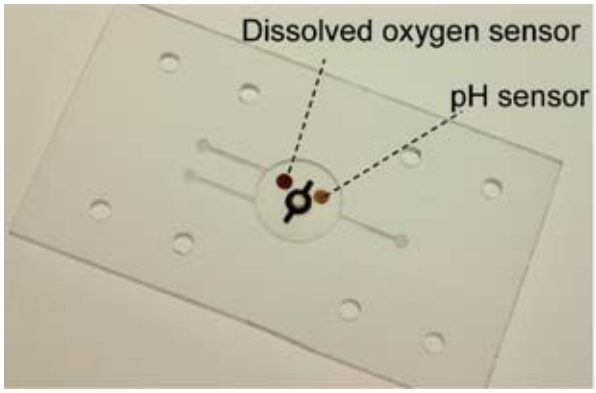

Figure 1: Photograph of the empty PMMA chamber of the microbioreactor. The magnetic stir bar in the center and the fluorescent sensors for DO and pH are visible.

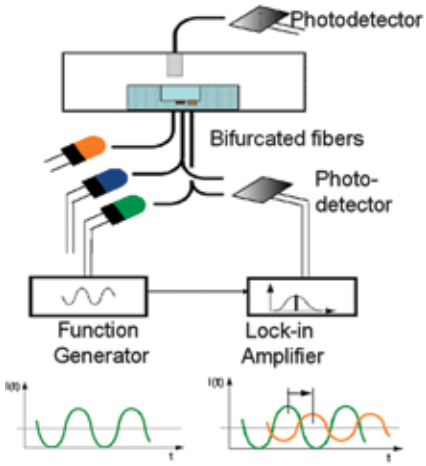

Figure 2: Experimental setup for optical measurements in the microbioreactor. Dissolved oxygen and pH are monitored by luorescence lifetime measurements. Biomass concentration is obtained by optical density, the transmission measurement by using an orange LED.

REFERENCES:

[1] Zanzotto, A., N. Szita, P. Boccazzi, P. Lessard, A.J. Sinskey, K.F. Jensen, "A Membrane-Aerated Microbioreactor for High-Throughput Bioprocessing," *Biotechnology and Bioengineering*, vol. 85, pp. 376-381, 2004.

[2] Zhang, Z., N. Szita, P. Boccazzi, A.J. Sinskey, K.F. Jensen, "Monitoring and Control of Cell Growth in Fed-Batch Microbioreactors," in *Proc. of µTAS*, 2003, pp. 765-768.

[3] Zhang, Z., P. Boccazzi, H.-G. Choi, N. Szita, A.J. Sinskey, K.F. Jensen, "A Microchemostat – Continuous Cell Culture in Microbioreactors," in *Proc. of µTAS*, 2004, pp. 231-233.

[4] Boccazzi, P., A. Zanzotto, N. Szita, S. Bhattacharya, K.F. Jensen, A.J. Sinskey, "Gene Expression Analysis of Escherichia Coli Grown in Miniaturized Bioreactor," *Applied Microbiology and Biotechnology*, published on-line DOI: 10.1007/s00253-005-1966-6 .

[5] Szita, N., P. Boccazzi, Z. Zhang, A. Zanzotto, A.J. Sinskey, K.F. Jensen, "Multiplexedmicrobioreactor System for High-Throughput Bioprocess," in *Proc. of µTAS*, 2004, pp. 390-392.

[6] Perozziello, G., M.F. Jensen, J.E. Mc Cormack, F. Bundgaard, O. Geschke, "Plug'n'pump Fluidic Interconnection," in *Proc. of µTAS*, 2004, pp. 575-577.

Cell Stimulation, Lysis, and Separation in Microdevices

J. Albrecht, J. El-Ali, S. Gaudet, K.F. Jensen
Sponsorship: NIH

Quantitative data on the dynamics of cell signaling induced by different stimuli requires large sets of self-consistent and dynamic measures of protein activities, concentrations, and states of modification. A typical process flow in these experiments starts with the addition of stimuli to cells (cytokines or growth factors) under controlled conditions of concentration, time, and temperature, followed at various intervals by cell lysis and the preparation of extracts (Figure 1). Microfluidic systems offer the potential to do these experiments in a reproducible and automated fashion.

Figure 1 shows a schematic of a microfluidic device for rapid stimulus and lysis of cells. The fluidic systems with stimulus and lysis zones are defined using soft lithography in a poly(dimethylsiloxane) (PDMS) layer, which is then bonded to a glass slide. Temperature regulation for the two zones is achieved by using a thermo electric (TE) heater at 37°C to mimic physiological conditions during stimulation and a TE cooler at 4°C to inhibit further stimulus during lysis. Mixing in the device is enhanced by the use of segmented gas-liquid flow.

To extract meaningful data from cellular preparations, current biological assays require labor-intensive sample purification to be effective. Micro-electrophoretic separators have several important advantages over their conventional counterparts, including shorter separation times, enhanced heat transfer, and the potential to be integrated into other devices on-chip. A PDMS isoelectric focusing device has been developed to perform rapid separations by using electric fields orthogonal to fluid flow (Figure 2). This device has been shown to separate low molecular weight dyes, proteins, and organelles [1].

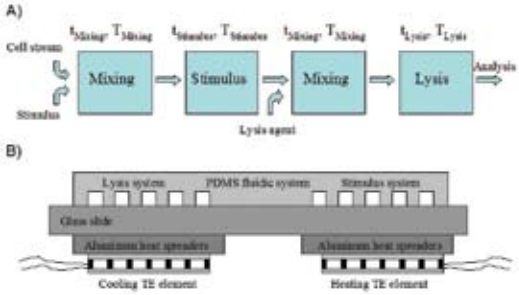

Figure 1: A) Typical process flow for cell stimulus. B) Schematic of cell stimulus device. A PDMS fluidic system is bonded to a glass slide and TE elements attached on the back through aluminum heat spreaders, which are used to control the temperature on the device.

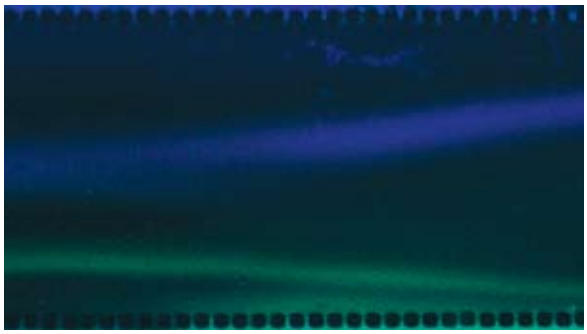

Figure 2: Rapid isoelectric focusing of two fluorescently labeled dyes. Flow is right to left. The anode is above the top row of posts, and the cathode at the bottom. Image shows focusing occurs in as little as 10 seconds.

REFERENCES:

[1] H. Lu, S. Gaudet, M.A. Schmidt, and K.F. Jensen, "A Microfabricated Device for Subcellular Organelle Sorting," *Analytical Chemistry*, vol. 76, pp. 5705-5712, 2004.

Microfluidic Devices for Biological Cell Capture

A.L. Gerhardt, M. Toner, M. Gray, M.A. Schmidt
Sponsorship: MGH, Shriners Burns Hospital

Over the past century, cellular biology and biomechanical engineering blazed ahead in areas, such as: genome sequencing, optical probes, and high-throughput biochemical testing. For example, an increasing variety of optical imaging probes now are available for chemical and biological analyses of molecular events, physiological processes, and pathologic conditions. In contrast, cell culture techniques have remained virtually stagnant [1]. Advances in MEMS, including microfluidics and soft lithography, are providing a toolset from which to develop biological MEMS devices. In addition to miniaturizing macro biological analysis tools, techniques, and assays, microfluidic devices can utilize microscale phenomena and systems to probe single- and multi-cellular levels yielding complimentary static and dynamic data sets [1,2]. Combining these advances with more traditional microtechnology provides groundwork for developing a new generation of cell culture and analysis. Assay protocols can be run in parallel, and dynamic single-cell event information can be collected on a small or large population of cells. Cells can be probed rapidly and inexpensively in large or small quantities with small sample sizes in custom, portable microenvironments developed to more physiologically resemble in vivo conditions [2]. Modular microfluidic devices are expanding possibilities, enabling snap-in modifications for different or second-pass assays. Biological cell capture and analysis devices are shown in Figure 1 and Figure 2. Designed to capture and maintain a specific number of cells in predetermined locations, the devices yield a mechanism by which to study isolated cells or cell-to-cell interaction. Once captured, the cells can be probed and static and dynamic data extracted on the single- and multi-cellular levels.

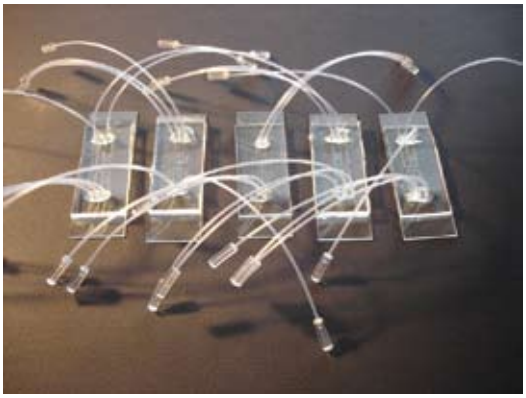

Figure 1: Packaged microfluidic devices for biological cell capture. Composed of a polydimenthylsiloxane (PDMS) cast bonded to a glass substrate, each device has standard microscope slide horizontal dimensions (25 mm x 75 mm) and a vertical dimension of about 10 mm (excluding macro connections). Captured cells can be viewed using non-inverted and inverted optical techniques.

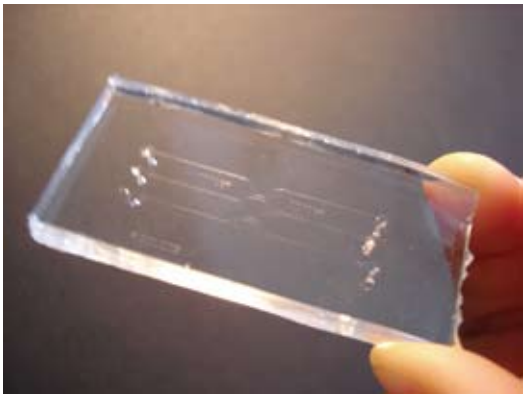

Figure 2: SU-8 masters define the microfluidic channel patterns, which are then cast in PDMS. Custom-machined hollow needles are used to punch holes for macro fluidic connections. Shown above is a 25 mm x 50 mm punched PDMS cast with 3 channels. Multiple channels enable process parallelization and more cell capture sites, increasing the statistical significance of collected data.

REFERENCES:

[1] Beebe, D. A. Folch, "The Science and Applications of Cell Biology in Microsystems," *Lab on a Chip*, vol. 5, pp. 10-11, 2005.

[2] Gerhardt, A.L., "Arrayed Microfluidic Actuation for Active Sorting of Fluid Bed Particulates," M.Eng. EECS. Thesis, Cambridge: Massachusetts Institute of Technology (MIT), 2003.

Manipulating Solid Particles In Microfluidic Systems

J.G. Kralj, M. Sultana, M.A. Schmidt, K.F. Jensen
Sponsorship: MIT Microchemical Systems Technology Center, Merck

Microfluidic systems offer a unique toolset for the separation of microparticles and for the study of the growth kinetics of crystal systems because of laminar flow profiles and good optical access for measurements. Conventional separation techniques for particles, such as sieving, are limited to sizes larger than ~ 50 microns with large dispersion. Sorting microparticles (e.g. small crystals, single cells), requires different techniques. Dielectrophoresis is particularly attractive for microfluidic systems because large electric field gradients that drive the force are easily generated at low voltages using microfabricated electrode structures, and fixed charges are not required as in electrophoresis. It is possible to continuously separate particles of 1-10 microns with ~ 1 micron resolution (Figure 1) using dielectrophoresis with asymmetric electric fields and laminar flow (Figure 2).

Microfluidic devices can also be used to study crystallization and extract kinetic parameters of nucleation and growth, and to study different polymorphs of a system. Crystallization has been achieved in some batch processes that do not have uniform process conditions or mixing of the reactants, resulting in polydisperse crystal size distributions (CSD) and impure polymorphs. Microsystems allow for better control over the process parameters, such as the temperature and the contact mode of the reactants, creating uniform process conditions. Thus, they have the potential to produce crystals with a single morphology and uniform size distribution.

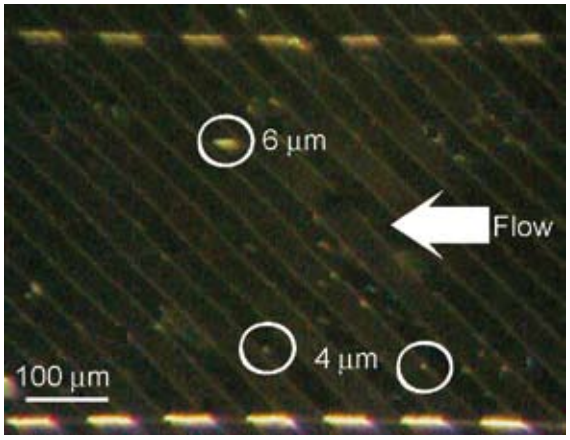

Figure 1: Dielectrophoretic forces generated by AC voltage and slanted electrode structures separate 4 & 6 micron particles, shown here near the device outlet.

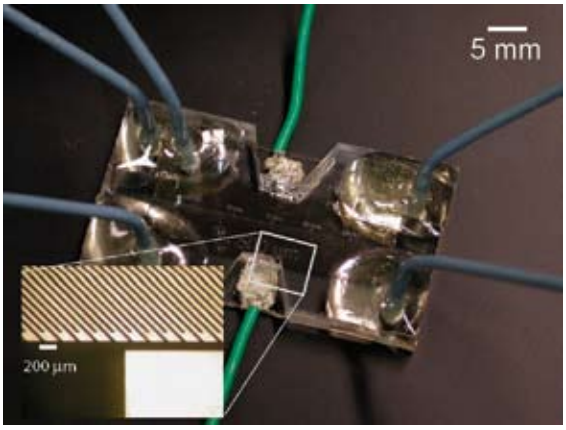

Figure 2: The packaged separator device is made of silicone rubber (PDMS), using soft-lithography techniques on interdigitated electrodes.

BioMEMS for Control of the Stem Cell Microenvironment

L. Kim, A. Rosenthal, J. Voldman
Sponsorship: NIH

The stem cell microenvironment is influenced by several factors, including: cell-media, cell-cell, and cell-matrix interactions. Although conventional cell-culture techniques have been successful, they offer poor control of the cellular microenvironment. To enhance traditional techniques, we have designed a microscale system to perform massively parallel cell culture on a chip.

To control cell-matrix and cell-cell interactions, we use dielectrophoresis (DEP), which uses non-uniform AC electric fields to position cells on or between electrodes [1]. We present a novel microfabricated DEP trap, designed to pattern large arrays of single cells. We have experimentally validated the trap using polystyrene beads, and have shown excellent agreement with our model predictions without the use of fitting parameters (Figure1A) [2]. In addition, we have demonstrated trapping with cells by using our traps to position murine fibroblasts in a 3x3 array (Figure 1B).

To control cell-media interactions, a 4x4 microfluidic parallel cell culture array has been designed and fabricated (Figure 2A). Each of the 16 culture chambers has microfluidic inlets and outlets that geometrically control the flow rate and type of media in each cell culture chamber. Reagent concentration is varied along one axis of the array, while the flow rates are varied along the other axis. The system is fabricated out of multilayer polydimethylsiloxane (PDMS) on glass and includes an on-chip diluter to generate a range of concentrations. We have cultured murine fibroblasts in a similar PDMS-on-glass environment at comparable flow rates (Figure 2B).

This microfabricated system will serve as an enabling technology that can be used to control the cellular microenvironment in precise and unique ways, allowing us to do novel cell biology experiments at the microscale.

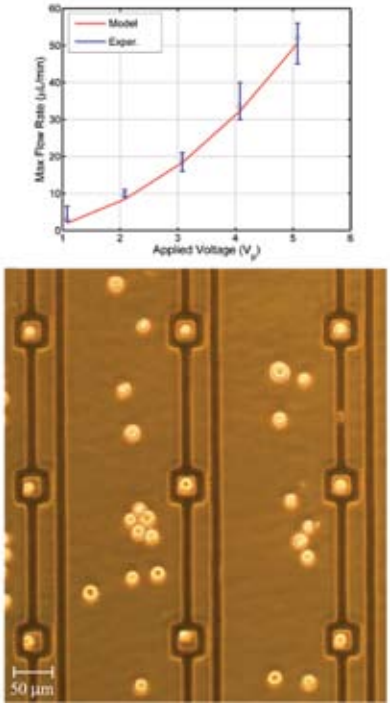

Figure 1: DEP trapping results. A. Maximum flow rate for trapped beads compared to our modeling predictions [2]. B. Trapping of murine fibroblasts in a 3x3 array.

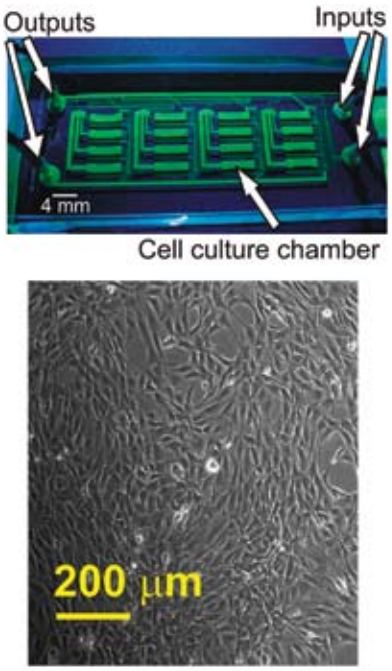

Figure 2: Parallel cell culture on chip. A. Microfluidic 4x4 array of cell culture chambers for creating a range of flow rate and reagent concentration conditions. B. 3T3 fibroblast perfusion culture on a comparable chip.

REFERENCES:

[1] Pohl, H.A., "Dielectrophoresis: The Behavior of Neutral Matter in Nonuniform Electric Fields," Cambridge University Press, New York, NY, 1978.
[2] Rosenthal, A. J. Voldman, "Dielectrophoretic Traps For Single-Particle Patterning," *Biophysical Journal*, vol. 88, 2193-2205, 2005.

Development of Microfluidic Channels for Endothelial Cell Chemotaxis

C.Y. Park, C.F. Dewey Jr
Sponsorship: NIH

Many cells have the ability to sense the direction of external chemical signals and respond by polarizing and migrating toward chemoattractants or away from chemorepellants. This phenomenon, called chemotaxis, has been shown to play an important role in embryogenesis, neuronal growth and regeneration, immune system response, angiogenesis, and other biological phenomena.[1] In addition, cell migration is also important for emerging technologies, such as tissue engineering and biochemical implants.[2] This simple behavior is apparently mediated by complex underlying diffusion and migration mechanisms that have been the focus of many studies and models. These mechanisms may be studied by various chemotactic assays. There have been several chemotaxis assay chambers developed in the past. The most widely used is the Dunn chamber.[3] The drawback of this chamber is that the cells that are squeezed between the cover glass and the chamber walls might release toxic enzymes and organells, and their effect, if any, on the viable neighborhood cells can not be easily quantified. Additionally, the linear gradient of chemokines lasts only 1 to 2 hours. The Whitesides group at Harvard designed a chemotaxis assay chamber using soft lithography.[4] They incorporated several serial mixers to generate multi-profile chemical gradient. This chamber can generate gradient with a simple linear or complex profile without limit in time, but it needs continuous flow to maintain gradient in the direction normal to gradient direction, which is not physiological.

A novel chemotaxis chamber using diffusion characteristics to develop a chemotactic gradient has been developed.[5] This chamber generates a stable and linear gradient along a narrow channel without limitation in time and unnecessary physical stresses. The chamber has 2 inlet ports for 2 kinds of solutions and 1 outlet. One of the input solutions is mixed with a growth factor, and the other solution is mixed with a fluorescent dye or microspheres to verify that there is no bypass flow through the cross channel that supports diffusion. There are two main channels through which the input solutions flow and one narrow cross channel that connects the two main channels, into which a growth factor diffuses from one main channel by diffusion.

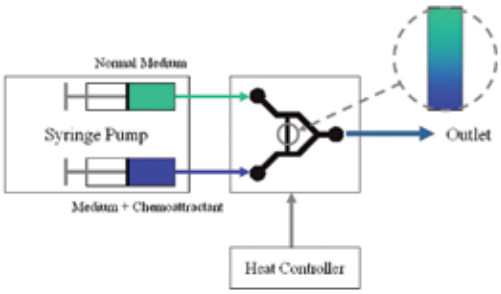

Figure 1: Diagram of experimental setup using syringe pump

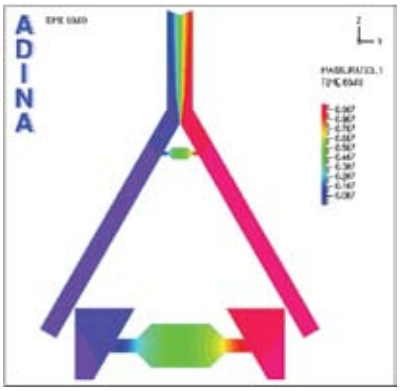

Figure 2: Numerical simulation of diffusion profile across the cross channel

REFERENCES:

[1] Jeon, N.L.,"Neutrophil Chemotaxis in Linear and Complex Gradients of Interleukin-8 Formed in a Microfabricated Device," *Nat. Biotechnol.*, vol. 20, pp. 826-830, August 2002.
[2] Muschler, G.F.,"Engineering Principles of Clinical Cell-Based Tissue Engineering," *J. Bone Joint Surg. Am.*, vol. 86-A, pp. 1541-1558, July 2004.
[3] Zicha, D.,"A New Direct-Viewing Chemotaxis Chamber," *J. Cell Sci.*, vol. 99, pp. 769-775, August 1991.
[4] Jeon, N.L.,"Generation of Solution and Surface Gradients Using Microfluidic Systems," *Langmuir*, vol. 16, pp. 8311-8316, October 2000.
[5] Shur, M.,"Microfabrication Methods for the Study of Chemotaxis," Thesis for master of science, Massachusetts Institute of Technology, MA, 2004.

A Microfabricated Sorting Cytometer

B. Taff, S. Desai, J. Voldman
Sponsorship: NSF Graduate Fellowship, NIH NCRR

This research involves the development of a microfabricated sorting cytometer for genetic screening of complex phenotypes in biological cells (Figure 1). Our technology combines the ability to observe and isolate individual mutant cells from a population under study. The cytometer merges the benefits of both microscopy and flow-assisted cell sorting (FACS) to offer unique capabilities on a single technology platform. Biologists will be able to use this platform to isolate cells based upon dynamic and/or intracellular responses, enabling new generations of genetic screens.

We are implementing this technology by developing an array of switchable traps that rely upon the phenomena known as dielectrophoresis (DEP) [1,2]. The DEP-enabled traps allow for capturing and holding cells in defined spatial locations, and subsequently, releasing (through row-column addressing) a desired subpopulation for further study. Using DEP, non-uniform electric fields induce dipoles in cells that, in turn, enable cellular manipulations. At present, no scalable DEP-based trap configuration exists that can robustly capture single cells and is also amenable to high-throughput microscopy. Such a platform requires performance characteristics that can only be met through quantitative modeling. We have undertaken much of the front-end work necessary for such a system and are continuing our efforts to realize this desired functionality.

To date, we have developed second-generation trap geometries implemented in 4x4 trap arrays (Figure 2) to compare our front-end simulation-based modeling with the performance of actual devices. We have designed, fabricated, and tested both n-DEP (cells held at electric-field minima) and p-DEP (cells positioned at electric-field maxima) based configurations [3]. Our first design and test iteration demonstrated partial functionality and first-order proof of concept, while offering insight for future design improvements. We are also investigating the effects of DEP trapping on cell health and the impact that it may have on our ability to assess specific complex phenotypic behaviors.

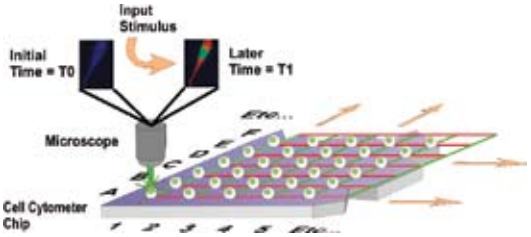

Figure 1: A sorting cytometer for screening complex phenotypes. The cytometer consists of a two-dimensional array of traps, each of which holds a single cell. After loading the traps, the array is optically interrogated, and cells with phenotypes of interest are sorted. In this case, the putative screen is for cells exhibiting altered kinase activation. Such a mutation would dynamically and spatially alter associated intracellular fluorescent responses.

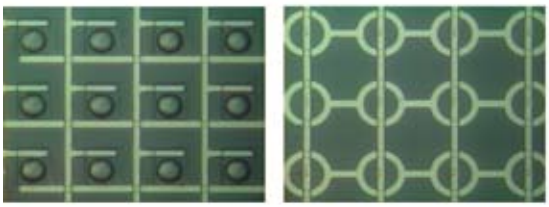

Figure 2: Fabricated traps. Left shows a Nomarski image of the n-DEP trap configuration in plan view, while right shows the ring-dot geometries of the p-DEP layout

REFERENCES:

[1] Pethig, R. "Dielectrophoresis: Using Inhomogeneous AC Electrical Fields to Separate and Manipulate Cells," *Critical Reviews In Biotechnology*, 1996. 16 (4), pp.331-348.

[2] Voldman, J., et al., "A Microfabrication-Based Dynamic Array Cytometer," *Analytical Chemistry*, 2002 74 (16), pp. 3984-3990.

[3} Taff, B., "Design and Fabrication of an Addressable MEMS-Based Dielectrophoretic Microparticle Array" S.M. Thesis, Massachusetts Institute of Technology, June 2004.

Vacuum Sealing Technologies for Microchemical Reactors

K. Cheung, K.F. Jensen, M.A. Schmidt
Sponsorship: ARO MURI

Current portable power sources may soon fail to meet the increasing demand for larger and larger power densities. To address this concern, our group has been developing MEMS power generation schemes that are focused around fuel cells and thermophotovoltaics. At the core of these systems is a suspended tube microreactor that has been designed to process chemical fuels [1]. Proper thermal management is critical for high reactor efficiency, but substantial heat loss is attributed to conduction and convection through air, as shown in Figure 1. A straightforward solution is to eliminate the heat loss pathways associated with air by utilizing a vacuum package. We are exploring a glass frit bonding method for vacuum sealing.

The leading cause of failure for a glass frit hermetic seal is large voids that are formed in the frit while bonding [2]. Progress has been made toward the optimization of presintering and bonding parameters to reduce or eliminate void formation. A vacuum package of 150 mTorr was obtained after optimization, but became leaky shortly after. An alternate packaging method using a two-step bond process, inspired by [3], was devised and developed. Recent experiments of the process, depicted in Figure 2, show that the initial box bond is capable of producing a hermetic seal. Enhancements through the incorporation of non-evaporable getters will be assessed once a vacuum package is achieved.

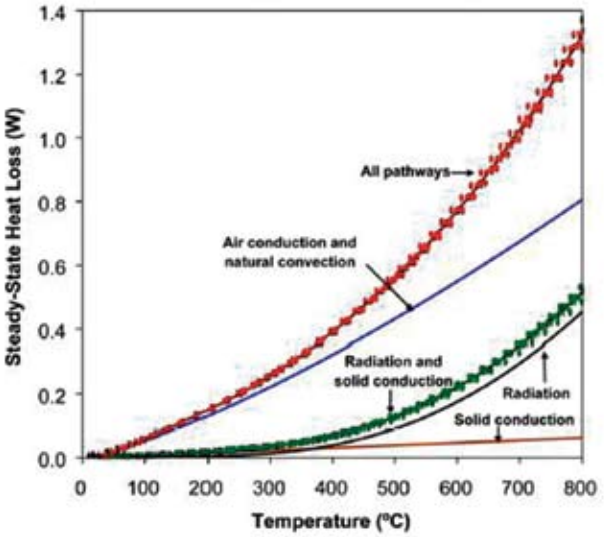

Figure 1: Experimental data for the heat loss of a suspended tube microreactor as a function of temperature in atmosphere (red) and in vacuum (green), plotted with the heat loss components through air, radiation, and solid conduction (blue, black, and orange respectively) [1]

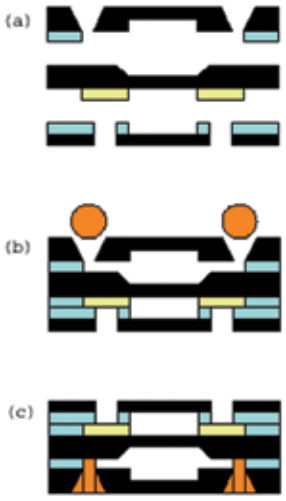

Figure 2: Basic concept of the two-step approach (a) initial bond in box furnace (blue = frit, black = silicon, yellow = metallization) (b) place solder/frit (orange) into pump-out hole, and (c) final seal-off

REFERENCES:

[1] L.R. Arana, "High-Temperature Microfluidic Systems for Thermally-Efficient Fuel Processing," ChemE PhD Thesis, MIT, 2003.
[2] J. Chou, "A Study of Vacuum Packaging Methods for a Microfabricated Suspended Tube Reactor," EECS MEng Thesis, MIT 2002.
[3] K.S.Ryu, S.J. Kwon, "Glass Packaging of the 0.7 Inch Diagonal FED Panel," SMDL Annual Report, 1998.

Scaled-out Multilayer Microreactors with Integrated Velocimetry Sensors

N. de Mas, A. Günther, T. Kraus, M.A. Schmidt, K.F. Jensen
Sponsorship: MIT Microchemical Systems Technology Center

Microreactors are a new class of continuous reactors, with feature sizes in the submillimeter range, which have emerged over the last decade and, for a number of applications, present capabilities exceeding those of their macroscale counterparts. Unlike conventional reactors, the throughput of microreactors is increased by "scale-out," i.e., operating a large number of identical reaction channels in parallel under equal reaction conditions. We have developed a scaled-out gas-liquid microreactor, built by silicon processing, which consists of three vertically stacked reaction layers, each containing twenty reaction channels. The reaction channels are operated in parallel from single gas and liquid feeds with a liquid volumetric throughput of 80 mL/h. Gas and liquid are introduced to the device through single inlet ports, flow vertically to each reaction layer, and are distributed horizontally to the reaction channels via individual auxiliary channels that provide a significantly larger pressure drop than that across a single reaction channel. These auxiliary channels eliminate cross-talk between reaction channels and ensure uniform flow distribution. The product mixture flows out of the device through a single outlet port. The design rationale of the scaled-out microreactor is illustrated in Figure 1. It is based on flow visualization studies and pressure drop measurements, obtained in a single channel, with the same channel geometry as the reaction channels of the scaled-out device (triangular cross section, channel width = 435 μm, channel length ~ 20 mm) [1]. A photograph of the scaled-out unit is presented in Figure 2. Flow visualization by pulsed-fluorescence microscopy across the top reaction layer reveals that the same flow regime is present in all channels. To further validate the reactor design and monitor flows during continuous operation, pairs of integrated multiphase flow regime sensors are integrated into the device [2]. Comparable slug velocities are measured across the reaction layers.

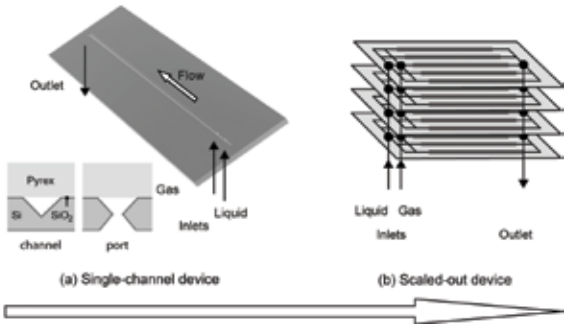

Figure 1: (a) Single-channel device (drawn to scale) formed in silicon and capped by Pyrex (Pyrex not shown). (b) Schematic of scaled-out device with several reaction layers and a large number of channels operating in parallel.

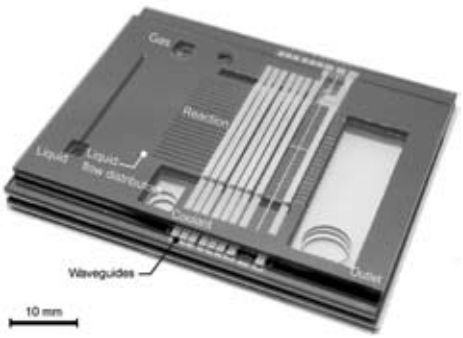

Figure 2: Scaled-out multilayer microreactor with three pairs of flow regime optical sensors, each integrated into the top and middle reaction layers. All channels are formed in silicon by nested potassium hydroxide etching and capped by silicon–Pyrex anodic bonding. The Pyrex layers are used as waveguides.

REFERENCES:

[1] de Mas, N., A. Günther, M.A. Schmidt, K.F. Jensen, "Microfabricated Multiphase Reactors for the Selective Direct Fluorination of Aromatics," *Ind. Eng. Chem. Res.*, vol. 42, pp. 698-710, 2003.

[2] Kraus, T., A. Günther, N. de Mas, M.A. Schmidt, K.F. Jensen, "An Integrated Multiphase Flow Sensor for Microchannels," *Exp. Fluids*, vol. 36, pp. 819-832, 2004.

[3] de Mas, N., A. Günther, T. Kraus, M.A. Schmidt, K.F. Jensen, "A Microfabricated Scaled-out Multilayer Gas-liquid Microreactor with Integrated Velocimetry Sensors," *Ind. Eng. Chem. Res.,* in press (2005).

Multiphase Transport Phenomena in Microfluidic Systems

A. Günther, S.A. Khan, B.H.K. Yen, M.A. Schmidt, K.F. Jensen
Sponsorship: MIT Microchemical Systems Technology Center

Microscale multiphase flows (gas-liquid and liquid-liquid) possess a number of unique properties and have applications ranging from use in microchemical synthesis systems to heat exchangers for IC chips and miniature fuel cells. Our work is focused on gas-liquid flows in microfabricated channels of rectangular or triangular cross section. We characterize the phase distribution and pressure drop of such flows and apply such information to a systematic design of gas-liquid microchemical reactors. The inherently transient nature of such multiphase flows provides a rich variety of flow regimes and dynamic flow properties. Characterization is done using pulsed-laser fluorescence microscopy and confocal microscopy (spinning disk and scanning), as well as by integrated flow regime sensors. Superficial gas and liquid velocities were varied between 0.01-100 m/s and 0.001-10 m/s, respectively.

Particular attention is given to segmented (slug or bubbly) flows in hydrophilic channels. Figure 1a illustrates the distribution of gas and liquid in the channel. Gas bubbles are surrounded by thin liquid films (thickness ~ 1μm) at channel walls and liquid menisci in the corners. Such flows create a recirculation in the liquid segments (Figure 1b) and can, therefore, be used to efficiently mix two miscible liquids on the microscale within a length of only a few tens of the microchannel width [1,2]. We demonstrate that the transient nature of gas-liquid flows can be used to significantly improve mixing of miscible liquids compared with existing methods. After mixing is accomplished–Figure 2 (bottom) provides an illustration for mixing of two differently colored streams–the gas can be removed from the mixed liquid phase in a capillary phase separator for arbitrary velocities and flow patterns [1]. In addition to providing mixing enhancement, segmented flows narrow the distribution of residence times of fluid elements in the liquid phase, as compared to single-phase flows [1]. A narrower residence time distribution is particularly essential for particle synthesis on a chip.

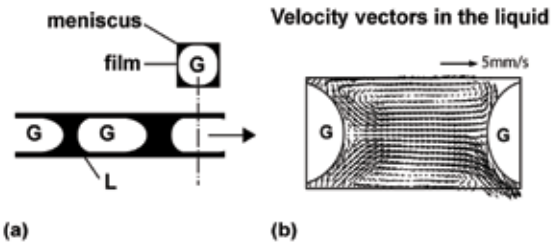

Figure 1: Segmented gas-liquid flow. (a) Gas-liquid phase distribution and (b) liquid phase velocity field obtained by microscopic particle image velocimetry (PIV). The mean velocity was subtracted from all velocity vectors to illustrate the recirculation motion in the liquid segment.

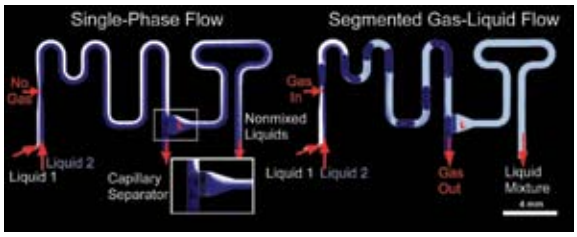

Figure 2: Illustration of enhanced liquid mixing in a microfluidic device by introducing a gas phase. Fluorescence micrographs show (a) the co-flowing liquid streams, L_1 and L_2, without the introduction of a gas phase, G, and (b) mixing in segmented gas-liquid flow and separation of the gas from the liquid in a single-stage microfluidic device.

REFERENCES:

[1] Günther, A., S.A. Khan, F. Trachsel, M. Thalmann, K.F. Jensen, "Transport and Reaction in Microscale Segmented Flow," *Lab on a Chip*, vol.4, pp. 278-286, 2004.

[2] Günther, A., M. Jhunjhunwala, M. Thalmann, M.A. Schmidt, K.F. Jensen, "Micromixing of Miscible Liquids in Segmented Gas-Liquid Flow," *Langmuir*, vol. 21, pp. 1547-1555, 2005.

[3] Trachsel, F., A. Güenther, S. Khan, K.F. Jensen, "Measurement of Residence Time Distribution in Microfluidic Systems," *Chem. Eng. Sci.,* vol. 60, pp. 5729 - 5737, 2005.

Integrated Microreactor System

H.R. Sahoo, E.R. Murphy, N. Imlinger, A. Günther, N. Zaborenko, K.F. Jensen
Sponsorship: Deshpande Center for Technological Innovation

Individual microreactors have been fabricated for many different chemical reactions, but the development of microreaction technology will require combining separation with microreactors to enable multi-step synthesis. The realization of integrated microchemical systems will revolutionize chemical research by providing flexible tools for rapid screening of reaction pathways, catalysts, and materials synthesis procedures, as well as, faster routes to new products and optimal operating conditions. Moreover, such microsystems for chemical production will require less space, use fewer resources, produce less waste, and offer safety advantages. The need for synthesizing sufficient quantities of chemicals for subsequent evaluation dictates that microchemical systems are operated as continuous systems. Such systems require fluid controls for adjusting reagent volumes and isolating defective units. The integration of sensors enables optimization of reaction conditions, as well as, the extraction of mechanistic and kinetic information.

We are developing integrated microchemical systems that have reactors, sensors, and detectors with optical fibers integrated on one platform. New approaches for connecting modular microfluidic components into flexible fluidic networks are being explored. Real-time control of reaction parameters, using online sensing of flowrate, temperature, and concentration, allows for precise attainment of reaction conditions and optimization over a wide range of temperatures and flow-rates. The multiple microreactors on the system can be used together to give higher throughputs or they can be used independently to carry out different reactions at the same time. Figure 1 shows a schematic of an integrated microreactor platform along with an early stage microreactor "circuit board" [1].

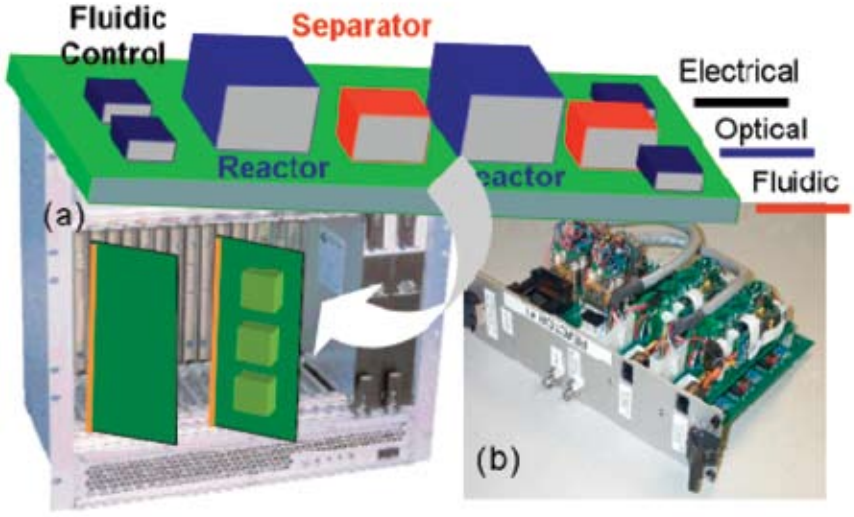

Figure 1: Schematic of an integrated microreactor platform along with an early stage microreactor "circuit board" [1]

REFERENCES:

[1] Quiram, D.J., PhD Chemical Engineering Thesis, Massachusetts Institute of Technology 2002.

Micro Gas Analyzer

L.F. Velásquez–García, L.Y. Chen, L. Lebel, A.I. Akinwande, M.A. Schmidt
Sponsorship: DARPA

The US Department of Defense is currently interested in developing the technology to sense, in real time, deployable agents used in chemical warfare. The Micro Gas Analyzer Project (MGA) is the result of this interest, and aims to develop a portable sensor of wide rage and robustness. Current state-of-the-art technology involves bulky equipment (not portable), high power consumption due to the use of thermionic sources and impact ionization mechanisms, high voltage (in the kilovolt range), and long processing times. Thus, the project has a number of key technological challenges, such as the enhancement of the state-of-the-art sensitivity and specificity capabilities, power consumption reduction, and portability, while keeping the processing time below two seconds.

The MGA is composed of an ionizer (a CNT field ionization array / CNT field emission array), a mass filter (a micro quadrupole mass spectrometer -μQMS), an ion counter/multiplier, an electrometer/mass detector, and a pumping system (passive – absorption pump/active – piezoelectric pump). A schematic of the MGA system is shown in Figure 1. The goal is to make low vacuum (in the millitor range), ionize the species inside the gas using the CNT arrays, filter them with the quadrupole, and then, sense them with the electrometer. The project team is composed of MIT (Ionizer, μQMS, μPump, Valves), University of Texas (Ionization, μPump), Cambridge University (Ion Counter), and Raytheon/CET (System Integration).

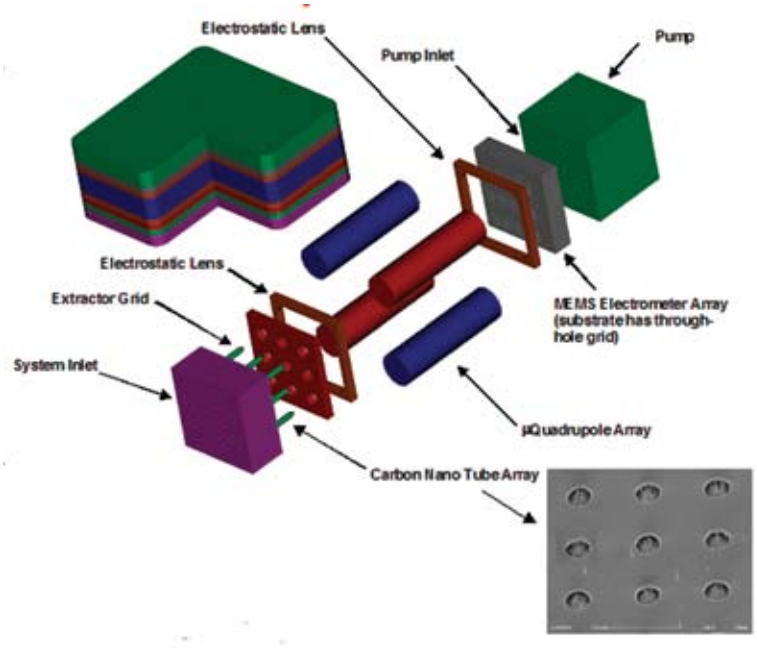

Figure 1: Schematic of the Micro Gas Analyzer

Micro Quadrupole Mass Spectrometer

L.F. Velásquez–García, L. Lebel, A.I. Akinwande
Sponsorship: DARPA

One of the subsystems of the Micro Gas Analyzer Project is a mass filter. The purpose of this filter is to select the kind of species that will be sensed downstream by the electrometer. A microfabricated quadrupole mass filter array is being developed for this purpose where a confining potential sorts the unwanted species (Figure 1). Both high sensitivity and high resolution are needed over a wide range of ion mass-to-charge ratios, from 20 to 200 atomic mass units, to achieve the versatility and resolution that are intended for the program. In order to achieve the high resolution and sensitivity, multiple micro-fabricated quadrupoles, each with specific geometrical parameters, are operated in conjunction with each other.

From a theoretical point of view, the Mathieu equations describe the dynamics of a particle inside the quadrupole. These equations predict a series of stability regions (Figure 2). Each stability region has its own strengths, such as: less power consumption, less operational voltage, or more sensitivity. For example, lower stability zones are used to improve ion transmission, whereas, higher stability zones are used to improve the selectivity of the filter. Therefore, we plan to explore the stability regions of the Mathieu equations to optimize our design. Two sets of variable voltage sources are needed for the mass filter to operate properly, with voltages ranging between 20 and 200 V, at frequencies of 250 and 500 MHz. We plan to try three different approaches to build the device: LIGA (a german acronym for the process that generates high aspect ratio metallic structures), rods assembled using micro-fabricated deflection springs [1], and rod mounts made with KOH [2]. The device has a cross-sectional area of 20 mm^2. The aperture of the individual quadrupoles ranges from 10 to 100 microns.

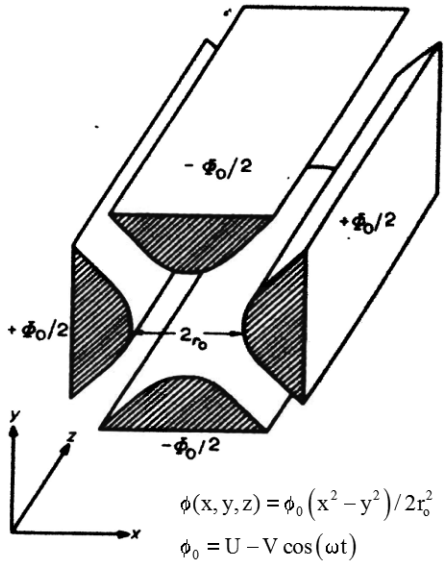

Figure 1: Electric potential inside a quadrupole. The electrodes of a quadruple are ideally hyperboloid surfaces, but quadruple implementations with circular rods perform satisfactorily.

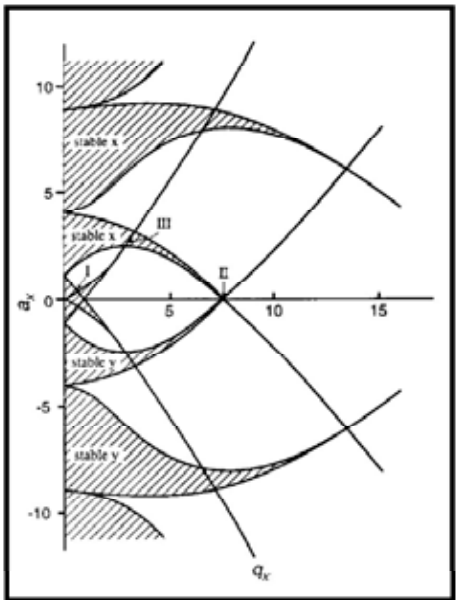

Figure 2: Stability regions of the Mathieu equations. The intersection of the x-stability and y-stability regions determines the possible parameters a and q where the trajectories of a charged particle traveling through a quadrupole is stable.

REFERENCES:

[1] Velásquez, L.F., "Precision Out-of-Plane Wafer Assembly Using DRIE-Patterned Spring Structures," submitted to *JMEMS*, 2004.

[2] Syms R.R.A., *et al.*, "Design of a Microengineered Electrostatic Quadrupole Lens," *IEEE Transcations on Electron Devices*, Vol. 45, No. 11, November 1998, p. 2304.

Design Tools for Bio-Micromachined Device Design

C. Coelho, N. Ngoc Son, D. Vasilyev, J. Han, J. Peraire, N. Hadjiconstantinou, J. Voldman, J. White
Sponsorship: SMA, NSF

Using micromachining for biological applications requires complicated structures such as mixers, separators, preconcentrators, filters, and pumps; and these elements are used to process biomolecules or biological cells. To accelerate the design of these complicated devices, new tools are needed that can efficiently simulate mixing and particle or cell motion in complicated three-dimensional flows. In addition, for microfluidic devices intended for use in molecular separation, the length scales are such that noncontinuum fluid effects must be considered, and therefore, hybrid approaches that combine molecular and continuum models must be developed. Finally, the wide variety of structures being developed implies that generating models for system-level simulation will require efficient simulation combined with automated model extraction [3]. Our recent work in addressing these problems includes: the development of efficient time integration techniques for cells in flow [1], techniques for accurately extracting diffusion constants from measurements [2], and efficient techniques for extracting models from detailed simulations [4].

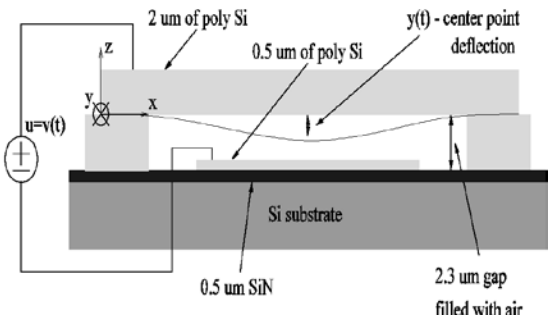

Figure 1: Micromachined clamped-clamped beam example. The input is the applied voltage, the output is the center deflection.

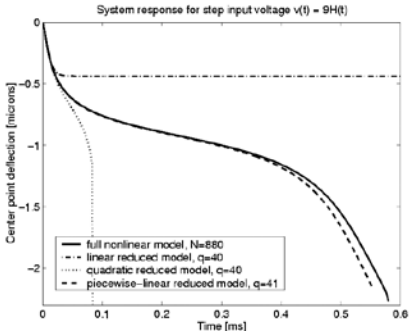

Figure 2: The Trajectory PWL extracted model (dashed line) agrees with the discretized PDE model of the device.

REFERENCES:

[1] Coelho, C.P., J.K. White, L.M. Silveira, "Dealing with Stiffness in Time-Domain Stokes Flow Simulation," *Proc. of Modeling and Simulation of Microsystems*, March, 2004.

[2] Coelho, C., S. Desai, D. Freeman, J. White, ``A Robust Approach for Estimating Diffusion Constants from Concentration Data in Microchannel Mixers," to appear in *Proc. of Modeling and Simulation of Microsystems*, May 2005.

[3] White, J., "CAD Challenges in BioMEMS Design," *Proceedings of the Design Automation Conference,* June, 2004, pp. 629-632.

[4] Vasilyev, D., M. Rewienski, J.K. White, "Perturbation Analysis of TBR Model Reduction in Application to Trajectory-Piecewise Linear Algorithm for MEMS Structures," *Proc. of Modeling and Simulation of Microsystems,* March, 2004.

Microfabricated Solid-Oxide Fuel Cell Systems

B.A. Wilhite, J. Hertz, D. Quinn, J. Cui, K.T. Deshpande, H. Tuller, B. Wardle, J. Ying, M.A. Schmidt, K.F. Jensen
Sponsorship: ARO MURI

Solid-Oxide Fuel Cells (SOFCs), employing ceramic electrolytes, are a promising alternative to low-temperature PEM (proton-exchange membrane) fuel cells for portable power applications. The use of an oxygen-ion conducting electrolyte, operating at high temperatures, offers the potential for internal reforming of a variety of fuels, with improved tolerance to competitively adsorbing species at the anode (e.g. CO); thus, removing the need for pretreatment stages for conversion of hydrocarbon fuel to high-purity hydrogen. However, the appropriate thermal management of this high-temperature fuel cell system is required to achieve an energy-efficient device.

A chip-scale micromembrane architecture has been developed for thermally efficient thin-film applications[1] and has been successfully demonstrated for hydrogen separation via ultra-thin palladium films. Resistive heaters placed directly upon a thermally-isolated membrane allow for rapid heating and cooling of the supported thin film at a minimum expenditure of energy. In addition, the mechanical strength provided by the micromembrane support allows the use of sub-micron films for significant improvement in ion permeability. For these reasons, the micromembrane architecture has been investigated for SOFC development. The extension of this technology is achieved, utilizing a silicon-nitride girder-grid support system to mechanically reinforce the solid-oxide thin films (Figures 1 and 2).

Efforts include: the determination of optimal free-standing fuel cell stack dimensions, integration of individual stacks into a reinforced membrane structure, design of current collectors, and electrical performance tests of fabricated devices. Stability tests of free-standing membranes of varying length scales and aspect ratios are performed for a variety of fuel cell stacks and individual stack layers, with results compared to mechanical models of layered free-standing films. The resulting information is incorporated into the design of a silicon-nitride reinforced free-standing membrane architecture. Lastly, microdevice testing stations allow for performance studies of prototype microdevices.

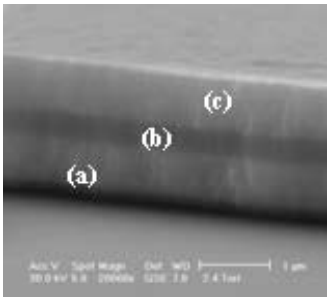

Figure 1: Cross section of ESEM image of solid-oxide fuel cell stack, comprised of (a) co-sputtered Pt-8%Y_2O_3-Zr_2O_3(YSZ) anode, (b) reactively sputtered YSZ electrolyte, and (c) co-sputtered Pt-YSZ cathode.

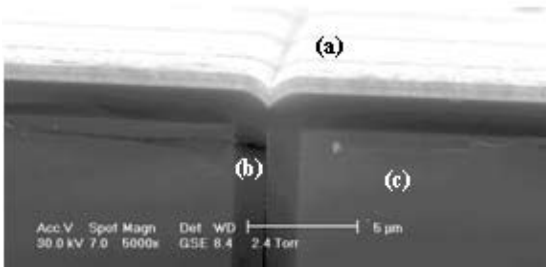

Figure 2: Cross section of ESEM image of (a) solid-oxide fuel cell stack, supported on (b) silicon nitride girders, formed in single-crystal silicon (c). Subsequent removal of silicon substrate produces free-standing fuel cell membrane.

REFERENCES:

[1] Wilhite, B.A., M.A. Schmidt, K.F. Jensen, "Palladium-Based Micromembranes for Hydrogen Separation: Device Performance and Chemical Stability," *Ind. Eng. Chem. Res.,* vol. 43, pp. 7083-7091, 2004.

Catalytic Micromembrane Devices for Portable High-Purity Hydrogen Generation

K. Deshpande, B.A. Wilhite, S.E. Weiss, J.Y. Ying, M.A. Schmidt, K.F. Jensen
Sponsorship: ARO MURI

The development of portable-power systems employing hydrogen-driven fuel cells continues to garner significant interest in the scientific community, with applications ranging from the automotive industry to personal electronics. While progress has been made in the development of efficient hydrogen-storage devices, it is still preferable for portable-power systems to operate from a liquid fuel with a high energy density (e.g., methanol, ammonia). This necessitates the integration of a hydrogen generator capable of converting stored fuels to hydrogen to drive the fuel cell.

Previous research has focused upon the development of novel catalysts and autothermal microreactor designs for efficient conversion of liquid fuels (e.g. methanol, ammonia) into hydrogen for use by a polymer-electrolyte fuel cell [1]. Additionally, micromembrane devices (Figure 1) have been developed for purification of the resulting hydrogen stream to remove impurities (e.g. CO) that adversely affect fuel cell performance [2]. Our current research aims to integrate (i) catalyst design, (ii) autothermal microreformer design, and (iii) micromembrane technology to realize microscale chemical systems capable of producing high-purity hydrogen for fuel cell operation. By combining microfabrication techniques for generation of micromembrane devices with wet-chemical deposition methods for a variety of catalysts, multiple membrane reactor applications for hydrogen generation can be realized, taking full advantage of superior mass transport and film permeabilities achievable at the microscale. Results obtained for $LaNi_{0.95}Co_{0.05}O_3$ perovskite catalysts integrated with 23 wt% Ag-Pd membranes (Figure 2) demonstrate promising high-purity hydrogen yields at low methanol feed compositions, and demonstrate the applicability of catalytic membrane reactors effected at the microscale for efficient production of high-purity hydrogen. Resulting microdevices are directly applicable as part of an integrated portable-power system.

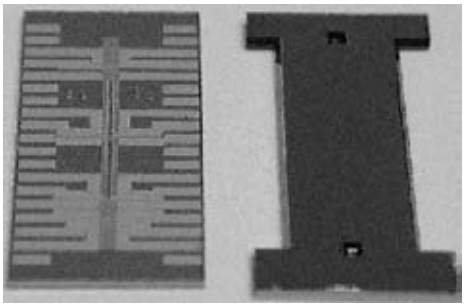

Figure 1: The micromembrane device, which provides a robust platform for the study of multiple thin-film applications.

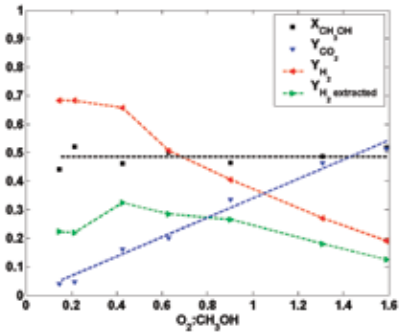

Figure 2: Results for 23 wt% Ag-Pd film (0.2 μm) coated with 1.7 mg of $LaNi_{0.95}Co_{0.05}O_3$ / Al_2O_3 catalyst for varying O_2:CH_3OH feed ratio at 400°C.

REFERENCES:

[1] Arana, L.R., S.B. Schaevitz, A.J. Franz, M.A. Schmidt, K.F. Jensen, "A Microfabricated Suspended-Tube Chemical Reactor for Thermally Efficient Fuel Processing," *Journal of Microelectromechical Systems.*, vol. 12, pp. 600-612, 2003.

[2] Wilhite, B.A., M.A. Schmidt, K.F. Jensen, "Palladium-Based Micromembranes for Hydrogen Separation: Device Performance and Chemical Stability," *Ind. Eng. Chem. Res.*, vol. 43, pp. 7083-7091, 2004.

Thermal Management in Devices for Portable Hydrogen Generation

B. Blackwell, M.A. Schmidt, K.F. Jensen
Sponsorship: ARO MURI

As power requirements of portable electronic devices continue to increase, the development of an efficient portable power generation scheme has remained an active research area. Specifically, hydrogen-driven fuel cells have received significant attention. This work focuses on microreaction technology for the conversion of fuel to electrical power. Emphasis has been placed on developing microreactors for high-purity hydrogen production. Critical issues in realizing high-efficiency devices capable of operating at high temperatures have been addressed: specifically, thermal management, the integration of materials with different thermophysical properties, and the development of improved packaging and fabrication techniques.

A microfabricated suspended-tube reactor (Figures 1, 2) has been developed for efficient combustion and reforming of chemical fuels.[1] The reactor, designed specifically to thermally isolate the high-temperature reaction zone from the ambient, consists of thin-walled U-shaped silicon nitride tubes formed by deep reactive ion etching (DRIE) and subsequent nitride deposition via chemical vapor deposition (CVD). Thin-film platinum resistors are integrated into the reactor for heating and temperature sensing. Detailed thermal characterization demonstrates reactor operation up to 900ºC and quantifies heat losses. Additionally, this high-temperature microcombustor is applicable for thermophotovoltaic generation.

A new fabrication scheme for the suspended-tube reactor incorporates wet potassium hydroxide (KOH) etching, an economical and time-saving alternative to DRIE]. In this design, pre-fabricated thin-walled glass tubes replace the silicon nitride tubing to provide inlet and outlet conduits. The thermal conductivity of the resulting tubes is 50% lower than that of silicon nitride. Hence, this technique allows for the incorporation of robust tubing, while maintaining thermal efficiency.

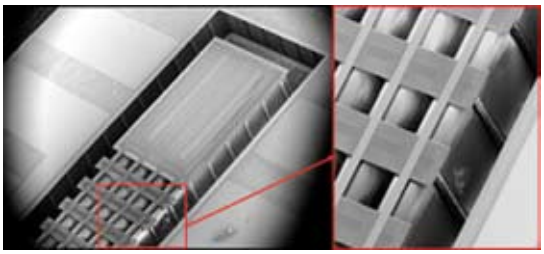

Figure 1: SEM of suspended tube reactor showing four SiN_x tubes, the suspended Si reaction zone with integrated Ti/Pt heater, and temperature-sensing resistor, and Si slabs thermally linking the four tubes.

Figure 2: Photograph of suspended tube reactor during hydrogen combustion. The suspended Si reaction zone glows (~800C) whereas the surrounding area remains cool.

REFERENCES:

[1] Arana, L.R., S.B. Schaevitz, A.J. Franz, M.A. Schmidt, K.F. Jensen, "A Microfabricated Suspended-Tube Chemical Reactor for Thermally-Efficient Fuel Processing," *J. MicroElectromechanical Systems,* vol. 12, pp. 600-612, 2003.

Materials and Structures for a MEMS Solid Oxide Fuel Cell

D. Quinn, P. Capozzoli, N. Wicks, N. Yamamoto, S.M. Spearing, B.L. Wardle, in collaboration with B.A. Wilhite, J. Hertz, K. Deshpande, K.F. Jensen, H. Tuller
Sponsorship: ARO MURI

Microfabricated solid oxide fuel cells are currently being investigated for portable power applications requiring high energy densities [1, 2]. Reducing the thickness of fuel cell stack materials improves the electrochemical performance versus traditional devices. This motivation for thinner structures, combined with significant temperature excursions during processing and operation (~600 – 1000 °C), presents the thermomechanical stability of such membranes as a major challenge. A buckled electrolyte/SiN thin film is shown in Figure 1. The prediction and management of structural stability (buckling) and failure require accurate knowledge of many parameters including: thermomechanical properties, residual stress, and fracture strength.

Our group has characterized the residual stress and microstructure of the electrolyte layer of the fuel cell stack. Residual stress in sputter-deposited yttria stabilized zirconia (YSZ) thin films (5nm – 1000nm thickness), as a function of deposition pressure and substrate temperature, has been completed [3]. The results indicate variations in intrinsic stress from ~0.5GPa compressive to mildly tensile (~50 MPa) (Figure 2). Changes in microstructure are subsequently characterized using X-ray diffraction of as-deposited and annealed films and correlated with relevant mechanisms/models of residual stress evolution. Frameworks for using such residual stress data to design mechanically stable membranes for μSOFC devices have also been developed.

Current research areas include: continued microstructural and residual stress characterization under thermal cycling, elastic/fracture properties characterization, design and fabrication of thermomechanically stable fuel cell stacks, exploration of proton conducting solid oxide thin films for lower-temperature operation, investigation of the mechanical properties of anode and cathode materials, and nonlinear modeling of film postbuckling and failure.

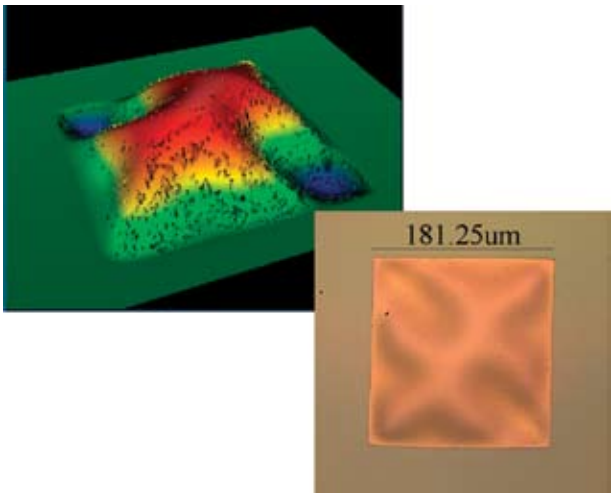

Figure 1: Postbuckled YSZ/SiN membranes on Si. Displacement contour plot (top) and top-down view (bottom).

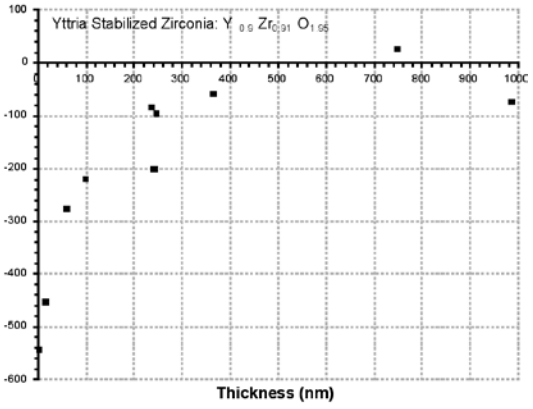

Figure 2: YSZ electrolyte film stress as a function of film thickness.

REFERENCES:

[1] Baertsch, C.D., K.F. Jensen, J.L. Hertz, H.L. Tuller, V. T. S. Vengallatore, S.M. Spearing, M. A. Schmidt, "Fabrication and Structural Characterization of Self-Supporting Electrolyte Membranes For A µSOFC," *Journal of Matls Research*, vol. 19, pp. 2604-2615, 2004.

[2] Srikar, V.T., K. Turner, T.-Z. A. Ie, and S.M. Spearing, "Structural Design Considerations for Micromachined Solid Oxide Fuel Cells," *Journal of Power Sources,* vol. 125, pp. 62-69, 2004.

[3] Quinn, D., S.M. Spearing, B.L. Wardle, "Residual Stress and Microstructural Evolution in Thin Film Materials for a Micro Solid Oxide Fuel Cell (SOFC," *Materials Research Society (MRS) Annual Fall Conference*, Boston, MA, December 2004.

Microfabricated Proton-Conducting Solid Oxide Fuel Cell System

K.T. Deshpande, J. Cui, B.A. Wilhite, J. Ying, M.A. Schmidt, K.F. Jensen
Sponsorship: ARO MURI

Owing to their high efficiency and energy density, miniaturized fuel cells are an attractive alternative to batteries in the mW-W power generation market for portable consumer and military electronic devices [cf. 1-3]. Hydrogen is being actively considered as a fuel for power generation. It can be supplied either by storage devices or its in-situ generation using reformers. However, safety and reliability issues persist with current storage choices, such as zeolites and carbon nanotubes [4]. For these reasons, fuel cells based on direct fuel reforming are advantageous. The processes typically involve either high temperature reforming of fuel to hydrogen combined with a low temperature Proton exchange membrane (PEM) fuel cell, which implies significant thermal loss. Alternatively, fuel reforming can be combined with solid oxide fuel cells capable of operating at high temperatures.

Typical components of a solid oxide fuel cell include electrodes and an electrolyte. Typically ZrO_2, CeO_2, and $LaGaO_3$, which are oxide ion conductors are used as separator materials [5]. However, one of the disadvantages of these materials is the need for operation at high temperatures (~700°C). These operating temperatures, in turn, lead to associated problems of materials compatibility and low tolerance with respect to variations in operating conditions. As an alternative, proton conducting solid oxide membranes, typically alkaline earth metal substituted perovskites, such as $BaCeO_3$, $SrCeO_3$, and $BaZrO_3$, exhibit high protonic conductivity even at 400°C [6].

In the current research, we explore the possibility of fabricating a fuel cell using these low temperature electrolytes. Previous work on Pd-based membranes on MEMS-supported membranes indicates that hydrogen yields up to 93% can be achieved for methanol using $LaNiCoO_3$ anode catalyst at 475°C. We plan to extend this concept further to prepare a complete fuel cell assembly and test its performance.

REFERENCES:

[1] Baertsch, C.D., K.F. Jensen, J.L. Hertz, H.L. Tuller, S.T. Vengallatore, S.M. Spearing, M.A. Schmidt, " Fabrication and Structural Characterization of Self-Supporting Electrolyte Membranes for a Micro Solid-Oxide Fuel Cell," *J. Mater. Res.*, vol. 19, pp 2604-2614, 2004.

[2] Morse, J.D., A.F. Jankowski, R.T. Graff, J.P. Hayes, " Novel Proton Exchange Membrane Thin-Film Fuel Cell for Microscale Energy Conversion," *J. Vac. Sci. Technol. A.*, vol. 18, pp 2003-2005, 2000.

[3] Fleig, J., H.L. Tuller, J. Maier, "Electrodes and Electrolytes in Micro-SOFCs: A Discussion of Geometrical Constraints," *Solid State Ionics*, vol. 174, pp 261-270, 2004.

[4] Wilhite, B.A., M.A. Schmidt, K.F. Jensen, "Palladium-Based Micromembranes for Hydrogen Separation: Device Performance and Chemical Stability," *Ind. Eng. Chem. Res.*, vol. 43, pp 7083-7091, 2004.

[5] Kreuer, K.D. " Proton-Conducting Oxides," *Annu. Rev. Mater. Res.*, vol.33, pp 333-359, 2003.

[6] Haile, S.M. " Fuel Cell Materials and Components," *Acta Materialia*, vol. 51, pp 5981-6000, 2003.

Thermophotovoltaic (TPV) MEMS Power Generators

O.M. Nielsen, K.F. Jensen, M.A. Schmidt
Sponsorship: ARO MURI

Batteries have, for a number of years, not kept up with the fast development of microelectronic devices. The low energy densities of even the most advanced batteries are a major hindrance to lengthy use of portable consumer electronics, such as laptops, and of military equipment that most soldiers carry with them today. Furthermore, disposing of batteries constitutes an environmental problem. Hydrocarbon fuels exhibit very high energy densities in comparison, and micro-generators converting the stored chemical energy into electrical power at even modest levels, are, therefore, interesting alternatives in many applications. This project focuses on building thermophotovoltaic (TPV) micro-generators, in which photocells convert radiation from a combustion-heated emitter, into electrical power. TPV is an indirect conversion scheme that goes through the thermal domain and therefore, does not exhibit very high efficiencies (10-15% max). However, because of its simple structure and because the combustor and photocell fabrication processes do not need to be integrated, the system is simpler to micro-fabricate than other generator types (e.g. thermoelectric systems and fuel cells). It is also a mechanically passive device that is virtually noiseless and less subject to wear than engines and turbines. In this TPV generator, a catalytic combustor, the suspended micro-reactor (Figure 1) is heated by combustion of propane and air, and the radiation emitted is converted into electrical energy by low-bandgap (GaSb) photocells (Figure 2). Net power production of up to 1 mW has been achieved [1], constituting a promising proof of concept. Work is underway to build a new micro-reactor more suited for the needs of TPV than the original design.

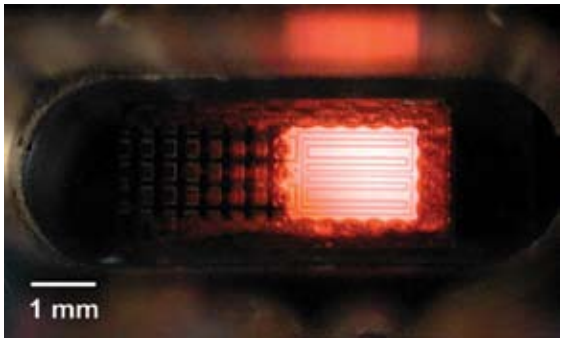

Figure 1: Suspended micro-reactor for fuel processing and TPV energy conversion.

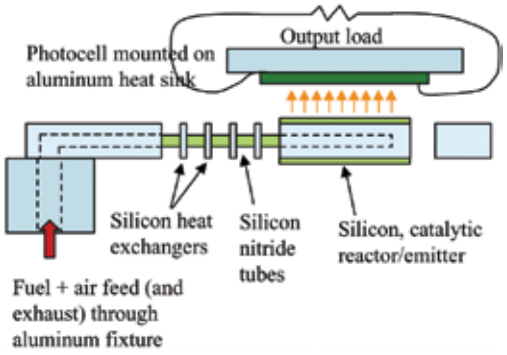

Figure 2: Suspended micro-reactor with photocell in TPV micro-generator configuration.

REFERENCES:

[1] Nielsen, O.M. *et al.*, "A Thermophotovoltaic Micro-Generator for Portable Power Applications," Transducers '03, Boston, MA, USA, June 2003, pp.714-17.

Thermoelectric Energy Conversion: Materials and Devices

H. Lee, Q. Hao, R.G. Yang, X. Chen, G. Chen, in collaboration with M.S. Dresselhaus (MIT), Z.F. Ren (Boston College), J.-P. Fleurial (JPL)
Sponsorship : NASA, Intel, Nanolab SBIR

Thermoelectric devices based on Peltier effect and Seebeck effect use electrons as a working fluid for energy conversion. These solid-state energy conversion devices have important applications in refrigeration and electrical power generation. Our work follows two directions: nanostructured materials and microdevices.

The efficiency of thermoelectric devices is characterized by the nondimensional thermoelectric figure of merit $ZT = S^2\sigma T / k$, where S is the Seebeck coefficient, σ the electrical conductivity, and k the thermal conductivity of their constituent materials, and T is the average device temperature. Identifying materials with a large ZT has been challenging because of the interdependency of those three properties. With both quantum size effects on electrons and classical size effects on phonons, nanostructures provide an alternative way to engineer thermoelectric properties.[1,2] Our current effort is focused on designing, synthesizing, and characterizing nanostructures in bulk form that can be produced for mass applications. Figure 1 illustrates ballistic phonon transport in a unit cell of a nanocomposite, which leads to low thermal conductivity.[3] We are also working on fabricating micro thermoelectric devices, first using thin film devices such as SiGe alloy and Si-Ge superlattices,[4] and more recently on thick films to reduce parasitic heat losses.[5] In addition, we are also exploring novel microdevice configurations that can improve energy conversion efficiency, by utilizing the hot electron concepts.[6,7]

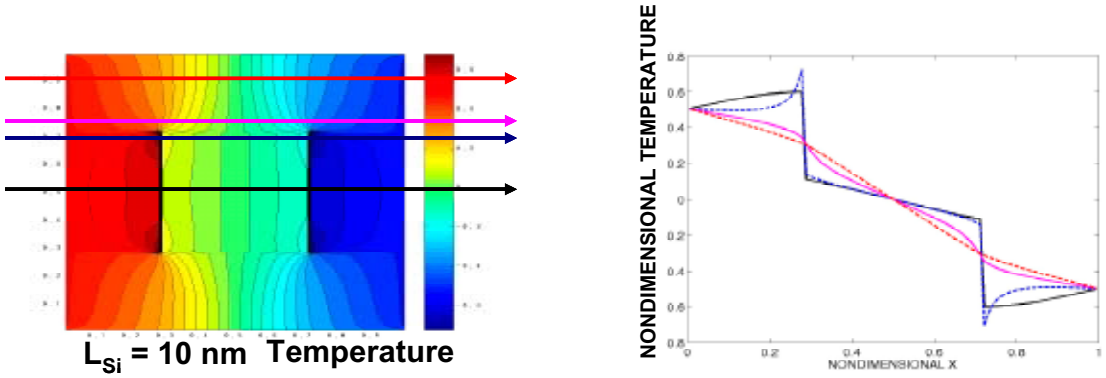

Figure 1: Temperature distributions in one unit cell of two-dimensional periodic structure made of Si nanowires embedded in a Ge matrix.

REFERENCES:

[1] Hicks, L.D., M.S. Dresselhaus, "Effect of Quantum-Well Structures on the Thermoelectric Figure of Merit," *Physical Review B*, Vol. 47, pp. 12727-12731, 1993.
[2] Chen, G., "Phonon Transport in Low-Dimensional Structures," *Semiconductors and Semimetals*, Vol. 71, pp. 203-259, 2001.
[3] Yang, R.G., G. Chen, "Thermal Conductivity Modeling of Periodic Two-Dimensional Nanocomposites," *Physical Review B*, Vol. 69, 195316, 1-10, 2004.
[4] Jacquot, A., W.L. Liu, G. Chen, J.-P. Fleurial, A. Dauscher, and B. Lenoir, "Fabrication and Modeling of a Thermoelectric Micro-Generator," Proceedings of International Conference on Thermoelectrics, ICT'02, pp.561-564, Long Beach, CA, August 24-29, 2002.
[5] Yang, R.G., G. Chen, J.P. Fleurial, G.J. Snyder, and J.-P. Fleurial, "Multistage Thermoelectric Micro Coolers," *Journal of Applied Physics*, Vol. 95, pp. 8226-8232, June 2004.
[6] Yang, R.G., A. Narayanaswamy, and G. Chen, "Surface-Plasmon Coupled Nonequilibrium Thermoelectric Refrigerators and Power Generators," *Journal of Theoretical and Computational Nanoscience*, in press.
[7] Chen, G., "Potential Step Amplified Thermal-Electric Energy Converters," *Journal of Applied Physics*, in press.

Far-Field Spectral Control and Near-Field Enhancement of Thermal Radiation Transfer for Energy Conversion Applications

A. Narayanaswamy, L. Hu, Z. Chen, G. Chen, in collaboration with J.D. Joannopoulos
Sponsorship: ONR, MURI (through UC Berkeley)

The performance of thermophotovoltaic (TPV) energy conversion systems is greatly affected by the radiation characteristics of the thermal emitter. Ideally, one would want a selective emitter with high emissivity above the band gap and low emissivity below the band gap. Various approaches have been proposed to fabricate effective selective emitters with 2D or 3D photonic crystals, which involve considerable intricate microfabrication. Instead, we have proposed a simpler-to-fabricate 1D structure that exhibits many of the features of its 2D and 3D counterparts [1]. The key has been to use ultra thin metallic films arranged as a periodic multilayer stack with a suitable non-absorbing dielectric material in-between. Figure 1 shows the numerical computation of the total hemispherical emissivity of two such structures as a function of wavelength.

In addition to improving the selective emission of thermal radiators, we are also exploring near field effects to improve the energy density and efficiency of thermal-to-electric energy conversion devices. Electromagnetic surface waves, like surface phonon polaritons or surface plasmon polaritons, can increase the energy transfer by two or three orders of magnitude compared to the near-field enhancement between materials that do not support such surface waves. Our work has shown that such enhancements in thermal radiative transfer can not only increase the power density and efficiency of TPV devices [2] but can also contribute to the improvement of thermoelectric devices [3]. We are also exploring a new TPV device structure involving interdigitized hot-and-cold fingers with increased surface area, built-in photon recycling, and potentially built-in spectral control [4]. Experimental work involving microfabrication and device testing is in progress.

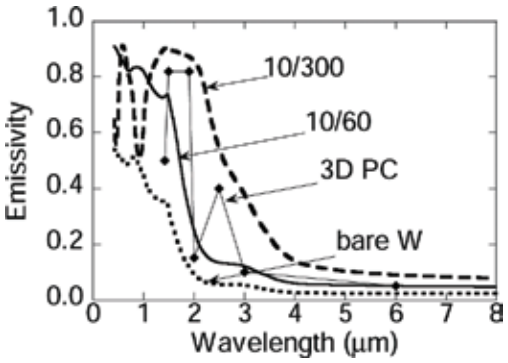

Figure 1: Spectral emissivity of 1D photonic crystal. The curves with legend 10/60 (10/300) refers to 10 nm of tungsten and 60 nm (300 nm) of alumina in each unit cell. For comparison, the emissivity of the 3D photonic crystal1 and bare tungsten are shown.

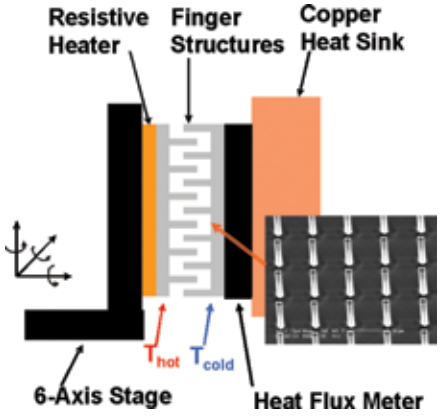

Figure 2: Illustration of the testing rig for the interdigitized thermophotovoltaic device structure. The SEM picture shows one set of figure structures.

REFERENCES:

[1] Narayanaswamy, A., G. Chen, "Thermal Emission Control with One-dimensional Metallodielectric Photonic Crystals," *Phys. Rev. B*, vol. 70, pp. 125101, September 2004.

[2] Narayanaswamy, A., G. Chen, "Surface Modes for Near-field Thermophotovoltaics," *Appl. Phys. Lett.*, vol. 82, pp. 3544-3546, May 2003.

[3] Yang, R., A. Narayanaswamy, G. Chen, "Surface plasmon Coupled Nonequilibrium Thermoelectric Refrigerators and Power Generators," *Journal of Computational and Theoretical Nanoscience*, in press.

[4] Narayanaswamy, A., G. Chen, "Thermal Radiation in 1D Photonic Crystals," *Journal of Quantitative Spectroscopy and Radiative Transfer*, vol. 93, pp. 175-183, June 2005.

Development of a High Power Density Microscale Turbocharger

N. Savoulides, L. Ho, H. Li, M. Schmidt, C.J. Teo, L. Wang, S. Jacobson, A. Epstein
Sponsorship: ARL

A microscale turbocharger has been fabricated as part of a program to develop a microfabricated gas turbine generator to serve as a battery replacement with seven times the energy density of today's best batteries. The turbocharger will evolve into the gas turbine generator with minimal fabrication process changes. The turbocharger lacks an electric generator, and its turbine and compressor flow paths are independent; otherwise, the two devices are virtually identical. The turbocharger is a test vehicle for developing fabrication processes and turbomachinery/bearing technology. The turbocharger is formed by fusion bonding six silicon wafers. The hatched structure in Figure 1 is the rotor, which is free to spin within the device on hydrostatic gas bearings. The turbocharger has a design rotation rate of 1.2 million rpm and a design compressor pressure ratio of 2.2.

Journal bearing dimensional control is a key challenge: 15 +/- 0.75 μm in width and 330 +/- 5 μm in depth. The bearing width tolerance, which is half that of previous devices in this program, is achieved through refinements in the etch recipe as well as modifications to the masking material profile. The masking material must be carefully controlled because of its finite etch rate and the effects of sidewall-passivation-layer erosion from ions deflected by the resist slope. The journal bearing specification is met on device wafers with a yield of more than 60%. Another challenge for this device is obtaining a rotor blade height uniformity of about 1%, which is critical for low levels of imbalance in the rotor.

A turbocharger has been operated to a rotation rate of 480,000 rpm, which is equivalent to a tip speed of 200 m/s (450 miles per hour). Figure 2 shows the measured compressor pressure ratio for two runs of the same device with different throttle settings. The compressor achieved a pressure ratio of 1.21 with a flow rate of 0.14 g/s at its top speed. The measured pressure and flow characteristics are consistent with the design models for this device.

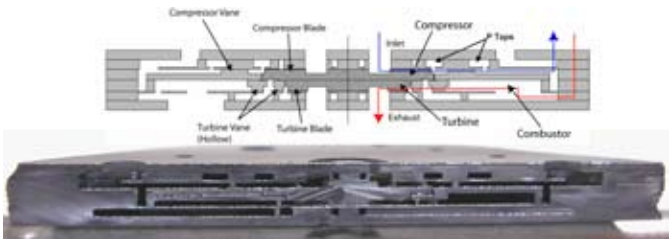

Figure 1: Turbocharger Cross Section: Compressor Rotor Diameter = 8.2 mm, Turbine Rotor Diameter = 6 mm, Die Size = 23 x 23 x 2.9 mm.

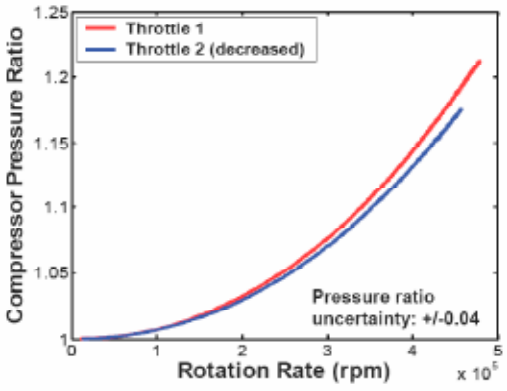

Figure 2: Turbocharger high speed operation.

REFERENCES:

[1] Li, H., N. Savoulides, L. Ho, S.A. Jacobson, R. Khanna, C.-J. Teo, L. Wang, D. Ward, A.H. Epstein, M.A. Schmidt, "Fabrication of a High Speed Microscale Turbocharger," presented at Hilton Head 2004: A Solid-State Sensor, Actuator and Microsystems Workshop, Hilton Head Island, SC, 2004.

[2] Jacobson, S.A., S. Das, N. Savoulides, J.L. Steyn, J. Lang, H.Q. Li, C. Livermore, M.A. Schmidt, C.J. Teo, S.D. Umans, A.H. Epstein, D.P. Arnold, J.-W. Park, I. Zana, M.G. Allen, "Progress Toward a Microfabricated Gas Turbine Generator for Soldier Portable Power Applications," presented at the US Army Science Conference 2004, Orlando, FL, 2004.

A MEMS Electroquasistatic Induction Turbine-Generator

J. Lodewyk Steyn, J.H. Lang, C. Livermore
Sponsorship: DARPA, ARL

Presented here is a microfabricated electroquasistatic (EQS) induction turbine-generator that has generated net electric power. A maximum power output of 192 μW was achieved under driven excitation. We believe that this is the first report of electric power generation by an EQS induction machine of any scale in the open literature. This work forms part of a program at MIT to fabricate a MEMS-scale gas turbine-generator system. Such a system converts the enthalpy of combustion of a hydrocarbon fuel into electric power. For even modest efficiency levels of the gas turbine engine cycle (10-15%), a small gas turbine would be a portable energy source with higher energy density than the best batteries available [1]. In MIT's device, this small engine provides the shaft power needed to drive a small electric generator. Although magnetic machines are preferred at large scales, EQS machines become attractive at small scales, primarily because very small airgaps between the rotor and stator allow higher breakdown electric fields of approximately 10^8 V/m. The generator comprises five silicon layers (Figure 1) fusion bonded together at 700°C. The stator is a platinum electrode structure formed on a thick 20 μm recessed oxide island. The rotor is a thin film of lightly doped polysilicon also residing on an oxide island, which is 10 μm thick. We also present a generalized state-space model for an EQS induction machine that takes into account the machine and its external electronics and parasitics. This model correlates well with measured performance, and was used to find the optimal drive conditions for all driven experiments. Figure 2 shows the results of an experiment under driven excitation. In this particular experiment, 108 μW was generated at 245krpm. Good correlation with the models is observed. In other experiments, self-excited operation was attained. In this case, the generator self-resonates and generates power without the use of any external drive electronics [3].

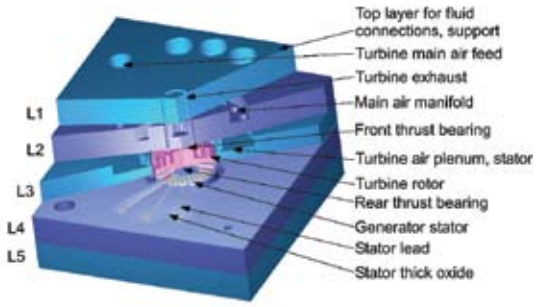

Figure 1: 3D section view of the turbine generator device. The device consists of five silicon layers fusion bonded together. The electric generator is located in Layers 3 and 4 and consists of a stator with 786 electrodes. Every 6th electrode is connected to form a 6-phase machine with 6 sets of 131 electrodes.

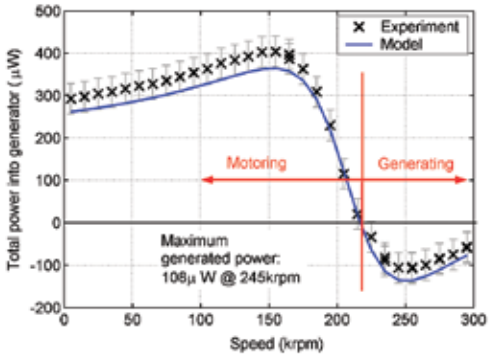

Figure 2: Power output vs. speed for the generator device. This figure shows the sum of the power from all 6 phases of the generator. This curve is typical of an induction machine. As indicated, when the rotating speed is slower than the synchronous speed, it acts as a motor. Beyond the synchronous speed, it acts as a generator.

REFERENCES:

[1] Epstein, A.H., "Millimeter Scale MEMS Gas Turbine Engines", Proc. of ASME Turbo Expo 2003, Power for Land, Sea, and Air, June 16-19, 2003, Atlanta, Georgia, USA.

[2] Livermore, C. *et al.*, "A High Power MEMS Electric Induction Motor," *J. MEMS*, v30, No. 3, June 2004.

[3] Steyn, J.L. *et al.*, "Generating Electric Power with a MEMS ElectroQuasiStatic Induction Turbine-Generator," Proc. of the IEEE MEMS2005 conference, 30 Jan - 3 Feb 2005, Miami Beach, Florida, USA.

Multi-Watt Electric Power from a Microfabricated Permanent-Magnet Generator

S. Das, D.P. Arnold, I. Zana, J.W. Park, J.H. Lang, M.G. Allen
Sponsorship: DARPA, ARL

Presented here are the design, fabrication, and characterization of three-phase permanent magnet (PM) machines that convert 2.3 W of mechanical power and deliver 1.1 W of DC electrical power to a resistive load at a rotational speed of 120,000 rpm. Such microgenerators are an important system-level component of compact MEMS-based power sources, such as combustion-driven or air-driven microengines [1].

The generators are three-phase, eight-pole, synchronous machines, each consisting of a surface-wound stator (Figure 1) and a multi-poled PM rotor (Figure 2(a)). The stator uses three Cu windings that are dielectrically isolated from a 1-mm thick NiFeMo (Supermalloy) substrate by a 3 µm spin-on-glass layer and/or 5 µm polyimide layer. The coils were fabricated using a two-layer electroplating process [2]. They were measured to be 80-120 µm thick and 50-550 µm in width. The microfabricated coils, with their small inter-conductor gaps and variable width geometry, are the key for enabling high power output. The rotor contains an annular SmCo PM and a ferromagnetic FeCoV (Hiperco50) backiron, each 9.525 mm OD, 3.175 mm ID, and 500 µm thick. The SmCo PM and FeCoV backirons were, then, assembled and glued into a pre-formed PMMA cup, which was fit onto a 1.6 mm shaft (Figure 2(b)).

For characterization, a high-speed spinning rotor test stand, incorporating an air-turbine driven spindle, was constructed. The stator was positioned under the rotor using an xyz-micropositioner, which permitted precise (± 5 µm) adjustment of the air gap. A three-phase step-up transformer (1:6 turn ratio) and Schottky diode bridge were used to rectify the output voltage for DC power generation across a load resistor. The power data for the 2-turn/pole machine shows a quadratic dependence on speed for a fixed load (Figure 2(c)) and typical power transfer dependence for varying loads (Figure 2(d)), with a maximum demonstrated power of 1.1 W (2.9 MW/m^3 power density).

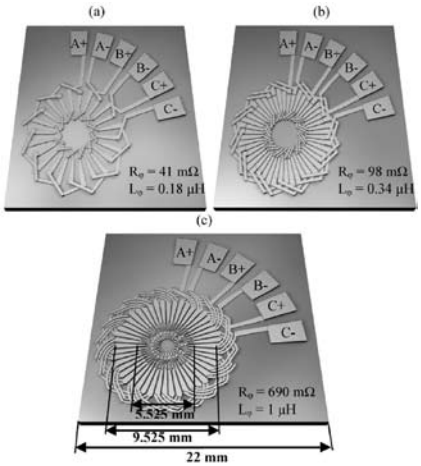

Figure 1: Conceptual drawings of (a) 1-turn/pole, (b) 2-turn/pole, and (c) 4-turn/pole surface wound stators. The measured phase resistance and inductance are indicated for each type.

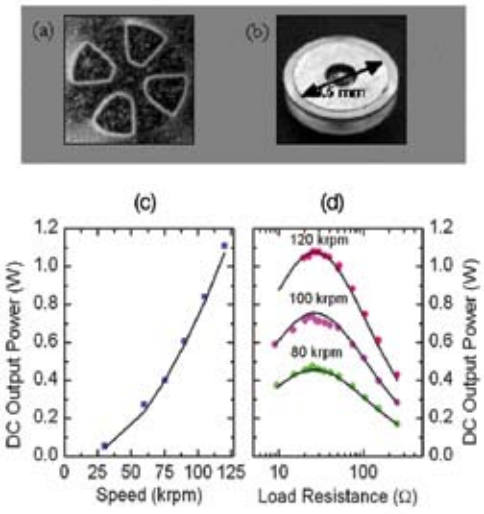

Figure 2: (a) Magnetic pole pattern using magnetic viewing paper and (b) 500 µm thick PM rotor and backiron mounted onto shaft. DC output power across load resistor for 2-turn stator at 100 µm air gap vs. (c) rotational speed for 30 Ω load and (d) load resistance at 80, 100, and 120 krpm.

REFERENCES:

[1] Jacobson, S.A., A.H. Epstein, "An Informal Survey of Power MEMS," *ISMME*, 2003.

[2] Park, J.W., M.G. Allen, "Ultralow-Profile Micromachined Power Inductors with Highly Laminated Ni/Fe Cores: Application to Low-Megahertz DC-DC Converter," *IEEE Trans. Mag.*, vol. 39, pp. 3184-3186, 2003.

High-speed Micro-scale Gas Bearings for Power MEMS

L.X. Liu, C.J. Teo, F. Ehrich, L. Ho, H. Li, S. Jacobson, Z.S. Spakovszky
Sponsorship: ARL

The high-speed micro hydrostatic gas journal bearings used in the high-power density MIT micro-engines are of very low aspect ratio, with a bearing length-to-diameter ratio of less than 0.1, and are running at surface speeds of order 500 m/s. These ultra-short high-speed bearings exhibit whirl instability limits and dynamic behavior very different from conventional hydrostatic gas bearings. The design space for stable high-speed operation is confined to a narrow region and involves singular behavior [1]. The narrow design space together with the limits on achievable fabrication tolerance that can be achieved in the silicon chip manufacturing technology severely affects journal bearing operability and limits the maximum achievable speed of micro turbomachinery. The hydrostatic gas thrust bearings are located near the center of the rotor, and play a vital role in providing axial support for the rotor. The thrust bearing geometry is designed to provide the required axial and tilting stiffness, and ensures stable thrust bearing operation at high-speed [2].

Our technical approach involves the combination of numerical simulations, experiment, and simple, first principles based on modeling of the gas journal and gas thrust bearing flow fields and the rotordynamics. A novel variation of the axial-flow hydrostatic micro-gas journal bearing concept is introduced that yields anisotropy in bearing stiffness [3]. By departing from axial symmetry and introducing biaxial symmetry in hydrostatic stiffness (Figure 1), the bearing's top speed is increased and fabrication tolerance requirements are substantially relieved, making more feasible extended stable high-speed bearing operation. An existing analytical hydrostatic gas journal bearing model [4] is extended and modified to guide the journal bearing design with stiffness anisotropy. In addition, a novel micro gas thrust bearing model is established. High-speed experimental spin tests were conducted in several micro-bearing test devices, and all 11 test devices were spun to high-speed, achieving an average rotor speed of 720,000 rpm. Figure 2 depicts a typical test run, and shows good agreement between the newly established bearing theory and the measurements.

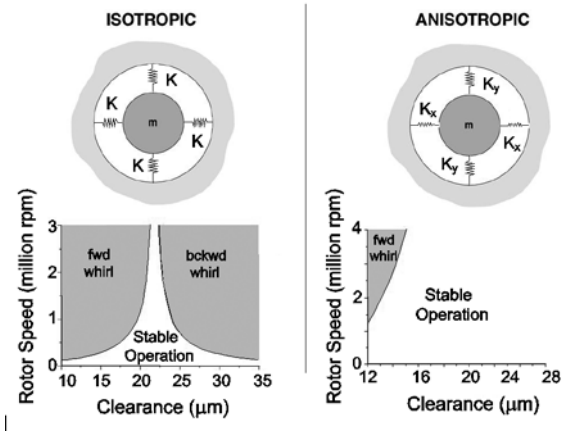

Figure 1: Elimination of singular behavior of whirl instability limit and extension of geometric design space for stable high-speed operation using bearing stiffness anisotropy in ultra-short hydrostatic micro-gas journal bearings [3].

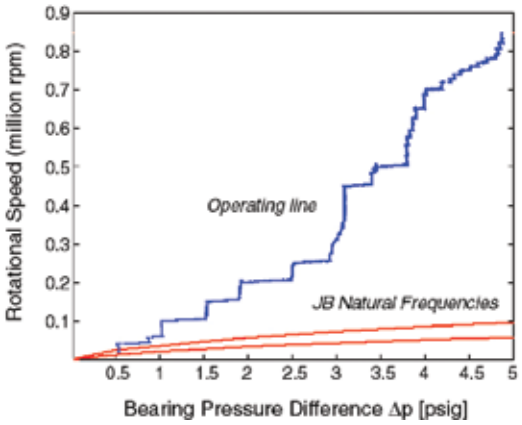

Figure 2: Experimental demonstration of operating schedule for a micro-electrostatic turbine-generator which achieved a maximum speed of 850,000 rpm (93% design speed) [2].

REFERENCES:

[1] Spakovszky, Z.S., L.X. Liu, "Scaling Laws for Ultra-Short Hydrostatic Gas Journal Bearings," 19th Biennial Conference on Mechanical Vibration and Noise, *ASME DETC*, 2003. Accepted for publication in *ASME Journal of Vibration and Acoustics*.

[2] Teo, C.J, Z.S. Spakovszky, "Modeling and Experimental Investigation of Micro-Hydrostatic Gas Thrust Bearings for Micro-Turbomachines," paper GT-2005-68222, to be presented at ASME IGTI Turbo Expo, Reno, NV, June 2005.

[3] Liu, L.X., Z.S. Spakovszky, "Effects of Bearing Stiffness Anisotropy on Hydrostatic Micro Gas Journal Bearing Dynamic Behavior," paper GT-2005-68199, to be presented at ASME IGTI Turbo Expo, Reno, NV, June 2005.

Piezoelectric Micro Power Generator (PMPG): A MEMS-based Portable Power Device

W. Choi, R. Xia, J. Brewer, S.-G. Kim
Sponsorship: NSF, Korean Institute of Machinery and Materials

A thin-film lead zirconate titanate $Pb(Zr,Ti)O_3$ (PZT), MEMS energy-harvesting device is developed to enable autonomous sensors for in-service integrity monitoring of large scale infrastructures. It is designed to resonate at specific frequencies from external vibrational energy sources, thereby creating electrical energy via the piezoelectric effect. The corresponding energy density of the 1st prototype is 0.74 mW-h/cm^2, which compares favorably to lithium ion batteries. [1] Current efforts are focused on improving the harvest efficiency of the device. A geometric optimization of the cantilever design is made to suppress damping contributions from air and structural dissipation. Additionally, a serpentine cantilever has been designed to achieve a low resonant frequency structure. The dominant contributors to low Q factor at the MEMS scale are air damping and internal structure damping. For 2nd generation PMPG [3], we have optimized the cantilever shape to minimize the damping effect. Analytical modeling of PMPG predicts a 77% decrease of the damping coefficient of a new PMPG device.[4] This reduced damping coefficient enables 4.3 times larger resonance amplitude of the cantilever structure and 10.2 times larger maximum strain of the PZT layer. As a result, power density increases up to 1850% of the old PMPG device at the same footprint. We also designed a serpentine cantilever to achieve a low resonant frequency structure, as well as, a low damping effect, when it resonates. (Figure 2)

PMPG has been integrated with a commercial wireless sensor, Telos, to simulate a self-powered RF temperature monitoring system. Such devices will play an important role in remote sensing network applications. Telos on average consumes 350μJ for 38 ms per measurement. Since PMPG offers limited power, a storage capacitor and a power management module are implemented to power the node at discrete time intervals.

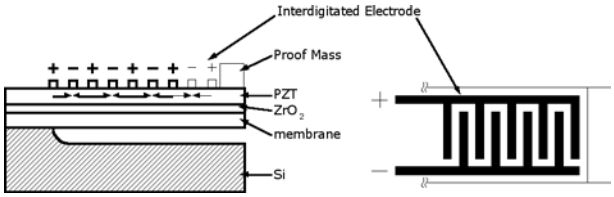

Figure 1: Schematic of 1st generation PMPG

Figure 2: Design of a low resonant frequency serpentine structure

REFERENCES:

[1] Jeon, Y. R. Sood, J.H. Jeong, S.G. Kim, "Piezoelectric Micro Power Generator for Energy Harvesting," *Sensors and Actuators A: Physical,* 2005, in press.

[2] Xu, B., Y. Ye, L.E. Cross, J. Bernstein, R. Miller, "Dielectric Hysteresis from Transverse Electric Fields in Lead Zirconate Titanate Thin Films," *Applied Physics Letters*, vol. 74, pp. 3549-3551, 1999.

[3] Hosaka, H., K. Itao, S. Kuroda, "Evaluation of Energy Dissipation Mechanisms in Vibrational Microactuators," MEMS '94, Proc, IEEE Workshop, 25-28 January 1994

[4] Wardle, B. L., N.E. DuToit, S.G. Kim, "Design Considerations for MEMS-Scale Piezoelectric Viaration Energy Harvesters," *Intergrated Ferroelectric,* accepted for publication

MEMS Piezoelectric Ambient Vibration Energy Harvesting for Wireless Sensors

N.E. duToit, A. Mracek, B.L. Wardle, in collaboration with W. Choi, S.-G. Kim
Sponsorship: CMI

Recently, numerous investigations have focused on the development of distributed wireless sensor node networks. Power for such devices can be supplied through harvesting ambient environmental energy, available as: mechanical vibrations, fluid motion, radiation, or temperature gradients [1]. Envisioned applications include: building climate control and warehouse inventory control, identification and personalization (RFID tags), structural health monitoring (aerospace and automotive sectors), agricultural automation, and homeland security.

Advances in "low-power" DSP's (Digital Signal Processors) and trends in VLSI (Very Large Scale Integration) system design have reduced power requirements to 10's-100's of μW. These power levels are obtainable through piezoelectric harvesting of ambient vibration energy. Current work focuses on harvesting this energy with MEMS resonant structures. Coupled electromechanical models have been developed to predict the electrical and mechanical performance obtainable from known low-level ambient vibration sources. These models have been validated by comparison to prior published results [2] and tests on a MEMS device. A non-optimized, uni-morph beam prototype (Figure 1) has been designed and modeled to produce 30 μW/cm^3 [3]. A MEMS fabrication process for a prototype device is presented based on past work at MIT [4]. Dual optimal frequencies with equal peak powers and unequal voltages and currents are characteristic of the response of such coupled devices when operated at optimal load resistances (Figure 2).

Future work will explore active sources, such as: aircraft skin for harvestable power, fabrication and testing of the uni-morph prototype beam, and optimization of device configurations for aerospace structural health monitoring applications. System integration and development, including modeling the power electronics, will be included.

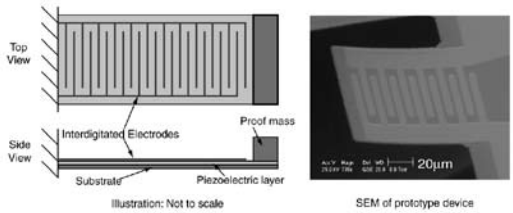

Figure 1: Illustration of MPVEH unimorph configuration (left) and SEM of a prototype device (right).

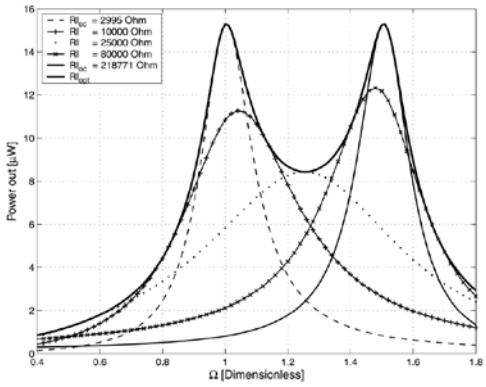

Figure 2: Power vs. normalized frequency with varying electrical load resistance [3].

REFERENCES:

[1] Roundy, S., P.K. Wright, J.M. Rabaey, Energy Scavenging For Wireless Sensor Networks With Special Focus On Vibrations, Kluwer Academic Publishers, 2004.

[2] Sodano, H.A., G. Park, D.J. Inman, "Estimation of Electric Charge Output for Piezoelectric Energy Harvesting," *Strain* 40 (2), pp. 49-58. (2004).

[3] duToit, N., B.L. Wardle, S-G. Kim, "Design Considerations for MEMS-Scale Piezoelectric Mechanical Vibration Energy Harvesters," accepted to *Integrated Ferroelectrics*, 2005. Presented at the XIII International Materials Research Congress, August 2004.

[4] Sood, R., Y.B. Jeon, J-H. Joeng, S-G. Kim, "Piezoelectric Micro Power Generator for Energy Harvesting," Proc. of Solid-State Sensor and Actuator Workshop, Hilton Head, South Carolina, June, 2004.

Micro Chemical Oxygen Iodine Lasers (MicroCOIL)

T. Hill, B. Wilhite, L.F. Velásquez-García, H. Li, A. Epstein, K. Jensen, C. Livermore
Sponsorship: DARPA, MDA

Conventional Chemical Oxygen Iodine Lasers (COIL) offer several important advantages for materials processing, including short wavelength (1.3 μm) and high power. However, COIL lasers typically employ large hardware and use reactants relatively inefficiently. This project is creating an alternative approach called microCOIL. In microCOIL, most conventional components are replaced by a set of silicon MEMS devices that offer smaller hardware and improved performance. A complete microCOIL system includes: microchemical reactors, microscale supersonic nozzles, and micropumps. System models incorporating all of these elements predict significant performance advantages in the microCOIL approach [1].

Initial work is focused on the design, microfabrication, and demonstration of a chip-scale Singlet Oxygen Generator (SOG): a microchemical reactor that generates singlet delta oxygen gas to power the laser. Given the extensive experience with microchemical reactors over the last decade [2-4], it is not surprising that a microSOG would offer a significant performance gain over large scale systems. The gain stems from basic physical scaling; surface to volume ratio increases as the size scale is reduced, which enables improved mixing and heat transfer. The SOG chip being demonstrated in this project employs an array of microstructured packed-bed reaction channels interspersed with microscale cooling channels for efficient heat removal. Figure 1 shows a schematic top view of the microSOG chip, including inlets and outlets for the reactant and product flows, and packed-bed reaction channels. Figure 2 shows a schematic diagram of stacked microSOG chips, micronozzles, and micropumps forming a complete microCOIL system.

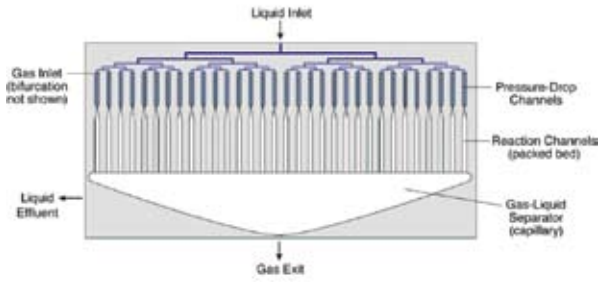

Figure 1: Schematic diagram of microSOG chip, showing reactant inlets, packed-bed reaction channels, and flow outlets.

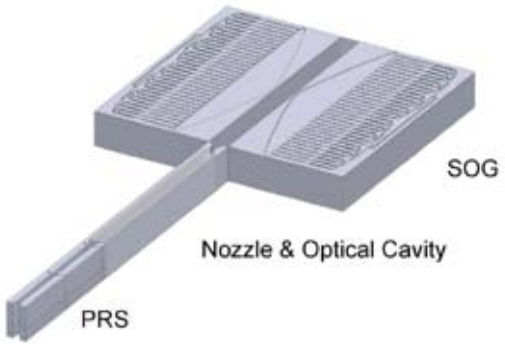

Figure 2: Schematic diagram showing multiple SOG chips, micronozzles, and micropumps (PRS) combined to form a microCOIL system.

REFERENCES:

[1] Wilhite, B.A., C. Livermore, Y. Gong, A.H. Epstein, K.F. Jensen, "Design of a MEMS-Based Microchemical Oxygen-Iodine Laser(mCOIL) System," *IEEE J. of Quantum Electronics* 40, 1041-1055 (2004).

[2] de Mas, N., R.J. Jackman, M.A. Schmidt, K.F. Jensen, "Microchemical Systems for Direct Fluorination of Aromatics," *Proc. Fifth International Conference on Microreaction Technology* (IMRET5) (2001).

[3] Ajmera, S.K., C. Delattre, M.A. Schmidt, K.F. Jensen, "Microfabricated Cross-Flow Chemical Reactor for Catalyst Testing," *Sensors and Actuators B (Chemical)*, B82, 297-306 (2002).

[4] Losey, M.W., M.A. Schmidt, K.F. Jensen, "Microfabricated Multiphase Packed-Bed Reactors: Characterization of Mass Transfer and Reactions," *Ind. Eng. Chem. Res.*, 40, 2555-2562 (2001).

Linear Array of Electrospray Micro Thrusters

L.F. Velásquez–García, A.I. Akinwande, M. Martínez–Sánchez
Sponsorship: AFOSR

Electrospray thrusters are electrostatic accelerators of charged particles that use the electrohydrodynamic effect known as *Taylor cone* as propulsive effect [1]. These particles could be charged droplets, solvated ions, or a mix of the two. Since the new advances in electrospray technology that occurred in the late 1980s [2], the field of electrospray propulsion has experienced a renaissance, specifically aiming to provide efficient high-tunable precision low-thrust engines for micro-satellites and high accuracy astrophysics missions [3]. The MIT Space Propulsion Laboratory and the Microsystems Technology Laboratories are currently pursuing the development of a micro-fabricated electrospray emitter array for space propulsion. The project is developing in parallel two radically different concepts, a pressure-fed engine, and a surface tension-fed engine. This abstract reports the design, fabrication, and experimental characterization of a micro-fabricated, internally-fed linear array of electrospray emitters (Figure 1). This work demonstrates the feasibility of high clustering of electrospray emitters. The linear array is composed of 1 plenum, 12 manifolds, and 240 emitters. The emitters are sharpened to reduce the startup voltage. The electrodes are micro-fabricated with conductive paths made of tungsten and electrical insulation provided by vacuum gaps 350 µm wide and 10 µm thick PECVD silicon oxide. The electrodes are hand-assembled to the engine using a novel technique that relies on clusters of micro-fabricated springs [4]. This assembly scheme allows us to have two independent process flows for the electrodes and the engine hydraulics. The emitter-to-emitter separation is 130 μm, and the hydraulic diameter is 12 µm. The length of each channel is 15 mm. The engine uses highly doped formamide as propellant, with electrical conductivity in the 0.3 – 3.0 S/m range. The electrospray array operates in the single Taylor cone droplet emission regime, and it requires about 2000 V to become activated. The engine implements the concept of hydraulic and electrodynamic flow rate matching to achieve electrical control. Current versus flowrate characteristics of the engine are in agreement with a well-established reduced order model (Figure 2). Experimental data, demonstrating the low divergence of electrospray emitter arrays operated in the single Taylor cone, is in qualitative agreement with a reduced order mode that assumes the absence of a thermalized tail in the plume.

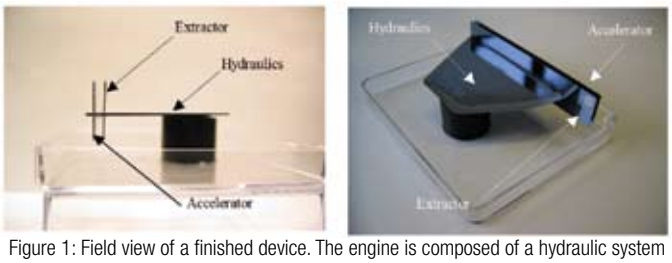

Figure 1: Field view of a finished device. The engine is composed of a hydraulic system and two electrodes, involving a total of four substrates. The electrodes are assembled to the hydraulic system using microprecision mesoscale silicon springs.

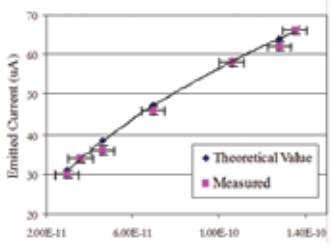

Figure 2: Experimental flowrate vs. emitted current using formamide with an electrical conductivity equal to 0.612 Si/m

REFERENCES:

[1] Taylor, G.I., "Disintegration Of Water Drops In An Electric Field," *Proc. R. Soc. London*, A 280, no. 1382, pp. 383-397, 1964.
[2] Fenn, J., "Colloid Ionization For Mass Spectrometry Of Large Biomolecules," *Science*, 246, pp. 64-71, 1989.
[3] Mueller, J., "Thruster Options For Microspacecraft: A Review And Evaluation Of Existing Hardware And Emerging Technologies," *AIAA*, 77-3058, Seattle, WA, 1997.
[4] Velásquez, L.F., "Precision Out-Of-Plane Wafer Assembly Using DRIE-Patterned Spring Structures," submitted to *JMEMS*, 2004.

Planar Array of Electrospray Micro Thrusters

L.F. Velásquez–García. A.I. Akinwande, M. Martínez–Sánchez
Sponsorship: AFOSR, NASA

Electrospray thrusters are electrostatic accelerators of charged particles using the electrohydrodynamic effect known as *Taylor cone* to generate thrust [1]. These particles could be charged droplets, solvated ions, or a mix of the two. Since the new advances in electrospray technology that occurred in the late 1980s [2], the field of electrospray propulsion has experienced a renaissance, specifically aiming to provide efficient high-tunable precision low-thrust engines for micro-satellites and high accuracy astrophysics missions [3]. The MIT's Space Propulsion Laboratory and the Microsystems Technology Laboratories are currently pursuing the development of a micro-fabricated electrospray emitter array for space propulsion applications. The project is developing, in parallel, two radically different concepts, a pressure-fed engine and a surface tension-fed engine. This abstract reports the design, fabrication, and experimental characterization of a hybrid macro-fabricated/micro-fabricated, externally fed planar array of micro-fabricated electrospray emitters with macro-fabricated electrodes (Figure 1). An externally-fed engine has a number of advantages compared to the other implementations reported in the literature. For example, the engine lacks a static pressure difference between the plenum and the emitters; therefore, there cannot be propellant emission unless it is electrically activated. In this sense, the planar array is less vulnerable to unplanned propellant emission compared to pressure fed schemes. Additionally, clogging is not an issue in this engine because the propellant is not doped, and the flow channels are open. The planar array uses the ionic liquid EMI-BF_4 as a propellant. The ionic liquid EMI-BF_4 has a very low vapor pressure, making it suitable to be used in an open architecture engine. The array is composed of a set of spikes, i.e., emitters, coming out from a propellant pool. There are two configurations for the emitters: fully sharpened slender emitters, i.e., pencils, and truncated pyramidal emitters, i.e., volcanoes. The arrays have between 4 and 1024 emitters in an active area of 0.64 cm^2. The surface of the engine (tank and emitters) is covered with "black silicon" that acts as wicking material. The hydraulic system has been experimentally characterized, including: start-up tests (Figure 2), wettability tests, current-per-emitter versus voltage characteristics, imprints of the exit stream on a collector, and a thrust test in agreement with the current-per-emitter versus voltage characteristics and the time-of-flight measurements that we have independently obtained at the Space Propulsion Laboratory. Preliminary results demonstrating the feasibility of obtaining substantially larger emission currents at the same extraction voltage by controlling the temperature have also been obtained. The emission from the array seems to be described by a Schottky emission mechanism.

Figure 1: Field view of a highly packed planar emitter array *(left)*; field view of a hybrid macro-fabricated/micro-fabricated planar array *(right)*.

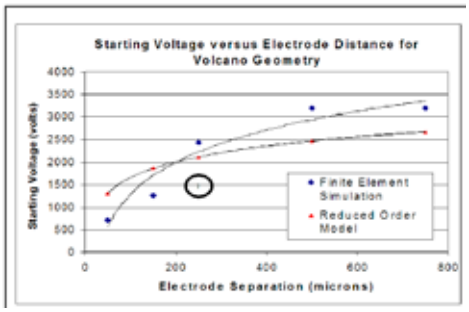

Figure 2: Start-up voltage vs. extractor separation for volcano emitters. The experimental points (from the testing facility with a fixed emitter-to-electrode separation equal to 250 μm) fall inside the circle drawn on the left plot.

REFERENCES:

[1] Taylor, G.I., "Disintegration of Water Drops in an Electric Field," *Proc. R. Soc.* London A 280, No 1382, pp 383 – 397, 1964

[2] Fenn, J., "Colloid Ionization for Mass Spectrometry of Large Biomolecules," *Science*, 246, pp. 64 – 71, 1989

[3] Mueller, J. "Thruster Options for Microspacecraft: A Review and Evaluation of Existing Hardware and Emerging Technologies," *AIAA* 77-3058, Seattle, WA, 1997.

Numerical Techniques for Integral Equations

M. Altman, J. Bardhan, X. Hu, S. Kuo, D. Willis, L. Daniel, J. Peraire, B. Tidor, J. White
Sponsorship: MARCO IFC and GRC, NSF, SRC, SMA, NIH

Finding computationally efficient numerical techniques for simulation of three-dimensional structures has been an important research topic in almost every engineering domain. Surprisingly, the most numerically intractable problem across these various disciplines can be reduced to the problem of solving a three-dimensional potential problem with a problem-specific Greens function. Application examples include: electrostatic analysis of sensors and actuators, electromagnetic analyses of integrated circuit interconnect and packaging, detailed analysis of frequency response and loss in photonic devices, drag force analysis of micromachined structures, and potential flow based aircraft analysis. Over the last fifteen years, we have been developing fast methods for solving these problems, and have developed widely used programs such as FastCap (capacitance), FastHenry (magnetoquasistatics), FastLap (general potential problems), FastImp (full wave impedence extraction),and FastStokes (fast fluid analysis). Our most recent work is in developing higher order methods[1], methods that efficiently discretize curved geometries[2], methods that are more efficient for substrate problems [3], and methods for analyzing rough surfaces [4].

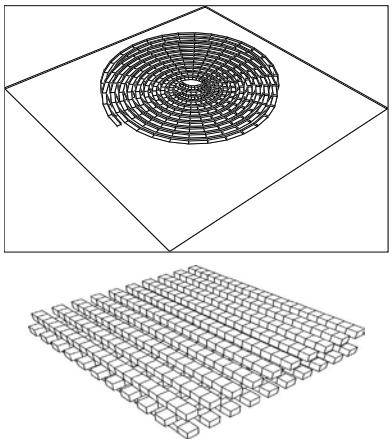

Figure 1: A buss crossing structure and a spiral inductor over a substrate. Analyzed by FastImp in minutes.

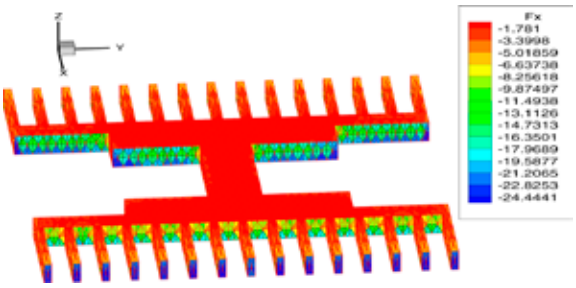

Figure 2: The fluid drag force distribution for a micromachined comb, computed using FastStokes in under five minutes.

REFERENCES:

[1] Willis, D.J., J.K. White, J. Peraire, "A pFFT Accelerated Linear Strength BEM Potential Solver," *Proc. of Modeling and Simulation of Microsystems*, March, 2004.

[2] Bardhan, J., M.D. Altman, S.M. Lippow, B. Tidor, J.K. White, "A Curved Panel Integration Technique for Molecular Surfaces," to appear in *Proc. of Modeling and Simulation of Microsystems*, May 2005.

[3] Hu, X., J. White, L. Daniel, "Analysis of Conductor Impedance over Substrate Using Novel Integration Techniques," To Appear, *Proceedings of the Design Automation Conference*, Anaheim, CA, 2005.

[4] Zhu, Z., A. Demir, J. White, "A Stochastic Integral Equation Method for Modeling the Rough Surface Effect on Interconnect Capacitance," *Proceedings of the IEEE Conference on Computer-Aided Design*, San Jose, November 2004.

Characterization and Modeling of Nonuniformities in DRIE

H.K. Taylor, H. Sun, T.F. Hill, D.S. Boning
Sponsorship: CMI, SMA

We contribute a quantitative and systematic model to capture etch nonuniformity in the deep reactive ion etching (DRIE) of microelectromechanical systems (MEMS) devices [1]. DRIE is commonly used in MEMS fabrication where high-aspect ratio features are to be produced in silicon. It is typical for many devices, of diameters on the order of 10 mm, to be etched simultaneously into a silicon wafer of diameter 150 mm. Devices containing a range of feature diameters exhibit aspect ratio-dependent etching rates, a phenomenon that is well understood [3]. In addition, equivalent features within supposedly identical devices are observed to etch at varying rates. These spatial variations have been explained in terms of uneven distributions of S_xF_y ions and fluorine neutrals at the wafer scale, and of competition for those species at the device, or die, level. An ion–neutral synergism model [7] is constructed from data obtained by etching several layouts of differing pattern opening densities (Figure 2). Such a model is used to predict wafer-level variation with an r.m.s. error below 3% (Figure 1). This model is combined with a die-level model, which we have reported previously [2,8], on a MEMS layout. The two-level model is shown to enable prediction of both within-die and wafer-scale etch rate variation for arbitrary wafer loadings.

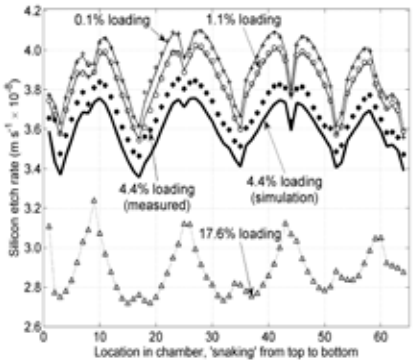

Figure 1: Four silicon wafers were etched in a deep reactive ion etcher, each wafer having one of the following proportions of its total surface area exposed for etching: 0.1%, 1.1%, 4.4%, 17.6%. An ion–neutral synergism model was fitted to etch rate data from wafers with 0.1%, 1.1% and 17.6% 'loading'. The 0.1%, 1.1% and 17.6% traces on this graph indicate that the model has successfully been fitted to the data. Lines represent the model's predictions; markers represent measured etch depths. The model can predict etch rates across a wafer with 4.4% loading, with an r.m.s. error of less than 3%.

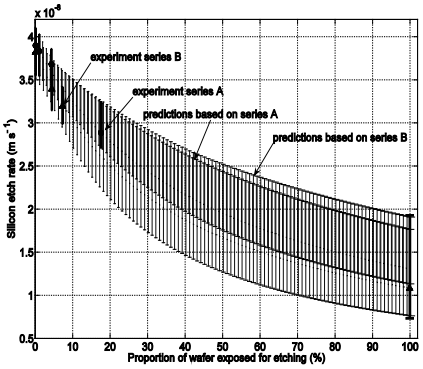

Figure 2: Measured and predicted etch rates as a function of the proportion of the wafer exposed for etching ("loading"). Data is presented for two sets of experiments performed on different dates using the same tool. At any given value of loading, a range of etch rates is observed across a wafer. The heights of the vertical bars in this figure indicate the size of that range. The thick vertical bars indicate the measured data; the bands constructed from thin lines indicate predictions of etch rates made using parameters extracted from the measured data.

REFERENCES:

[1] Sun, H. *et al.*, in 18th IEEE Int. Conf. MEMS (2005).
[2] Hill, T. *et al.*, in Tech. Digest of 2002 Hilton Head Solid State Sensors and Actuators Workshop, Hilton Head Island, SC, 2004.
[3] Ayon, A.A. *et al.*, *J. Electrochem. Soc.*, 146, 339 (1999).
[4] Yeom, J. *et al.*, in 12th Int. Conf. On Solid State Sensors, Actuators, and Microsystems, p. 1631, Boston, MA, 2003.
[5] Kiihamaki, J. *et al.*, *JVST*, A, 18, 2280 (2000).
[6] Bhardwaj, J. *et al.*, "Dry Silicon Etching For MEMS," Annual Meeting of the Electrochemical Society, Montreal, Quebec, Canada, May 1997.
[7] Gottscho, R.A. *et al.*, *JVST* B, 10, 2133 (1992).
[8] Sun, H., T. Hill, M.A. Schmidt, D. Boning, in 2003 Materials Research Society Fall Meeting, Boston, MA, 2003.

Measuring the Mechanical Properties of Thin Films Using MEMS Structures

R. Bernstein, D. Moore, C. Thompson
Sponsorship: CMI, SMA

Simple micromechanical devices are being developed to measure the mechanical properties of thin films in localized areas after processing. The simplest devices to fabricate are cantilevers overhanging a pit formed using an anisotropic etch. Cantilevers formed from a material of interest can be used to measure the through-thickness stress-gradient and the elastic modulus of that material. Measuring the elastic modulus requires applying a known force to the tip of the cantilever and measuring the subsequent deflection or curvature. We have developed a technique for high accuracy modulus measurement by application of a force with a beam having known properties, with deflection measurements made in an optical profilometer.

Membrane devices, as shown in Figure 1, can be used to measure the stress in a thin film without further processing. The membranes are fabricated using an SOI wafer as the starting material. An anisotropic etch from the backside is used to form the membrane, which consists of two layers: buried silicon dioxide under the device single crystal silicon. The membrane buckles because the buried silicon dioxide is under compressive stress relative to the silicon. The amount of buckling is determined by the mechanical properties and the geometry of the membrane, and is measured using optical profilometry. Depositing a film on either side of the membrane changes the buckling, and therefore, the stress of the new material can be determined. Films deposited on both sides of the membrane contribute to the change in deflection; consequently, the stress in CVD films can be measured.

Buckling of doubly-supported beams can be used to characterize compressive stresses. To characterize tensile stresses, we have recently developed a new type of device, a V-shaped beam, as shown in Figure 2(a). The V-beam is made from a material of interest. A tensile stress causes out-of-plane bending that can be measured using an optical profilometer. The measured deflections are then compared to finite element analyses. Two modes of bending have been seen in V-beams produced from silicon nitride thin films. Finite element models of the 2 modes showing vertical deflection contours can be seen in Figures 2(b) and 2(c). Mode 1 bending is symmetric and produces very large deflections that are often too large to measure in an optical profilometer. Most beams tend to bend into Mode 2, which is asymmetric, but easily measured using an optical profilometer. Mode 2 deflections also have the advantage that the through-thickness stress gradient does not change the deflection. Because all the devices described above are small, they can be placed in many locations on the wafer.

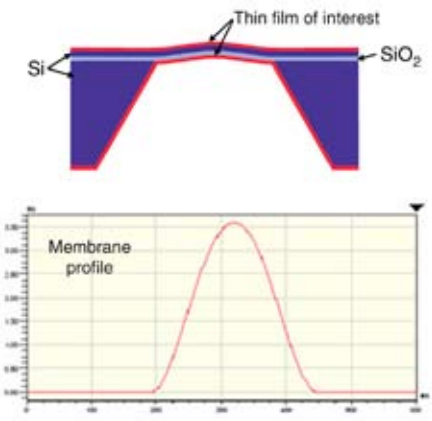

Figure 1. Cross section of a square membrane after the CVD thin film of interest has been deposited, with measured deflection from optical profilometry.

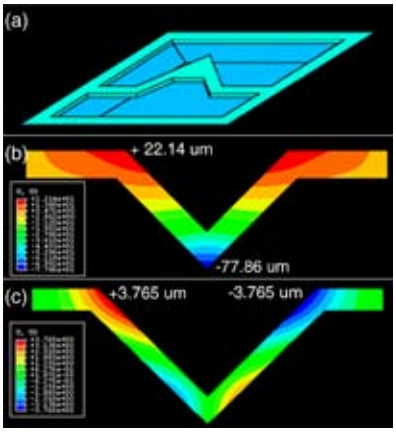

Figure 2. (a) V-beam device released by anisotropic etch. (b) Finite element analysis (FEA) of Mode 1 bending in a v-beam, with maximum deflection at tip of V. (c) FEA of Mode 2 bending.

Scanning Probe Microscopy with Inherent Disturbance Suppression Using Micromechanical Devices

A.W. Sparks, S.R. Manalis
Sponsorship: AFOSR

Scanning probe microscopes are notoriously susceptible to disturbances, or mechanical noise, from the surrounding environment that couple to the probe–sample interaction. These disturbances include vibrations of mechanical components, piezo drift, and thermal expansion. Disturbance effects can be substantially reduced by designing a rigid microscope, incorporating effective vibration isolation, and selecting an appropriate measurement bandwidth and image filter. However, it is not always possible to satisfy these requirements sufficiently, and as a result, critical features in an image can be obscured.

The cause of this problem is that the actuator (control) signal is used both to readout topography and correct for disturbances. We have introduced a general approach for inherently suppressing out-of-plane disturbances in scanning probe microscopy [1]. In this approach, two distinct, coherent sensors simultaneously measure the probe-sample separation. One sensor measures a spatial average distributed over a large sample area, while the other responds locally to topography underneath the nanometer-scale probe. When the localized sensor is used to control the probe-sample separation in feedback, the distributed sensor signal reveals only topography. This configuration suppresses disturbances normal to the sample. We have applied this approach to scanning tunneling microscopy (STM) with a microcantilever that integrates a tunneling tip and an interferometer (Figure 1) and have shown that it enables Angstrom resolution imaging of nanometer-sized gold grains in a noisy environment (Figure 2). For disturbances applied normal to the sample, we measured disturbance suppression of -50 dB at 1 Hz, compared to 0 dB with conventional imaging.

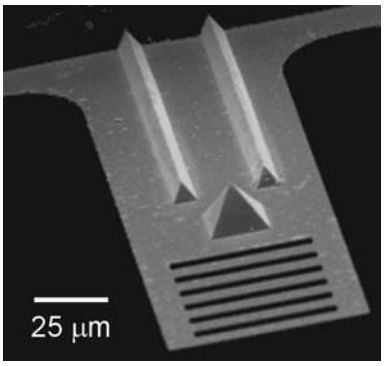

Figure 1: Scanning electron micrograph of the silicon nitride cantilever with integrated tunneling probe and interferometer.

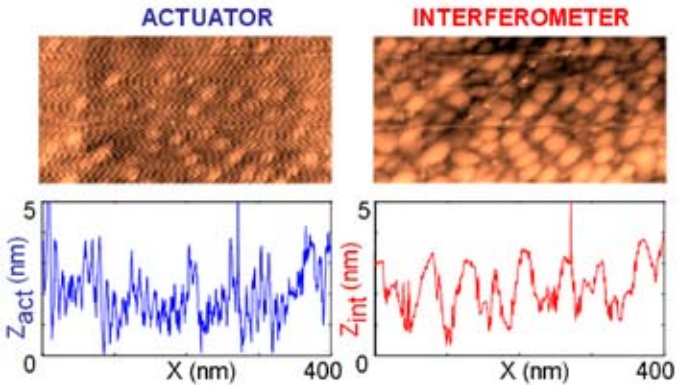

Figure 2: 400 x 200 nm^2 STM images of Au/Pd/Ti on a silicon substrate, imaged at 0.2 Hz on a mechanically grounded optics table. Cross sections from each image are shown for the same scan line.

REFERENCES:

[1] Sparks, A.W., S.R. Manalis, "Scanning Probe Microscopy with Inherent Disturbance Suppression," *Appl. Phys. Lett.,* vol. 85, pp. 3929-3931, 2004.

In-Plane AFM Probe with Tunable Stiffness

C. Mueller-Falcke, S.-G. Kim
Sponsorship: IMC

We developed an in-plane Atomic Force Microscope (AFM) probe that is specifically tailored to the needs of biological applications. It features a variable stiffness, which makes the stiffness of the probe adjustable to the surface hardness of the sample [1]. The inherent capability of the in-plane AFM probe for building a massively parallel array is also an important feature that greatly affects the speed of the AFM scanning process.

Concept and Functionality

The switchable stiffness probe allows the scanning of biological samples with varying surface hardness without changing probes during scanning and therefore, prevents a loss of positional information, as is unavoidable with conventional devices. For the integration of the components into a MEMS device, the conventional cantilever-type design of AFM probes has been abandoned in favor of an in-plane design. The new design has an advantage in that it facilitates a high-density array of AFM probes and allows for easy surface micromachining of the integrated device. It also enables the integration of micro-fluidic channels for reagent delivery and nanopipetting. For scanning nano-scale trenches and grooves, a multi-walled carbon nanotube, embedded in a nanopellet [2], is mechanically assembled to the AFM probe as a high-aspect-ratio tip.

Design and Fabrication

The variable stiffness is accomplished in a mechanical way by engaging or disengaging auxiliary beams to the compliant beam structure by the means of electrostatically actuated clutches (Figure 1). Figure 2 shows the integrated AFM probe system. For actuation, an electrostatic combdrive is considered to move the probe tip up and down. The vertical displacement of the tip can be measured by a capacitive sensor, which can easily be integrated into the system.

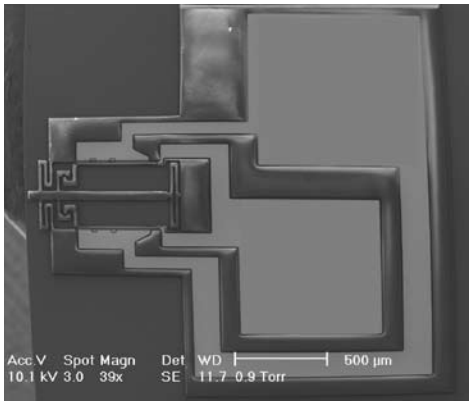

Figure 1: Unreleased in-plane AFM probe with electrostatic actuators that engage the clutches.

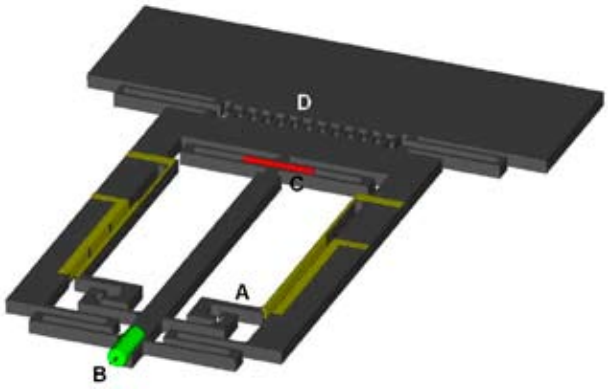

Figure 2: Device design (A: Electrostatic clutch, B: High-aspect-ratio carbon nanotube tip, C: Capacitive sensor, D: Combdrive actuator).

REFERENCES:

[1] Mueller-Falcke. C., Y-A. Song, S.-G. Kim, "Tunable Stiffness Scanning Microscope Probe," Optics East, Philadelphia, PA, October, 2004.

[2] El-Aguizy, T., J.-H. Jeong, Y.B. Jeon, W.Z. Li, Z.F. Ren S-G. Kim, "Transplanting Carbon Nanotubes," *Applied Physics Letters,* vol. 85, no. 25, P.5995, 2004.

Direct Patterning of Organic Materials and Metals Using a Micromachined Printhead

V. Leblanc, J. Chen, S.H. Kang, P.J. Benning, M.A. Baldo, V. Bulovic, M.A. Schmidt
Sponsorship: Hewlett-Packard

Organic optoelectronic devices are promising for many commercial applications, if methods for fabricating them on large area low-cost substrates become available. Our project investigates the use of MEMS in the direct patterning of materials needed for such devices.

In our first demonstration, we used an electrostatically actuated micromachined shutter integrated with an x-y-z manipulator to modulate the flux of evaporated organic semiconductors and metals and to generate patterns of the deposited materials. The micromachined printhead consists of a free-standing silicon microshutter actuated over a 25 micron square aperture by a comb-drive actuator. Figure 1 shows the microshutter and aperture. The device is fabricated, starting with a SOI (silicon on insulator) wafer, and using deep reactive ion etching to pattern both the through-wafer aperture and the free-standing structure and actuation mechanism. An operating voltage of 30 V is needed to obstruct the aperture with the microshutter. The simulated first mechanical resonant frequency of the device is 6 kHz.

We tested the printing method in a vacuum chamber by depositing an organic semiconductor, Alq_3 (tris (8-hydroxyqunolinato) aluminum), and silver on glass substrates. We also printed arrays of organic light emitting devices (OLED). Figure 2 shows patterns obtained using this method: photoluminescence image of 40 micron pixels of Alq_3, optical microscope image of 30 microns wide line patterns of silver, and electroluminescence of 30 micron pixels arrays of TPD:10%DCM/Alq3/TAZ at 20 V (with blue filter), and of TPD/Alq3/TAZ at 10V (no filter). The results show that this printing technique is capable of patterning small molecule organic light emitting devices at high resolution (800 dpi in our case).

The next stage of this project will involve investigating the use of a microporous layer with integrated heaters for local evaporation of the materials.

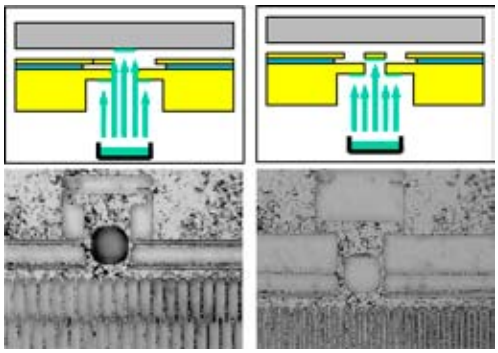

Figure 1: Schematic of printing principle and microscope image of aperture (dark area) and shutter. Left: when no voltage is applied, the material deposits on the substrate. Right: the shutter covers the aperture, and no material can be deposited on the substrate.

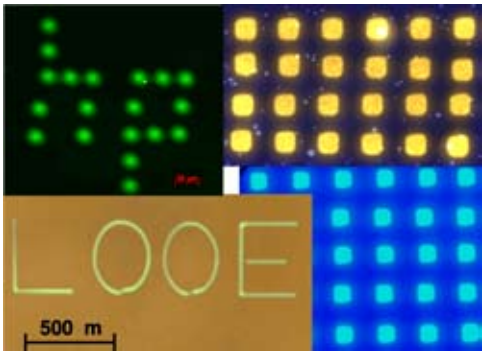

Figure 2: Patterns obtained using our direct patterning method. Clockwise from top right: photoluminescence of Alq3 pixels, electroluminescence of 2 different OLED arrays with 30 micron pixels, and reflection image of silver pattern.

Nanometer-Level Positioning in MEMS without Feedback Control

M. Culpepper, S. Chen, C. DiBiasio
Sponsorship: NSF Nanomanufacturing Program

Traditional macro-scale nanopositioners rely on sensors and feedback control to achieve nanometer-level accuracy and repeatability. The need for low-cost, high-speed precision positioning devices has led to a trend in miniaturization of these machines. Miniaturization of precision positioning devices is problematic as precision positioners require feedback control, and feedback control is not readily adapted to small-scale machines. The difficulty in adaptation is due mainly to the challenges encountered during the integration of small-scale sensors, mechanisms, and actuators. In this work, we are designing multi-axis MEMS that are capable of nanometer-level positioning without sensing/feedback control. The approach has grown from binary actuation technologies used in macro-scale robotics [1,2].

In our approach, Digital Nanoactuation Technology (DNAT), a positioner is equipped with actuator-flexure building blocks. The blocks consist of a pair of binary actuators that work together to generate discrete, repeatable positions. The actuators are attached to a positioning stage via flexures such that the actuator-flexure sets are diametrically opposed. An actuator set is shown on the left side of Figure 1. The opposed flexures differ in stiffness, one compliant, K_C, and one stiff, K_S. When both actuators are activated (four possible on-off combinations), four repeatable positions may be obtained. DNAT building blocks may be superimposed to provide many position states. For example, the 64 states shown on the right side of Figure 1 are obtained by superimposing the output of three blocks. The number of states scales with the number of actuator pairs, N, as 2^{2N}. A positioner with N = 6 is capable of over 4000 discrete positions. If these points are encompassed within a space of a few microns, simple on and off actuator commands may be used to obtain nanometer-level repeatability without sensing/feedback. A macro-scale analogy of a small-scale device has been constructed and tested [3] to demonstrate that nanometer-level positioning is possible. The small-scale prototype shown in Figure 2 is being tested to characterize a 64 state prototype before we progress to a smaller, 4000 state device.

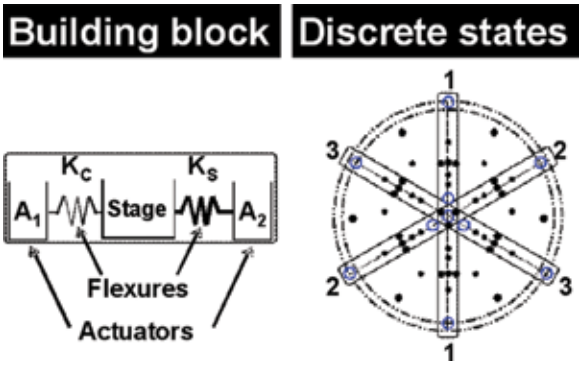

Figure 1: DNAT building block (left) and 64 Discrete position states obtained with three building blocks (right)

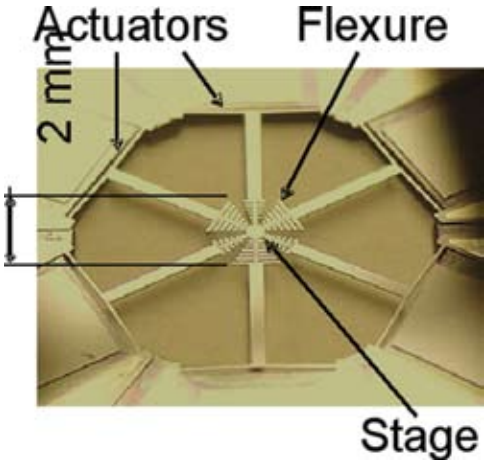

Figure 2: Small-scale DNAT positioner

REFERENCES:

[1] Mukherjee, S., S. Murlidhar, "Massively Parallel Binary Systems" *ASME Journal of Mechanical Design.*, pp 68-73, March 2001
[2] Lichter, M.D., V.A. Sujan, S. Dubowsky, Lect Notes Contr INF, 271, 219, 2001
[3] Culpepper, M.L., S. Chen, "Design of Precision Manipulators Using Binary Actuation and Differential Compliant Mechanisms," in Proc. ASPE Annual Meeting, 2003, pp. 279-282.

An Electrostatic, Circular Zipping Actuator for the Application of a Tunable Capacitor

X. Yang, A.H. Slocum, J.H. Lang
Sponsorship: Deshpande Center for Technological Innovation

A tunable capacitor is devised using a circular zipping actuator, based on its ability to potentially control a gap between two large surfaces with nanometer resolution [1]. The device consists of three wafers; a SOI (Silicon-On-Insulator) wafer sandwiched by two *Pyrex* glass wafers that are anodically bonded together, as shown in Figure 1. In the center of the device is a circular membrane that is supported by tethers that are connected to the outer walls. A cylindrical fulcrum, fabricated by the deep reactive ion etching technique, acts as the pivot for the membrane and divides the membrane into the outer actuator region and the center capacitor region. The top of the fulcrum is bonded to the top glass wafer for structural rigidity. The SOI layer is used as the membrane-actuator because of its uniform thickness and the low stress of single-crystal silicon. Thermally grown silicon dioxide is used as dielectric insulation. The bottom wafer contains the bottom electrodes for the actuator and the capacitor. The actuator electrode is etched into the glass to form the gap of the actuator. Gold is deposited on top of the glass wafer as both actuator and capacitor electrodes. Voltage is applied between the top and the bottom actuator electrodes. At a certain threshold, the outer membrane snaps down. With increasing actuation voltages, the membrane zips along the radial direction, as shown in Figure 2, and results in the separation of the two capacitor surfaces. Because of the poor adhesion of gold to oxide, the membrane will not be bonded to the gold surface, although the two are in close contact during operation. Thus, the design makes it possible to have two initially closed-contacted surfaces that can be pried apart. By changing the gap between the two plates of the capacitor, the capacitance can be tuned.

The device is modeled using both numerical methods with Matlab and FEM with ANSYS. Tests are done using a laser interferometer to measure the center displacement and a network analyzer to measure the capacitance change.

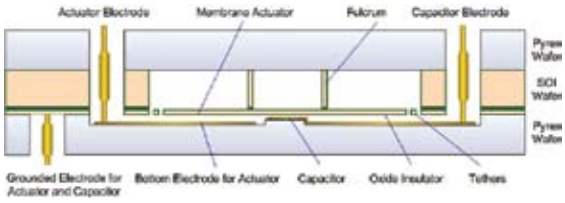

Figure 1: Cross-sectional view of the circular, zipping actuator device before actuation.

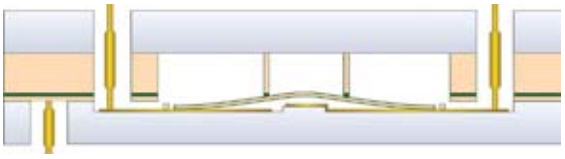

Figure 2: Cross-sectional view of device after actuation.

REFERENCES:

[1] White, J., H. Ma, J. Lang, A. Slocum, "An Instrument To Control Parallel Plate Separation For Nanoscale Flow Control," *Rev. Sci. Inst.* v. 74 no. 11, November 2003.

A Low Contact Resistance MEMS Relay

A.C. Weber, A.H. Slocum, J.H. Lang
Sponsorship: ABB Corporate Research

An electrostaticaly driven, bulk micromachined, low contact resistance MEMS cross bar relay has been designed, and is currently under fabrication. This relay will be used to study and optimize the behavior of micro-scale contacts for power applications.

Many MEMS relays have been reported in the literature [1,2,3]; most, however, are not suited for practical power applications due to their high contact resistance. A contact resistance of 50 mΩ [4] has been achieved by our group using a bulk micromachined, externally actuated structure as a proof of concept for this design [4].

The electrostatic "zipper" actuators [4,5] are designed for low pull-in voltage (~100 V) and large contact travel (~40 µm) to prevent arcing as the load circuit (up to 600V) is switched on and off. Figure 1 shows the MEMS relay. Figure 2 shows a detailed view of the actuator. The two arms of the parallelogram flexure are used as the traveling electrodes of the electrostatic actuators. Each traveling electrode, or arm of the parallelogram flexure, is adjacent to a pair of stationary electrodes: an engaging and a disengaging stationary electrode. The relay is engaged by electrostatic attraction between the traveling electrodes and the engaging stationary electrodes. Similarly, the MEMS relay is disengaged through electrostatic attraction between the traveling electrodes and the disengaging stationary electrodes. Each stationary electrode is comprised of a stiff component and a compliant, cantilevered component. The cantilevered component reduces the pull-in voltage by reducing the distance between the electrodes. As the actuator is energized, the compliant end of the stationary electrode, having the lower stiffness, is attracted by and deflected toward the moving electrode, making initial contact at the loose end of the cantilever. As the actuation voltage is increased, the contact point between the electrodes is displaced along the stationary electrode over the stiff component of the electrode in a "zipping" motion.

Our group continues to develop these MEMS relays for power applications.

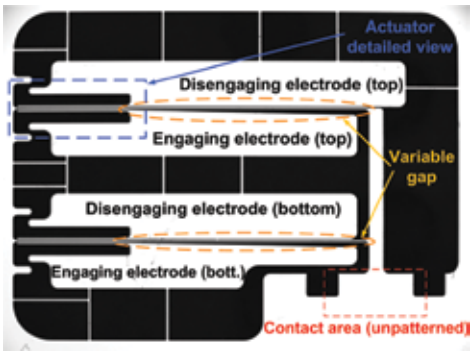

Figure 1: MEMS relay top view

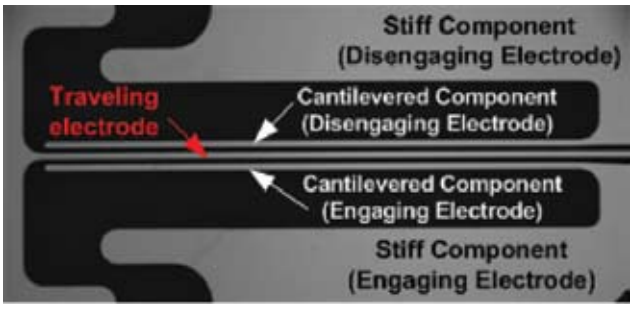

Figure 2: Actuator detailed view

REFERENCES:

[1] Lee, H. *et al*, "Electrostatically Actuated Copper-Blade Microrelays," *Sensors and Actuators A*, 100 (2002), pp. 105-113.
[2] Wong, J. *et al*, "An Electrostatically-Actuated MEMS Switch for Power Applications," in *Proc. IEEE MEMS '00,* Miyasaki Japan , pp. 633-638.
[3] Taylor, W. *et al*, "Fully Integrated Magnetically Actuated Micromachined Relays," *Journal of MEMS,* 7 (1998), pp. 181-191.
[4] Li, J., "Electrostatic Zipping Actuators and Their Application to MEMS," PhD thesis, Massachusetts Institute of Technology, 2004.
[5] Li, J. *et al*, "DRIE Fabricated Curved-Electrode Zipping Actuator with Low Pull-In Voltage," *12th Int. Conference on transducers, Solid-State Sensors, Actuators and Microsystems*, 2003, vol. 1, pp. 480-483.

A Variable Capacitor Made from Single Crystal Silicon Fracture Surfaces

A. Sprunt, A. Slocum, J.H. Lang
Sponsorship: Center for Bits and Atoms

A process for the fracture fabrication of single crystal silicon surface pairs with nanoscale roughness has been developed, and a prototype variable capacitor, featuring fracture surfaces as the moveable parallel plates, has been fabricated. The surfaces are fabricated by notching a portion of a compliant structure with either potassium hydroxide (KOH) or Focused Ion Beam (FIB) milling to produce a stress concentration. The device is fractured by pulling on the compliant structure with a probe. Post-fracture, the compliant structure acts as a bearing so the two surfaces can be brought back into intimate contact without misalignment. Proper alignment ensures that nanometer scale gaps can be maintained with surfaces that are perfectly smooth or complementary. Complementary surfaces have been closed to gaps less than 20 nm. For a successful fracture, the notch must be very sharp and properly aligned to the crystal structure, and the compliant structure (typically etched into the device layer of a Silicon On Insulator (SOI) wafer) must attenuate stray forces and moments and withstand the trauma of fracture. Experiments with different specimens have shown 10 µm to be the optimal thickness (Figure 1).

An updated version of the device used for the surface fabrication experiments has been fabricated, assembled, and sealed (Figure 2). This device includes an integrated zipper actuator [1] for controlling the separation of the surfaces, as well as, provision for wirebonding the device into its hermetically sealed package. Testing has confirmed that the actuator functions properly and that the specimens survived the fabrication process. The device also validated the electrical model used to design the capacitance measurement circuitry. Unfortunately, fracturing of these new devices has been problematic: growing the actuator's thermal oxide has likely blunted the notches. The fabrication process has been debugged, and a new round of fabrication (with an improved design) is nearing fruition.

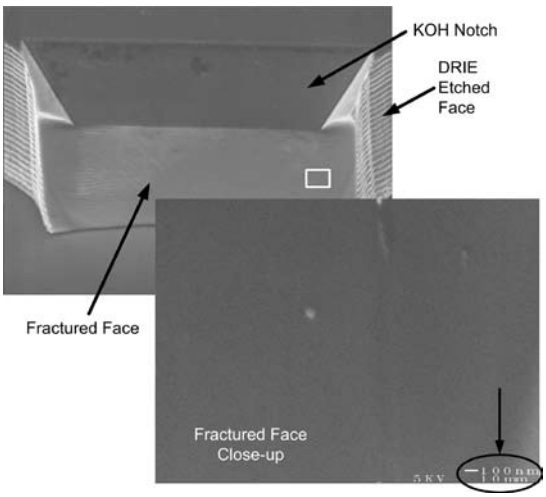

Figure 1: A high resolution SEM image of a fractured surface. Note the exceptionally good surface roughness.

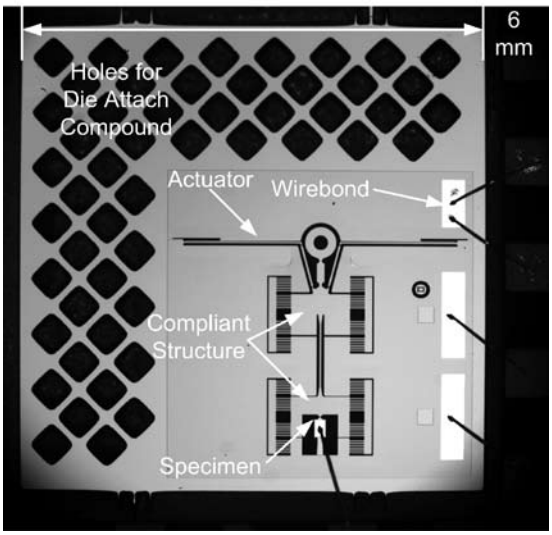

Figure 2: Integrated device for measuring the capacitance between pairs of fracture fabricated nanosurfaces.

REFERENCES:

[1] Li, J., "Electrostatic Zipping Actuators and Their Applications to MEMS," PhD thesis, Massachusetts Institute of Technology, Unpublished.

A High-*Q* Widely Tunable Gigahertz Electromagnetic Cavity Resonator

S.M. Hou, J.H. Lang, A.H. Slocum, A.C. Weber, J.R. White
Sponsorship: EECS, MechE

RF systems need high-frequency widely tunable high-*Q* bandpass filters for channel selection filters and local oscillators. Our work describes the design, fabrication, and testing of an electromagnetic cavity resonator designed for such applications. Alternative technologies provide wide tuning or high *Q*, but not both, and are generally not tunable. This resonator is distinguished by its simultaneous high *Q* near 200 and its wide high-frequency tuning range of 2.5 GHz to 4.0 GHz, which have been experimentally demonstrated. The resonator is fabricated using standard MEMS technologies and consists of a gold-lined capacitor and toroidal inductor cavity formed by etching silicon in potassium hydroxide (Figure 1). Frequency tuning is performed by compressing the cavity to close the capacitor gap. Testing was done with a piezoelectric actuator for this task. The match between the modeled and measured impedance is extremely good up to and beyond 5 GHz, with less than a 1% error in magnitude and phase.

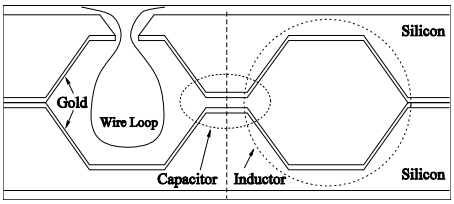

Figure: 1: Cross-sectional view of a cavity resonator with magnetic coupling.

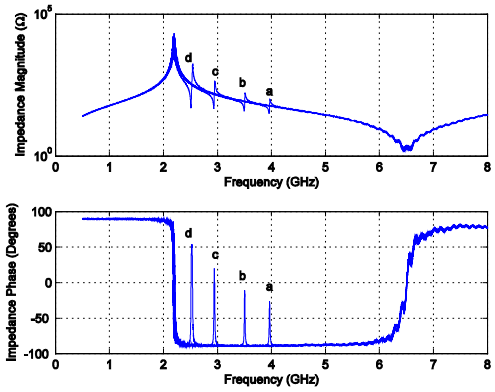

Figure 2: Superimposed impedances as functions of frequency when the capacitor gap is reduced by (a) 0 µm, (b) 5 µm, (c) 10 µm, and (d) 13.9 µm.

REFERENCES:

[1] Hou, S.M., J.H. Lang, A.H. Slocum, A.C. Weber, J.R. White, "A High-*Q* Widely-Tunable Gigahertz Electromagnetic Cavity Resonator," Proc. of the 2004 IEEE Solid-State Sensor, Actuator and Microsystems Workshop, Jun 2004.
[2] Hou, S.M., "Piezo-Tunable Gigahertz Cavity Microelectromechanical Resonator," Master's thesis, Mass. Inst. of Tech., 2004.
[3] Lin, L., R.T. Howe, A.P. Pisano, "Microelectromechanical Filters for Signal Processing," *JMEMS*, 7, #3, 286–294, Sep 1998.
[4] Wang, K., C.T-C. Nguyen, "High-Order Medium Frequency Micromechanical Electronic Filters," *JMEMS*, 8, #4, 534–557, Dec 1999.
[5] Wang, K., A.-C. Wong, C.T-C. Nguyen, "VHF Free-Free Beam High-*Q* Micromechanical Resonators," *JMEMS*, 9, #3, 347–360, Sep 2000.
[6] Wang, J., Z. Ren, C.T-C. Nguyen, "Self-Aligned 1.14 Ghz Vibrating Radial Mode Disk Resonators," Transducers 03, 947-950, Jun 2003.
[7] Borwick, R.L. *et al*, "A High Q, Large Tuning Range, Tunable Capacitor for RF Applications," MEMS 02, 669–672, Jan 2002.
[8] Grenier, K. *et al*, "Integrated RF MEMS for Single Chip Radio," *Transducers 01*, 4C1.01, Jun 2001.
[9] Haus, H.A., J.R. Melcher, Electromagnetic Fields And Energy, Prentice Hall, 1989.
[10] Hammond, H.P., Energy Methods In Electromagnetism, Oxford University Press, 1981

Lateral, Direct Contact RF MEMS Switch with PZT Actuation

W. Choi, Y. Shi, S.-G. Kim
Sponsorship: Korean Institute of Machinery and Materials

A novel direct contact MEMS switch is developed with compliant lateral metal contacts to address the need for low contact resistance and long life cycles. The device is unique in its self-alignment of the contact surfaces, self-cleaning of particles generated at each contact cycle, and mechanical anchoring method of the contact metal to the side of the Su-8 beam structures. The fabricated device maintains less than 0.1Ω contact resistance for up to 10 billions of cycles of contact. A fabricated device is shown in Figure 1 (a). Each switching member consists of two parallel beams with angled contact surfaces. One side of the contacting surfaces is undulated with micro grooves, as shown in Figure 1 (b). When the movable member is actuated to meet the fixed one, the gold on each side of the contact creates a short circuit. When the movable member is on the other side, enough gap is maintained to open the circuit with high isolation. The angled contact orientation makes the undulated surface slide over the static surface, which pushes entrapped particles or generated micro-weldments into the micro-grooves. By cleaning the surface at every cycle of switching, the micro-undulated surface ensures a low contact resistance over long cycles of switching operation. The grooved contact surfaces show successfully that the self-cleaning concept works and that a low contact resistance below 0.1Ω has been maintained over 10 billion cycles. (Figure 2)

Applications of the self-cleaning MEMS switch, such as tunable antennas, are being investigated to assess the commercial potential of our switch.

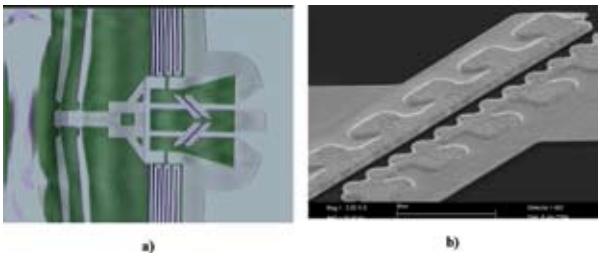

Figure 1: Fabricated device: a) Released device's layout, b) Contact metal at the later wall.

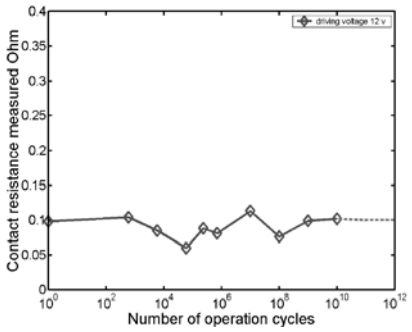

Figure 2: Contact resistance over operation cycles.

REFERENCES:

[1] Shi, Y. and Kim, S-G. "A Lateral, Self-Cleaning, Direct-Contact MEMS Switch," *Proc. IEEE MEMS 2005*, Miami, January 2005.

Design and Fabrication of Nano-Tweezers

F. Hashemi, G. Chen
Sponsorship: MIT

Since the invention of atomic force microscopes (AFM) that provided researchers with a convenient tool to observe objects at nanoscale, manipulation tools at nanoscale have been in high demand. There have been several attempts to create nanomanipulation devices, such as nano-tweezers, to address this challenge. Most such attempts have amounted to single proofs of concepts rather than a practical, readily producible manipulation tool. The goal of this project was to further the current state of nanomanipulators, by producing nano-tweezers that are consistently producible, using batch microfabrication processes. In addition, given the regularity and practicality of the AFM as a nano-scale research tool, the nano-tweezers were intended to also serve as a scanning probe for the AFM. This way, the same tool can to be used to both image and manipulate samples, and the utility of the devices is increased.

A two-fold approach was used to tackle the problem. First, using complete batch fabrication methods, a process was created to generate nano-scale tweezer tips separated by a nano-scale gap. This process uses standard micron scale batch lithography to define pyramidal walls in silicon. It then produces an extremely thin cut that self-aligns to the apex of the pyramid. Thus far, tip separations of 358nm and tip widths of 50nm have been repeatably produced. The alignment of the process is within 35nm and is much smaller than that of the lithography tool. The second phase was to create free standing, protruding structures that can serve as the tweezing arms and move with nano-scale resolution. Cantilevered flexural members, coupled with electro-static actuation, were successfully fabricated. These slender cantilevered flexural components measure only 1-2 um in width. A novel process was developed that overcomes problems due to surface tension, and protects the released devices all the way through die separation.

The devices have shown actuation behavior that is consistent with theory and design intent. Resolution of motion of 40nm has been verified using SEM through the entire working range of the device. Resolution of less than 10nm is expected based on data but has not been verified due to the limits of this SEM.

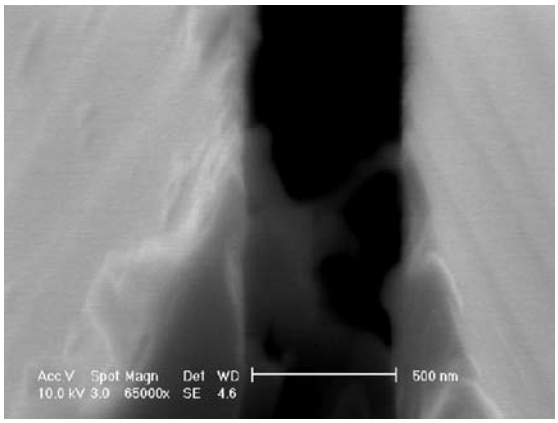

Figure 1: Close up cross-sectional view of the split pyramid showing tip separation.

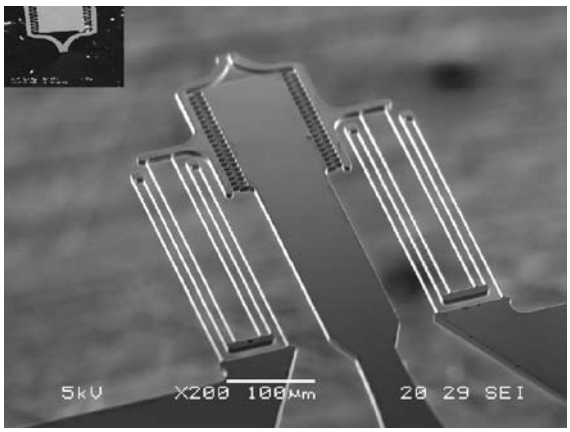

Figure 2: SEM image of the nano-tweezers. Image insert showing the nano-tweezers actuated, closed state.

Induced-Charge Electro-Osmotic Pumps and Mixers for Portable or Implantable Microfluidics

J.A. Levitan, Y. Ben, T. Thorsen, M.A. Schmidt, M.Z. Bazant
Sponsorship: Institute for Soldier Nanotechnologies, MIT-France Program

Microfluidic technology offers great promise in diverse fields such as bioinformatics, drug delivery, and analytical chemistry. In spite of involving microchannels, however, current lab-on-chip technologies are mostly limited to bench-top analysis due to various bulky external elements. For example, peristaltic pumping in soft-polymer channels requires complicated tubing and flow meters, and capillary electro-osmosis requires a high-voltage power supply. Miniaturizing and integrating the power source is a crucial next step toward portable or implantable devices for medical diagnostics, localized drug delivery, artificial organs, or pressure control to treat diseases such as glaucoma.

We are developing new kinds of pumps and mixers exploiting "induced-charge electro-osmosis" (ICEO) [1], as a potential platform for portable microfluidics. ICEO refers to the slip of a liquid electrolyte at a polarizable (metal or dielectric) solid surface, driven by an electric field acting on its own induced surface (double-layer) charge. Unlike classical (fixed-charge) electro-osmosis, which requires large DC voltages (>100V) applied down a channel, ICEO can be driven locally by small AC voltages (<10V). It is sensitive to the geometry, ionic strength, and driving frequency and scales with the square of the applied voltage. The effect generalizes "AC electro-osmosis" at planar electrode arrays [2] and offers some more flexibility.

We originally demonstrated ICEO flow in dilute KCl around a platinum wire by comparing flow profiles from micro-particle-image velocimetry (μPIV) to our theory [3]. We have also fabricated many devices involving electroplated gold structures on glass in PDMS microchannels, which exhibit mm/sec flow rates in 100 V/cm fields at kHz AC, and further optimization is underway. As a first application, we are developing a portable ICEO-powered biochip to detect blood exposure to toxic warfare agents by lysing cells and amplifying and detecting target genes.

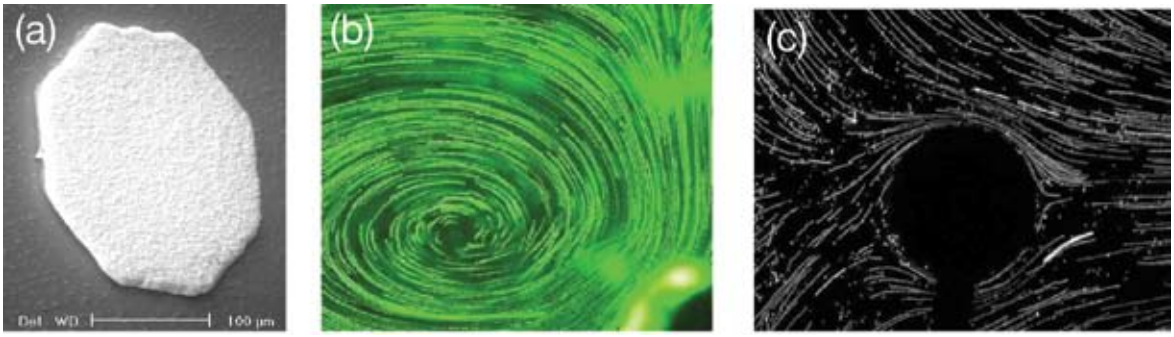

Figure 1: (a) SEM image of an electroplated gold post (12μm x 150μm). (b) ICEO convection around the post, visualized by streaks of fluorescent tracers used μPIV. (c) faster ICEO flow past a post held at fixed potential.

REFERENCES:

[1] Bazant, M.Z., T. M. Squires, "Induced-charge Electrokinetic Phenomena: Theory and Microfluidic Applications," *Physical Review Letters*, vol. 92, art. no. 066101 (2004).

[2] Ramos, A., H. Morgan, N.G. Green, A. Castellanos, "AC Electric-field Induced Flow in Microelectrodes," *Journal of Colloid and Interface Science*, vol 217 (2), pp. 420-422 (1999).

[3] Levitan, J.A., S. Devasenathipathy, V. Studer, Y. Ben, T. Thorsen, T.M. Squires, M.Z. Bazant, "Experimental Observation of Induced-charge Electro-osmosis around a Metal Wire in a Microchannel," *Colloids and Surfaces A*, in press (2005).